



12-1999

## **Control of CVD diamond nucleation and effects on microcomponent processing**

Samer Sima'an Ackleh

Follow this and additional works at: [https://trace.tennessee.edu/utk\\_graddiss](https://trace.tennessee.edu/utk_graddiss)

---

### **Recommended Citation**

Ackleh, Samer Sima'an, "Control of CVD diamond nucleation and effects on microcomponent processing.  
" PhD diss., University of Tennessee, 1999.  
[https://trace.tennessee.edu/utk\\_graddiss/8752](https://trace.tennessee.edu/utk_graddiss/8752)

This Dissertation is brought to you for free and open access by the Graduate School at TRACE: Tennessee Research and Creative Exchange. It has been accepted for inclusion in Doctoral Dissertations by an authorized administrator of TRACE: Tennessee Research and Creative Exchange. For more information, please contact [trace@utk.edu](mailto:trace@utk.edu).

To the Graduate Council:

I am submitting herewith a dissertation written by Samer Sima'an Ackleh entitled "Control of CVD diamond nucleation and effects on microcomponent processing." I have examined the final electronic copy of this dissertation for form and content and recommend that it be accepted in partial fulfillment of the requirements for the degree of Doctor of Philosophy, with a major in Metallurgical Engineering.

Carl McHargue, Major Professor

We have read this dissertation and recommend its acceptance:

R. A. Buchanan, T. T. Meek, M. Breinig

Accepted for the Council:

Carolyn R. Hodges

Vice Provost and Dean of the Graduate School



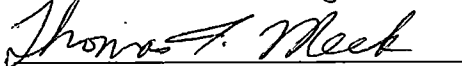
(Original signatures are on file with official student records.)

To the Graduate Council:


I am submitting herewith a dissertation written by Samer Ackleh entitled "Control of CVD Diamond Nucleation and Effects on Microcomponent Processing" I have examined the final copy of this dissertation for form and content and recommend that it be accepted in partial fulfillment of the requirements for the degree of Doctor of Philosophy, with a major in Metallurgical Engineering.

  
Carl McHargue, Major Professor

We have read this dissertation  
and recommend its acceptance:

Accepted for the Council:

  
Associate Vice Chancellor and  
Dean of The Graduate School

**CONTROL OF CVD DIAMOND NUCLEATION AND  
EFFECTS ON MICROCOMPONENT PROCESSING**

**A**

**Dissertation**

**Presented for the**

**Doctor of Philosophy**

**Degree**

**The University of Tennessee, Knoxville**

**Samer S. Ackleh**

**December 1999**

## DEDICATION

I dedicate this dissertation to my mom and dad whom I love.

*To*

*Mr. Sima'an Elias Ackleh*

*And*

*Mrs. Wedad Toufiq Ackleh*

Mom and Dad, without your love and sacrifice my achievements in life would have been impossible. Thanks and I love you.

## ACKNOWLEDGMENTS

I wish to thank my major professor, Dr. C. J. McHargue, for his support, guidance, patience, and good spirit throughout the course of this research. Dr. McHargue was very sincere and encouraging through the course of this project, and he also played as a role model for me in the fact that he is so active in the science field. I also wish to thank Dr. R. A. Buchanan and Dr. T. T. Meek, and Dr. M Breinig for serving as part of my committee.

I am grateful to a number of people at Oak Ridge National Laboratory. I am thankful without limits to Dr. R. E. Clausing for his unforgettable support and understanding through out this project. I am also very thankful to Mr. Lee Heatherly for all his helpful ideas and support concerning this research. Many thanks also go to Dr. John Hunn for his help on the ion implantation and analysis used in this study.

I would like to thank Dr. Peter Blau for allowing me to use his profilometry facilities and Mrs. Rebecca Martin for training me on them. Thanks also to Dr. Bob Shaw for helping on the silicon etching process and for supplying the needed materials. Special thanks to Dr. Bernart Frost for helping me on the AFM analysis. Thanks to Mrs. Dorothy Coffee for her help on the SEM training.

Last but not least I would like to thank all my family and friends for their continuous support throughout the course of this project. In particular, I would like to thank my mom and dad Mrs. And Mr. Wedad and Sima'an Ackleh, my brothers Dr. Essam Ackleh and his family, Dr. Azmy Ackleh and his family, and Mr. Loay Ackleh, my wonderful sister Mrs. Yamama Ma'alouf and her family. Without you them, this would not have been possible.

Research sponsored in part by the Division of Materials Science, U.S. Department of Energy under contract number DE-AC05-96OR22464 with Lockheed Martin Energy Research Corporation.

## ABSTRACT

Different surface pretreatments of the substrates and their effect on the nucleation and early growth stages of CVD diamond were studied, and the results were used to design a procedure for growing near-net shape diamond micro machine components. The mechanisms responsible for nucleation of diamond on various substrate material are still under study and have not been completely explained yet. Studies of different pretreatments that enhance or degrade the nucleation are important for the determination of controlling mechanisms and might lead to better applications of the CVD diamond industry.

The mechanical pretreatment consisted of ultrasonic abrasion of the silicon substrate with diamond, SiC, Al<sub>2</sub>O<sub>3</sub>, and TiB<sub>2</sub> powders mixed with ethanol. Scanning electron microscopy (SEM), profilometry, and AFM were used to characterize the surfaces before and after the CVD of diamond. Measurements of the surface roughness showed no significant difference between the roughness of the various abraded samples. Nucleation density was 4 to 8 orders of magnitude higher on the samples abraded with diamond-ethanol slurry than any other material. Increasing the abrasion time appears to have slight effect on the nucleation density. Gross deformation did not seem to affect the nucleation rate either.

The effect of ion implantation on the pretreated samples was investigated. Scanning electron microscopy and RBS/Channeling were used to analyze the results of this work. At an energy of 150 KeV, a dose of  $2 \times 10^{15}$  Si/cm<sup>2</sup> was the border line for suppression of nucleation and also for amorphization of both diamond and silicon.

Annealing of the substrates at various stages of the CVD process was also studied. SEM, RBS/channeling, and SEM channeling were used for the analysis in this study. Annealing the substrates did not seem to have a significant effect on the nucleation and growth of CVD diamond.

The results of the studies on pretreatment were used to design a process for fabrication of diamond microcomponents. The process included ion implantation, CVD

growth, and etching. Analysis on these samples was done using all the above mentioned techniques. Controlling the nucleation in the implanted regions is the major key to the control of the minimum resolution of features on the diamond near-net shape microcomponents.



## TABLE OF CONTENTS

CHAPTER	PAGE
<b>PART I: Nucleation of Diamond.....</b>	<b>1</b>
<b>1. Introduction.....</b>	<b>2</b>
1.1 Purpose of this Study.....	2
1.2 Properties and Application.....	3
1.3 Mophology and its Importance.....	7
1.4 Synthesis of Diamond.....	13
1.5 Ion Implantation-Introduction.....	28
<b>2. Literature Review of Nucleation of CVD diamond.....</b>	<b>33</b>
2.1 Nucleation Mechanisms.....	33
<b>3. Characterization Techniques.....</b>	<b>50</b>
3.1 Scanning Electron Microscopy (SEM).....	50
3.2 Energy Dispersive Spectrometry (EDS).....	51
3.3 Profilometry.....	53
3.4 Atomic Force Microscopy (AFM).....	54
3.5 Rutherford Back Scattering (RBS)/Channeling.....	57
3.6 Transportation and Range of Ions in Matter (TRIM).....	63

<b>4. Experimental Methods.....</b>	<b>65</b>
4.1 The Hot Filament Chemical Vapor Deposition apparatus (HFCVD).....	65
4.2 Experimental Procedures.....	70
<b>5. Results and Discussion.....</b>	<b>77</b>
5.1 Surface Mechanical Treatments.....	77
5.2 Ion Beam Treatment.....	98
5.3 Observations on Carbon Contamination – SiC.....	114
5.4 Annealing Effects on the Nucleation of CVD Diamond....	126
<b>6. Summary Part I.....</b>	<b>138</b>
6.1 Surface Mechanical Treatments.....	138
6.2 Ion Beam Treatments.....	138
6.3 Effects of Carbon Contamination of Surfaces.....	139
6.4 Annealing Studies.....	139
<b>PART II: Near Net Shape Micro Components.....</b>	<b>141</b>
<b>1. Introduction and Literature.....</b>	<b>142</b>
<b>2. Experimental Setup and Procedure.....</b>	<b>145</b>
<b>3. Results and Discussion.....</b>	<b>149</b>
<b>4. Summary of Part II.....</b>	<b>170</b>

<b>PART III: Conclusions.....</b>	<b>171</b>
<b>1. Conclusions for Part I.....</b>	<b>172</b>
<b>2. Conclusions for Part II.....</b>	<b>174</b>
<b>PART IV: Suggested Future Work.....</b>	<b>176</b>
<b>References.....</b>	<b>179</b>
<b>VITA.....</b>	<b>193</b>

## LIST OF TABLE

TABLE	PAGE
<b>PART I</b>	
1.1 Properties of diamond.	5
1.2 Some-Anisotropic Properties of Diamond Single Crystals	9
1.3 Theoretical cleavage energy for diamond.	10
4.1 Doses used in the implantation process.	73
4.2 Deposition parameters for the CVD process.	74
5.1 Results of profilometer measurements on surface roughness of substrates.	78
5.2 Average values for Ra and Rq based on the data in Table 5.1.	78
5.3 Densities for samples abraded with diamond SiC, Al <sub>2</sub> O <sub>3</sub> , and TiB <sub>2</sub> and their conditions.	84
5.4 Ratio of nucleation density on silicon substrates abraded with diamond SiC, Al <sub>2</sub> O <sub>3</sub> .	96
5.5 Nucleation densities of samples implanted with silicon and grown under various conditions.	99
5.6 damage energy values at the surface and peak damage scaled to ion dose for both silicon and diamond targets.	112

5.7 Nucleation on ion implanted silicon substrates.	113
5.8 History of sample J implanted with $1 \times 10^{17}$ Si/cm <sup>2</sup> and exposed in the growth chamber for indicated sequence.	115
5.9 Annealing conditions and results.	133

## **PART II**

3.1 Summary of growth parameters for the near-net-shape samples.	149
3.2 Parameters of CVD near-net-shape microcomponent of sample SSA07.	156
3.3 Parameters of CVD near-net-shape microcomponent of sample SSA42.	157
3.4 Parameters of CVD near-net-shape microcomponent of sample SSA43.	158
3.5 Parameters of CVD near-net-shape microcomponent of sample J.	159
3.6 Parameters of CVD near-net-shape microcomponent of sample M.	159

## LIST OF FIGURES

FIGURE	PAGE
<b>PART I</b>	
1.1 Diamond applications based on mechanical properties	6
1.2 Growth conditions change film structure and thereby the thermal conductivity	12
1.3 Schematic of the implantation and damage processes using energetic ion beams	30
2.1 Nucleation and growth kinetics of low-pressure diamond deposition on a non-reacting surface	35
2.2 Chemical interactions between different substrates and the gas phase containing $\text{CH}_x$ , $\text{H}_2$ , $\text{H}^\circ$ [77]	38
2.3 Nucleation and growth kinetics during low-pressure diamond deposition on a carbide-forming substrate surface.	40
2.4 A schematic showing nucleation by the carbide particles being heterogeneous.	42
2.5 Different mechanisms for diamond nucleation on scratches	44
3.1 Scanning conditions for selected area channeling	52
3.2 A list of common forces encountered in Atomic Force Microscopy	55
3.3 A schematic diagram showing the components of a tip on an AFM	56
3.4 Basic backscattering spectrometry	58
3.5 Schematic view of the channeling of ions direct at an angle $\psi$ to a close-packed row of atoms in a crystal	61
3.6 Model of lattice atoms, showing the atomic configuration in the diamond cubic structure.	62
3.7 Schematic diagram illustrating ion scattering from defects	64
4.1 A schematic of the experimental set up used for growing	

polycrystalline diamond films.	66
4.2 A HFCVD reactor during film growth (ORNL photograph YP-5852).	68
4.3 A schematic of the quartz tube reactor used for hot filament CVD deposition of diamond films.	69
5.1 AFM micrograph showing the roughness of a virgin silicon surface	80
5.2 AFM micrograph showing the roughness of a diamond polished silicon surface.	81
5.3 AFM micrograph showing the roughness of a SiC polished silicon surface.	82
5.4 AFM micrograph showing the roughness of a Al <sub>2</sub> O <sub>3</sub> polished silicon surface.	83
5.5 Scanning electron micrograph showing diamond nucleation density on a sample abraded with diamond slurry in the ultrasonic bath.	85
5.6 Scanning electron micrograph showing diamond nucleation density on a sample abraded with diamond slurry in the ultrasonic bath.	87
5.7 Scanning electron micrograph showing diamond nucleation density on a sample abraded with Al <sub>2</sub> O <sub>3</sub> slurry in the ultrasonic bath.	88
5.8 Scanning electron micrograph showing diamond nucleation density on a sample abraded with SiC slurry in the ultrasonic bath.	89
5.9 Scanning electron micrograph showing diamond nucleation density on a sample abraded with SiC slurry in the ultrasonic bath.	90
5.10 Scanning electron micrograph showing diamond nucleation density on a sample abraded with SiC slurry in the ultra-	

sonic bath for 15 minutes (compare to Figure 5.11).	91
5.11 Scanning electron micrograph showing diamond nucleation density on a sample abraded with SiC slurry in the ultrasonic bath for 3 hours.	92
5.12 Scanning electron micrograph showing diamond nucleation density on a sample that was polished on a felt pad using Al <sub>2</sub> O <sub>3</sub> slurry.	93
5.13 Scanning electron micrograph showing diamond nucleation density on a sample scratched with SiC abrasive paper.	95
5.14 AFM micrgraph showing a diamond particle which does not seem to be associated with any obvious features.	97
5.15 Scanning electron micrograph of sample implanted with $5 \times 10^{14}$ Si/cm <sup>2</sup> and exposed to 1.0% CH <sub>4</sub> concentration.	100
5.16 RBS/channeling spectra for a sample implanted with $1 \times 10^{15}$ Si/cm <sup>2</sup> .	101
5.17 Scanning electron channeling pattern of an annealed silicon sample showing that surface to be a single crystal.	103
5.18 Scanning electron micrograph showing the difference in nucleation density between an implanted and non-implanted region of a silicon sample that was implanted with $2 \times 10^{15}$ Si/cm <sup>2</sup> .	104
5.19 Scanning electron micrograph showing slight suppression of nucleation in the implanted regions for a sample implanted with a dose of , and inserted into a 0.5% CH <sub>4</sub> CVD reaction for 16.67 hours.	105
5.20 Scanning electron micrograph showing no suppression of diamond nucleation for a sample implanted with a dose of $2 \times 10^{15}$ Si <sup>+</sup> /cm <sup>2</sup> , and inserted into a 1.0% CH <sub>4</sub> CVD reaction for 16 hours.	106
5.21 Scanning electron micrograph showing almost complete suppression of nucleation.	107



5.22 RBS/channeling for sample J.	109
5.23 Scanning electron micrograph showing the boundary between the region that was affected by the etchant and the region that was unaffected.	117
5.24 Scanning electron micrograph showing a high magnification (300x) of the region where the etchant was effective.	118
5.25 Scanning electron micrograph showing a high magnification (300x) of the region where the etchant was not effective.	119
5.26 Scanning electron micrographs of different areas on J sample showing presence of a film between the silicon substrate and diamond particles.	120
5.27 Energy disperssion spectrum on sample J.	121
5.28 Energy disperssion spectrum for sample M, showing no carbon peak.	123
5.29 Scanning electron micrograph for sample J, after second run for six hours.	124
5.30 Scanning electron micrograph showing the area where part of the diamond grid fell off due to too much undercutting resulting from the etchant.	127
5.31 Scanning electron micrograph showing a center of three circles where diamond used to reside.	128
5.32 Scanning electron micrograph showing yet another center of three circles where diamond used to reside.	129
5.33 Scanning electron micrograph showing yet more areas where SiC is present under pre-existing diamond.	130

## **PART II**

2.1 A photograph showing a TEM grid used for masking the samples in the ion implantation process.	146
--	-----

3.1 Scanning electron micrograph showing the diamond pattern of sample SSA07.	150
3.2 Scanning electron micrograph showing the diamond pattern of sample SSA42.	151
3.3 Scanning electron micrograph showing the diamond pattern of sample SSA43.	152
3.4 Scanning electron micrograph showing the diamond pattern of sample J.	153
3.5 Scanning electron micrograph showing the diamond pattern of sample M.	154
3.6 Scanning electron micrograph showing a diamond pattern of a sample that was grown for 18 hours on a pretreated substrate, then the diamond grid was removed and palced on another substrate for another 36 hours of growth.	161
3.7 Free standing microcomponent, sample SSA07 small holes.	164
3.8 Free standing microcomponent, sample SSA07 large holes.	165
3.9 Free standing microcomponent, sample SSA42.	166
3.10 Free standing microcomponent, sample SSA43 small holes.	167
3.11 Free standing microcomponent, sample SSA43 large holes.	168
3.12 Free standing microcomponents, samples SSA07, SSA42, and SSA43 together.	169

**PART I**

**Nucleation of Diamond**

# CHAPTER 1

## INTRODUCTION

### 1.1 Purpose and Objectives of this study

The objectives of this study are:

- 1) To study the effects of surface pretreatment of the substrate (silicon) on the nucleation (and early growth stages) of Chemical Vapor Deposition (CVD) diamond; and
- 2) To use these results to design a procedure for growing near-net shape diamond micro machine components.

In some respects this study is an extension of the limited research done by Sunil Abraham [1], on the effect of ion-beam pretreatment on the nucleation of diamond on SiC (6H) single crystal substrate. However, because of the possible participation of the substrate material in chemical reaction with the reactant gases and with the deposited diamond itself, these prior results cannot directly be extended to growth on single-crystal silicon substrates.

An understanding of nucleation is necessary for the effective design of the deposition conditions that lead to high-quality diamond-coated components and free standing diamond components. For example, the type and orientation of grain boundaries strongly effect the chemical, thermal, mechanical, electronic and optical

properties. The ability to control nucleation can also allow the design of fabrication procedures to economically prepare diamond micro-machine components of near-net-shape dimensions for specific applications.

This introduction will first discuss the properties of diamond that make this material important and then briefly discuss the importance of morphology and its effect on diamond properties. Following that a review of deposition processes will be given, with emphasis on the “low-pressure” ones that have led to great worldwide research activities to produce high-quality diamond components for specific applications. The last section will introduce ion implantation, since it plays a significant role in the current study.

## **1.2 Properties and applications**

Why diamond? First, the fact that mankind can synthesize diamond is very interesting on its own, because it is thermodynamically stable only at high pressures. It also has great technological importance because it has better mechanical [2], physical, electrical [3], and optical [4] properties than many other materials used in many different applications, such as thermal management, cutting tools, wear resistant coatings, optics, and electronic devices [5]. Diamond is the hardest known material and that gives rise to many applications that are of even greater commercial value than the gemstones. Second to its use as a gemstone, is its use in applications that exploit its high thermal conductivity. Other mechanical and physical properties of diamond are its small coefficient of friction, and the velocity of sound is higher in diamond than in any other material [6]. Diamond also has excellent thermal, optical, and electrical

properties. Typical values of some of the properties of diamond are listed in Table 1.1 [1].

Applications for diamond include cutting tools, nozzles for very high pressure spraying systems, grinding, and heat sinks for integrated circuits in computerized chips, coatings, and more. For a detailed list of applications based on the mechanical properties of diamond, see Figure 1.1 [2].

Lowering the cost of producing diamond and improving its quality will increase the number of applications. If we can lower the temperature of heteroepitaxial growth then we can increase the variety of materials that can be used as substrates, thus increasing the application of diamond as coatings or films. In the shipping industry a thin film of diamond acting as a protective coating on large cargo ships, could slow or prevent the barnacles from sticking to the hulls of the ships, and that alone would save the large amount of money spent in cleaning the hulls. Diamond films could also be used on eyeglasses to prevent them from being easily scratched.

One of the major obstacles to higher computer speeds is the fact that Integrated circuits (IC's) have to be a minimum distance apart so that they won't over heat, and that limits the number of IC's that can fit in a given space. If the IC's chips are coated with a diamond film, the heat from the IC's will spread and be conducted away much faster and the spacing between the IC's can be decreased; thus computer speeds can be increased since more IC's can be fitted into a given space.

**Table 1.1: Properties of diamond**

---

Chemical Reactivity	Extremely Low
Density	3520 Kg m <sup>-3</sup>
Hardness	9000 kg mm <sup>-2</sup>
Heat Conductivity	20 w cm <sup>-1</sup> °K <sup>-1</sup> at 30 °C
Tensile Strength	0.5 x 10 <sup>6</sup> psi (natural)
Compressive Strength	14 x 10 <sup>6</sup> psi (natural)
Thermal Expansion Coeff.	0.8 x 10 <sup>-6</sup> °K <sup>-1</sup>
Refractive Index	2.41 at 590 nm
Transmissivity	225 μm -far IR
Friction Coefficient	0.05 (dry)
Band Gap	5.48 eV
Electrical Resistivity	10 <sup>16</sup> ohm-cm (natural)
Youngs Modulus	1050 GPa

---

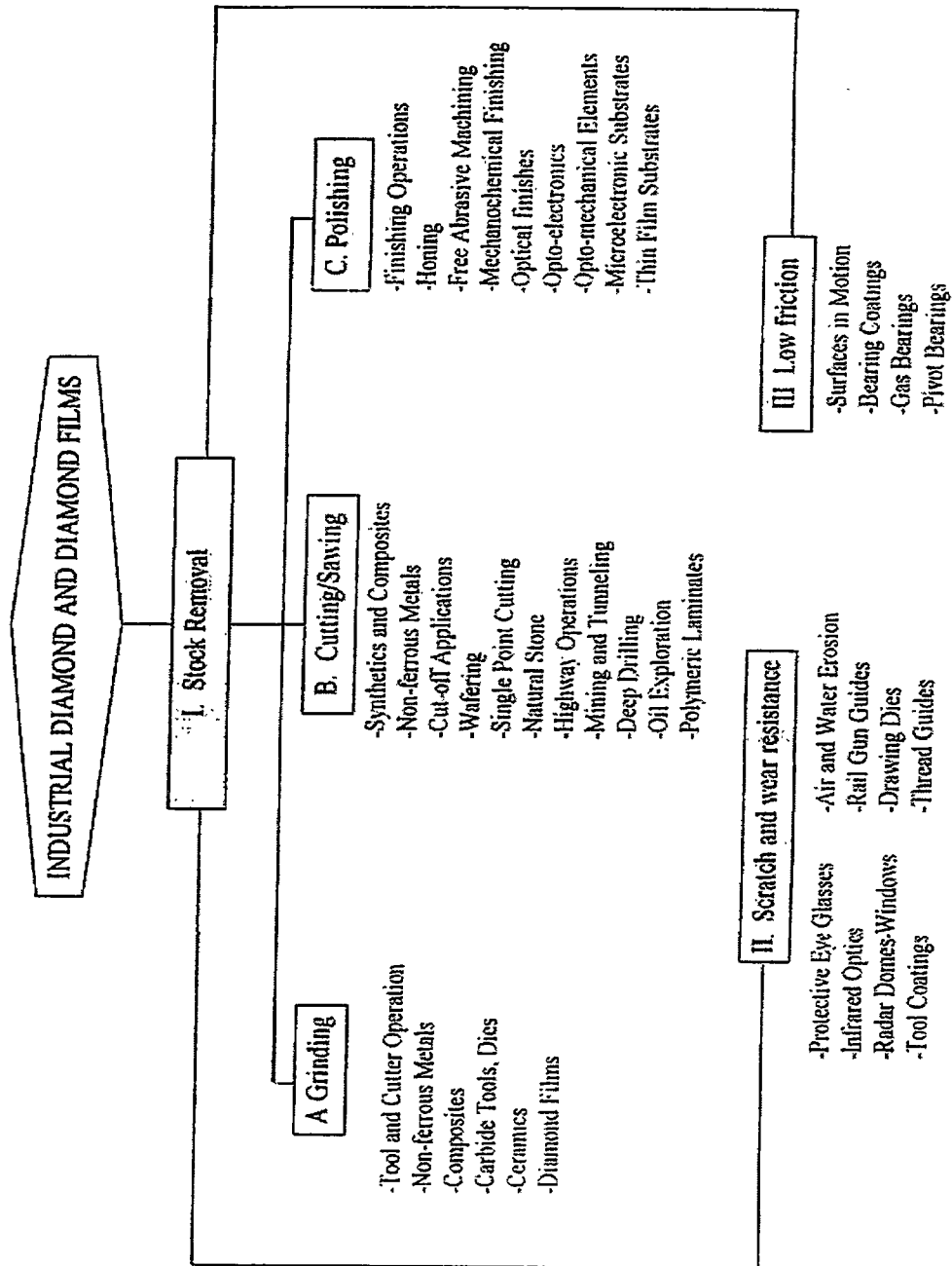


Figure 1.1: Diamond applications based on mechanical properties.



CVD diamond-coated drill bits, reamers, countersinks etc. are now commercially available for machining non-ferrous metals, plastics, and composite materials. Initial tests indicate that such CVD diamond-coated tools have longer lifetime, cut faster and provide a better finish than conventional tungsten carbide tool bits [5]. In some of the applications mentioned above either natural diamond or CVD diamond can be used. However, there are many applications that are in, or close to, the market place where CVD diamond offers wholly new opportunities. Wear resistant coatings are one such application. The ability to protect mechanical parts with ultra-hard coating, in for example, gearboxes, engines, and transmissions, may greatly increase the components lifetimes and reduce the lubrication requirements [5].

### **1.3 Morphology and its importance**

Different applications for diamond rely on different properties of diamond. As a result it is important to control the properties of diamond so that maximum efficiency can be achieved in a particular application. According to R.E. Clausing [7], the properties of diamond single crystals are dependent on the orientation, i.e. they are anisotropic, and on the defects and impurities incorporated in the crystal. In addition to that, polycrystalline diamond depends on the material at the boundaries of each crystallite. In order to control the properties of diamond, one must control the morphology of diamond, and in order to do so, the nucleation and growth techniques must be well understood.

Morphology, as defined by R. E. Clausing, is “the internal and external form and structure of a diamond material, either a single crystal or polycrystalline assembly.”

The basic diamond cubic crystal structure, and the quality and rate of crystal growth in different crystallographic directions, which are strongly affected by the growth conditions, can give diamond a wide variety of morphologies. Two main reasons for the importance of controlling morphology are the fact that many of the physical, chemical and mechanical properties of diamond single crystals are anisotropic, and the difficulty of altering the as-grown structure.

Some of the anisotropies of properties are listed in Table 1.2 [7]. Depending on the direction of polishing and the crystal face, the rate of wear may vary by orders of magnitude [8]. The material removal rate can change by a factor of 10 simply by rotating the crystal ten degrees in the plane of polishing or reversing the direction of polishing [8]. Oxidation rates are usually 10 times higher on the {111} faces than they are on the {100} faces [9]. The dominant cleavage plane for diamond is the (111), although there are several other planes on which diamond cleaves, and the theoretical energy necessary to cleave diamond varies from one plane to another. A list of the values of energies needed for each plane is listed in Table 1.3 [10].

In polycrystalline diamond, each of the crystallites will have its own orientation, shape and size, which may be similar or different from the ones surrounding it, depending on the growth conditions. Since each crystal can grow in different shape and size, the boundaries between the crystals will not be perfect. Each grain will have a boundary that is not aligned with the surrounding grains, and grain boundaries generally have higher concentration of defects and impurities. The mechanical strength of these

**Table 1.2: Some-Anisotropic Properties of Dimaond Single Crystals**

Property	Crystal Face or Direction	Relative Value	Reference
Abrasion/Wear Rate	{111} face/polishing direction 50o away from <111> toward cube	30	Wilks (1979)
	{111} face/polishing direction 60o away from <111> toward cube	3	Wilks (1979)
Oxidation Rate	{111}	1.5	Evans (1979)
	{110}	0.8	
Cleavage Energy	{100}	0.2	
	{111}	10.6	Field (1979)
	{110}	13.0	
	{100}	18.4	

**Table1.3: Theoretical cleavage energy for diamond**

<b>Plane</b>	<b>Angle between plane and (111) plane</b>	<b>Cleavage energy/ J m<sup>-2</sup></b>
111	0° and 70° 32'	10.6
332	10° 0'	11.7
221	15° 48'	12.2
331	22° 0'	12.6
110	35° 16' and 90'	13.0
322	11° 24'	13.4
321	22° 12'	14.3
211	19° 28'	15.0
320	36° 48'	15.3
210	39° 14'	16.4
311	29° 30'	16.6
100	54° 44'	18.4

Note: to obtain a fracture surface energy,  $\gamma$ , divide by 2.

boundaries is high, but the discontinuities in the structure affect properties that depend on crystal perfection, such as the thermal conductivity.

The mechanical, chemical and physical properties are also affected, by the presence of grain boundaries [7]. Oxidation rates are much faster at the grain boundaries of polycrystalline material than in a single crystal. The etch rates of polycrystalline films can be 100 times faster than single crystal {100} faces, especially when the grain size is small and the defect concentration is high.

Thermal conductivity depends on the rigidity of the bonds between the different crystallites. The higher the rigidity the more efficient is the motion of phonons through the grain boundaries. The higher intensity  $1332\text{ cm}^{-1}$  Raman spectroscopy lines correspond to more perfect films, and that means better thermal conductivity in that film, see Figure 1.2 [7]. From this, one can conclude that the thermal conductivity in polycrystalline diamond films is anisotropic. The smaller the grain size in the direction of flow, the more interaction between the phonons and the boundary and the lower the conductivity. On the other hand if the conductivity is measured in a direction where the single crystallites are elongated, perhaps to the thickness of the film, then the thermal conductivity can reach that of a single crystal diamond.

The grain boundaries increase the concentration of defects such as non-diamond impurities, and that can decrease the elastic modulus and hardness, and increase the fracture toughness.

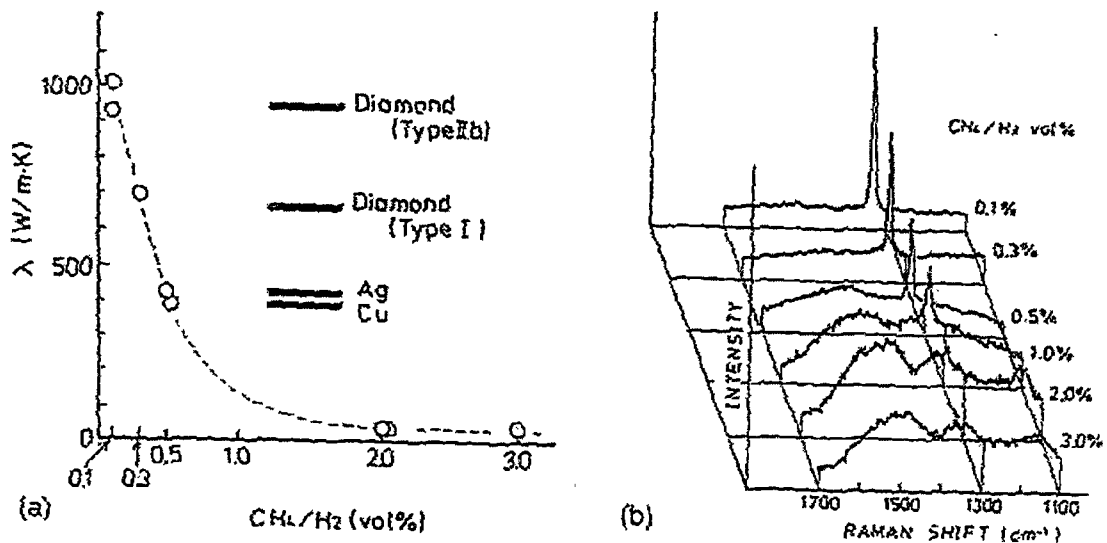


Figure 1.2: Growth conditions change film structure and thereby the thermal conductivity. (a) Thermal conductivity of CVD diamond films as a function of using different methane concentrations during film depositions. (b) The Raman spectra of the diamond films indicates increasing crystal perfection with decreasing methane concentration [11]

## 1.4 Synthesis of diamond

Many reports discuss the different methods used to synthesize diamond [12-19] and have been summarized by Anthony [20].

The several techniques for synthesizing diamond can be divided into two main categories: growth as a stable phase and growth as a metastable phase. The first method is High Pressure High Temperature (HPHT). This technique can be further divided into two processes under which diamond is the equilibrium phase. One process is called the static process, an indirect process, in which graphite is dissolved into liquid metal solvent, and under high pressure, diamond particles precipitate. The other HPHT process is a direct one called the dynamic process, where, by using explosives to reach high pressures and temperatures for a short time, graphite is directly converted to diamond. Under the dynamic process, the duration of the high-pressure high-temperature conditions is very short thus fine diamond particles are the product of this dynamic process. This kind of diamond is mainly used for polishing purposes.

Although people have tried to synthesize diamond for hundreds of years, the first reliable method was developed in 1954. Based on the fact that diamond is 1.56 times as dense as graphite, the logic was that at high pressures diamond is the stable phase of carbon. Most of the commercially produced diamond with the static process, was created using the indirect conversion process, where the metastable graphite is converted into diamond with the presence of a metal catalyst. There are several advantages for using the indirect static process over the direct static process. Pressures and temperatures used for the direct process are about twice those used for the indirect

process (120 Kbar and 2000° C, vs. 60 Kbar and 12000° C). Approximately, 90% of the diamond produced for commercial use is synthesized using the high-pressure, high-temperature, indirect static process using a liquid metal solvent [20].

The static high-pressure process has many advantages, but also some limitations. First, the size of the diamond crystals that can be produced is limited by the size of the growth chambers, which in turn is limited by the high pressures and maximum yield strengths of the materials from which those chambers are made. The second limitation is the fact that some of the liquid from the metal catalyst can be trapped as inclusions inside the diamond, unless the growth process proceeds at a very slow rate, which is not economical. Since those metal inclusions have different thermal expansion coefficient than diamond, they will cause internal stresses to exist inside the diamond and weaken it.

In the second technique for diamond synthesis, first reported in 1960, diamond is a metastable state grown under subatmospheric pressures (low pressures) from hydrocarbon gases in the presence of atomic hydrogen. The importance of atomic hydrogen for this technique will be discussed below.

Since the initial report of low-pressure growth of diamond, many different processes have been studied [21-58]. The main difference between the processes is how the atomic hydrogen is produced and moved around in the specific system [7]. The low-pressure technique initially was only of scientific interest because the growth rate was very slow, and the process required the use of diamond substrates. Eversole initiated these studies by exposing the diamond substrates to a hydrocarbon gas,

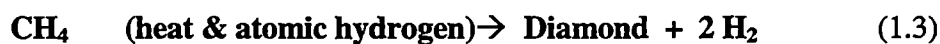


followed by molecular hydrogen, at high temperatures and low pressures [59]. Under these conditions, the hydrocarbon formed diamond and graphite, and the hydrogen then was used to react with the graphite to produce additional methane gas and to remove the graphite. This was a cyclic process that would be repeated until the desired diamond size was achieved. The reactions can be represented as follows:



This is the Chemical Vapor Deposition (CVD) process.

The need for the cyclic role of the reactions was eliminated in the 1970's, when a continuous method was developed. Not only did this newer method increase the growth rates, but it also eliminated the requirement for a diamond substrate. Spitsyn added the atomic hydrogen to the reaction, and that was the key to the new process [60]. This invention made the CVD process very important technologically. The reaction for the new process is shown as follows:



Atomic hydrogen plays a major role in the CVD diamond growth process. It is perhaps the most critical determinant of diamond film quality and growth rate. The carbon is deposited on the surface of the substrate as both  $sp^3$  (diamond) and  $sp^2$  (graphite) material in competition with the simultaneous etching of these materials by atomic and molecular hydrogen. The etching rate of graphite under atomic hydrogen environment is much faster than that of diamond, thus allowing a very low or zero net rate of graphite deposition while having a significant rate of diamond deposition.

The steady state level of atomic hydrogen in the system is a balance between the H atom production rate and the H atom loss rate. In the hot-filament systems, atomic hydrogen is produced heterogeneously by thermal decomposition of the  $H_2$  on the hot filament surface. The atomic hydrogen produced diffuses away from the filament resulting in a concentration gradient that decreases with increasing distance from the filament. Once the hydrocarbon content in the gas reaches a critical value, the H concentration takes a sudden drop [61]. The reason for that according to [62] is that a graphite layer covers the filament when critical hydrocarbon fraction is exceeded, poisoning H production. The loss mechanism for the atomic hydrogen is the homogeneous chemistry and wall recombination. For typical diamond CVD conditions, this is a slow process, and the H atoms are able to diffuse to the walls or to the substrate before recombining in the gas.

The low-pressure high temperature growth technique can be divided into three commonly used methods:

- a) Hot Filament CVD (HFCVD).

b) Hot Filament Electron-assisted CVD (EACVD).

c) Plasma CVD.

**a) Hot Filament CVD:**

The HFCVD apparatus typically consists of a hot filament, a heater block on which the substrate sits, a quartz tube in which the reactions take place, and a gas source to deliver hydrogen and methane gases. The hot filament is heated to temperatures in the range of 1950° C - 2300° C. The molecular hydrogen mixed with about 1-2% hydrocarbon, such as methane, flows through the quartz tube. The hydrogen then is adsorbed on the filament surface and dissociates into two hydrogen atoms that desorb back into the surrounding gas.



Hot Filament Material and Carburization:

Anthony summarizes the limitations to the material that can be used for the hot filament [20]. The material must be an electrically conductive refractory material; the material must have a melting point above the temperature at which the filament will operate. The operating temperature must be high enough to produce atomic hydrogen, and the filament must be able to resist any damage that might be caused by the H<sub>2</sub> at that temperature [63]. In order to prevent the melting and breakage of the filament, the

binary eutectic temperature of carbon and the filament material must be higher than the operating temperature. For a list of the various materials used for filament applications and their relative parameters see Table 1.4 [20]. Molybdenum is eliminated since a hot spot may form on the molybdenum filament and it may be higher than the Mo-C eutectic temperature of 2200° C, and thus cause the filament to fail by melting before it is fully carburized.

Although a carbon filament meets all the requirements mentioned above, its use does not produce CVD diamond. The reason is that any atomic hydrogen that forms on a carbon filament reacts with the carbon and releases hydrocarbons into the surrounding gas instead of atomic hydrogen. Unless there is atomic hydrogen on the substrate, graphite rather than diamond will be deposited. Such an observation suggests that the atomic hydrogen forms on the filament surface itself and reacts with the filament material and does not form in the gas surrounding it.

Tungsten, tantalum and rhenium have been used for the production of CVD diamond. Both tantalum and tungsten react with hydrocarbon in the gas to form carbides, so, in reality, the tungsten and tantalum filaments are tungsten carbide, and tantalum carbide filaments. From the point of view of the diamond growth rate, the two materials seem to produce similar results, although the tungsten carbide is a commonly used catalyst material in gaseous hydrocarbon chemistry.

The filament is usually carburized before the CVD growth process takes place. The carburization process occurs in two steps. The first step is the formation of  $M_2C$ , and the second is the formation of  $MC$  where  $M$  is one of the refractory metals.  $M_2C$

**Table 1.4: Filaments for Diamond Synthesis**

Material	Melting Point	Evaporation Rate	Carbon Eutectic Point
	°C	grams/cm <sup>2</sup> - sec	°C
Tungsten	3387	10 <sup>-9</sup>	2475
Carbon	3727	6 X 10 <sup>-8</sup>	3727
Rhenium	3180	7 X 10 <sup>-5</sup>	2486
Tantalum	2996	10 <sup>-8</sup>	2800
Molybdenum	2610	4 X 10 <sup>-7</sup>	2200
Niobium	2468	8 X 10 <sup>-9</sup>	2335

forms in all cases under typical CVD growth conditions, while MC does not always form due to the small activity coefficient of carbon under some conditions of CVD. As the inward radial carburization takes place, the filaments tend to crack, bend, swell, distort and embrittle, since the molar volume of the carbide is 40-70% larger than the metal. Since the grain boundary is the most effective region for the migration of carbon, the filament tends to crack along the grain boundaries. The carburization and cracking increase the resistance of the filament, and in order to maintain a constant temperature on the filament, the current and voltage must be monitored and changed accordingly.

Rhenium does not form carbides thus might be very attractive as a filament material. The drawback for rhenium is that it dissolves large quantity of carbon, causing rhenium to swell. Also, dissolved carbon can react with dissolved oxygen forming embrittling voids on grain boundaries. These voids and the dissolved carbon both cause the swelling of the filament. The ductility in the wire, which is due to the fine grain structure, decreases due to annealing which causes grain growth to very large grain sizes. In spite of the fact that the carburized rhenium wire is partially embrittled, its still much less so than tungsten or tantalum. Economically, the rhenium is not very attractive since it is two orders of magnitude more expensive than tantalum or tungsten.

#### **b) Hot Filament EACVD:**

The EACVD stands for electron-assisted chemical vapor deposition. The name is a result of adding a positive or negative electrical potential (bias) between the filament and the substrate. The effect of the EACVD on the nucleation and growth does

not seem to be very obvious [20]. If we take a normal CVD system, the filament usually has zero potential at one end, and some applied potential at the other end. The substrate is usually at zero potential, and thus it has a potential difference with every point on the filament except for the one end that is also at zero potential. Thus, if the effect of the bias between the substrate and the filament plays a significant role on nucleation and growth results, one would expect to see a difference in such results across the entire substrate in the direction that is parallel to the filament. The fact that no one has reported such observations in literature seems to suggest that EACVD effects are not significant at least at the potentials involved in the filament power supplies.

When the filament is negatively biased relative to the substrate, there is generally an increase in the nucleation and growth rates. On the other hand, if the filament is positively biased relative to the substrate, the nucleation and growth rates seem to decrease, while the quality of the deposited diamond crystals seems to increase. In either case the bias potential should not exceed the value of the breakdown point of the gases, since these favorable effects seem to cease with the formation of the plasma. Researchers heated their filaments differently. Some used AC and some used DC to heat their filament, and that created some confusion in the results of this process.

### **c) Plasmas**

The use of gas plasmas is a popular method to generate atomic hydrogen. There is a difference between the kinetic energy of the atomic hydrogen produced by this method and that produced by the hot filament methods. In the thermal methods, the

atomic hydrogen generated has a low kinetic energy since the hydrogen molecule is broken apart as a direct transfer of thermal energy, without the use of any excess energy that might be converted to kinetic energy for the hydrogen atom. In plasmas, the gas is typically ionized by forming a balanced mixture of electrons, negative ions, and positive ions, which are formed by exposing the gas to high temperatures or high electric fields. If the plasma is exposed to a high AC electric field, then the hydrogen dissociation is due to collisions with electrons. The dissociation energy of hydrogen is 4.5 eV, but electrons of energy above 9.5 eV are required for hydrogen dissociation by electron impact. The reason for the higher energy requirement comes from the mass difference between an electron and a hydrogen molecule. The strongest dissociation comes with electron energies of about 25 eV.

Typically, the charge density in plasma is low. Most of the molecules do not decompose into atoms or radicals and probably do not play a role in the diamond deposition. About 1% of the molecules in the plasma are converted into neutral radicals that are chemically active and those seem to play the main role in the CVD deposition of diamond. There are also about 0.01% of the molecules in plasma that are ions. These ions are also chemically active and they can take a part in the deposition of diamond, but the fact that their concentration is so small implies that they are not very important in the process of CVD diamond deposition. In spite of the low concentration of these ions, they might still have some effects during the CVD process.

There are two categories under which all the plasma deposition processes fall; low-pressure and high-pressure. The electrons and the molecules in a low-pressure gas



excited by an electric field will not be at thermal equilibrium with each other. In RF and microwave plasmas the electrons will gain much more energy, from the applied electric field than will the molecules, because it is easier to accelerate the light electrons compared to the heavier ions. In low-pressure plasma the mean free path for collisions between electrons and molecules is relatively large, so the electrons will attain and retain high energy leaving the molecules with slow motion. As a result, the low-pressure plasma ions will usually have a low temperature, and any generation of atomic hydrogen and reactive molecular radicals, will be a result of colliding with high-energy electrons. Since the electrons are spread across the plasma, and the mean free path is large, the absolute concentration of atomic hydrogen and molecular radicals will be low.

High-pressure plasmas have a short mean free path for the collisions between electrons and molecules. Before the electron can accelerate and gain much energy from the applied electric field, it will collide with and lose some of its energy to a more massive molecule. As a result the overall temperature of the molecules and the electrons will be more nearly the same, and the generation of atomic hydrogen and molecular radicals can be caused by a collision with an electron or a molecule. The atomic hydrogen concentration may be higher in the high-pressure plasma. As a direct consequence, the CVD diamond growth rate can be much higher in high-pressure plasma compared to low-pressure plasma. This has been confirmed experimentally where, high-pressure plasma may produce a growth rate of about 500  $\mu\text{m}/\text{hour}$  [20], while low pressure plasma would have a typical growth rate of about 1.0  $\mu\text{m}/\text{hour}$ .

It would seem that low pressure plasma methods are less interesting when growth rates are compared to the high pressure plasma methods. Other factors make the low pressure methods desirable. The high pressure plasmas have a very high energy content, and the substrates must be cooled to prevent melting. High pressure plasmas are more difficult to control than low pressure ones. So depending on the application at hand, one might prefer either of the plasma categories.

In the low pressure category we have the following methods:

- 1) Glow Discharge
- 2) Microwave Discharge
- 3) RF Discharge

In the high pressure category we have the following methods:

- 4) DC Discharge
- 5) Microwave Discharge jets
- 6) RF Discharge

These methods will be discussed in the listed order.

### **1. Low-Pressure Glow Discharge**

A stream of low pressure molecular hydrogen is passed through a glow discharge between two metal electrodes. Using pressures between 0.1 and 20 torr, produces atomic hydrogen in concentrations up to 25%. In order to generate the atomic hydrogen close to the substrate, either the substrate is placed in the glow discharge or

one of the electrodes will act as the substrate. As mentioned earlier in describing the hot filament method, the growth rates of diamonds are higher when the filament is at a negative bias. Although AC or DC can be used to form the discharge, the DC method has an advantage if one of the electrodes acts as the substrate. Some of the disadvantages of this process are the limited range of pressure that can be used, the erosion of the electrodes, the contamination from the electrodes, and the high stress and hydrogen content in the grown diamond films.

## **2. Low-Pressure Microwave Discharge**

Like glow discharge, this method generates up to 25% atomic hydrogen under typical CVD diamond growth conditions. Low pressure microwave discharge is the most common method to provide atomic hydrogen for CVD diamond growth. In this technique the problem of electrode erosion does not exist because the discharges have no electrodes. Also, because of the high number of production sources for microwave ovens, the microwave sources can be very economical. Microwave plasma deposition technique has been reported to achieve deposition with the lowest temperatures (365-500° C). The addition of the oxygen species allows, among other effects, a decrease in the gas pressure, which in turn is very important, because it will allow the plasma to be distributed more uniformly over a wider area, thus giving a more uniform deposit. The plasma must not touch the walls of the chamber because diamond can deposit on the walls. The deposited diamond can couple with the microwaves and heat up the walls and result in more deposition, and that can gradually make the walls (usually quartz) opaque to microwaves. Another problem that arises under different working conditions,

is the erosion of the chamber walls due to the atomic hydrogen reduction of the quartz. The above problems can be avoided by confining the plasma magnetically.

### **3. Low-Pressure RF Discharge.**

This method is not as commonly used as the microwave discharge method for CVD diamond growth. As mentioned before, there is a direct correlation between the growth rate of CVD diamond and the generation of atomic hydrogen and hydrogen radicals. The microwave plasma is a more efficient method for the generation of such radicals than the RF plasma. The reason is probably the fact that electrons have a higher density and higher energy in the microwave plasma [20]. Nevertheless, RF discharge can produce between 10 to 65% atomic hydrogen concentrations depending on the pressure, and it has been used to grow CVD diamond. Similar problems to the ones in the microwave plasma also exist in the RF plasma, but in addition, the RF can electromagnetically couple with a conductive body and heat up the chamber. Usually, diamond grown by the RF plasma technique has poorer quality than diamond grown by the microwave plasma technique.

### **4. High-Pressure DC Discharge**

This technique has been used to grow good quality diamond at very fast rates, up to 200  $\mu\text{m}/\text{hour}$ , and thickness greater than 1 mm. Even though these DC discharges are very stable, they still have a few disadvantages. First, the substrate must be cooled so that it won't melt from the high power density applied during the growth process. Second, the power consumption is very high, the electrodes are likely to erode, and the discharge is not uniform, plus the deposition area is usually small.

## **5. High-Pressure Microwave Discharge Jets.**

Good quality diamond at a fairly high rate of 30  $\mu\text{m}/\text{hour}$  has been grown at atmospheric pressure and over a square inch of area, using this method. A gas mixture of Ar-H<sub>2</sub>-CH<sub>4</sub> is used with a CH<sub>4</sub>/H<sub>2</sub> ratio up to 10%. An electric breakdown around the central electrode gives the plasma its initial ignition. Then the plasma is sustained by microwave energy applied between the walls of the chamber and the central electrode. The plasma is very unstable and the substrate must be cooled vigorously and that makes sustaining the plasma very difficult. One disadvantage of the high pressure microwave discharge, compared with the low pressure microwave discharge, is that it uses electrodes, which can erode, while the low pressure microwave plasma is electrodeless.

## **6. High-Pressure RF Discharge**

High pressure radio frequency discharges are very unstable and addition of argon to the hydrogen-hydrocarbon mixture is needed to increase the stability of the discharge. The discharge is typically run for a short time, and must be monitored continuously. CVD diamond can be grown at high rates during these short times. Like other high pressure discharges, the substrate must be cooled due to the high power consumption.

## **High and Low-Pressure Flames**

Using an oxygen flame, such as the one in a plumber's torch at atmospheric pressures, hydrogen or hydrocarbons can be burned to produce atomic hydrogen. Hirose [28] discovered that CVD diamond could be grown, just downstream from the flame front. The substrate is placed in the feather of the flame where the high temperatures (2800-3400°C) cause plasma to form, and atomic hydrogen can be produced in large quantities due to the fuel rich conditions under which these flames are operated. The carbon to diamond conversion rate with this inexpensive method is very low, and the substrate has to be vigorously cooled due to the large heat input rate of the flame.

### **1.5 Ion Implantation – Introduction:**

There have been many reports on the importance of surface features of the substrate and the role they play in the nucleation of diamond. For this reason, it was the goal of this research to modify the structure of the surface and study the effects of such modifications on the nucleation and growth of CVD diamond. A widespread method to modify the surface structure, especially of semiconductors, is ion implantation.

Ion Implantation is a process in which an energetic beam of ions is injected into a substrate material. The goal of ion implantation is to modify a solid via addition of the ion [64]. There are four basic processes that are a direct result of such ion bombardment, see Figure 1.3 [64]. As illustrated in Figure 1.3, a single ion impinging onto a substrate with KeV energy will have several collisions along its trajectory with both target atoms (nuclear collisions) and electrons (electronic collisions). Thus, it will

lose its energy in several collisions until it finally comes to rest at some hundreds of atom layers depth into the substrate. When a beam of mono-energetic ions are implanted into the substrate, the ion depth distribution will follow approximately a Gaussian distribution. Such a distribution is due to the statistical nature of such nuclear and electronic energy-loss collisions. The peak of such a Gaussian distribution will correspond to the most projected ion range. The density of implanted atoms and irradiation-produced defects is a function of the dose of the incident ions i.e. the concentration of implanted atoms will increase with increasing ion dose. Figure 1.3 also depicts the damage cause by the collisions [64]. In such radiation the lattice atoms are displaced from their regular sites, and a single heavy ion can result in the displacement of many hundreds of lattice atoms within a volume surrounding the ion trajectory.

Most of the ion energy is deposited in elastic displacement collisions with the shielded atomic nuclei and electronic excitations of the atomic electrons, while some is deposited into inelastic ionizing collisions. In metals, semiconductors and some insulators, it is the nuclear stopping (elastic collisions) which results in the displacement of atoms. The electronic excitations are also a mechanism for energy-loss, to slow the ion down.

There are three stages that describe the phenomena associated with ion implantation [66-69].

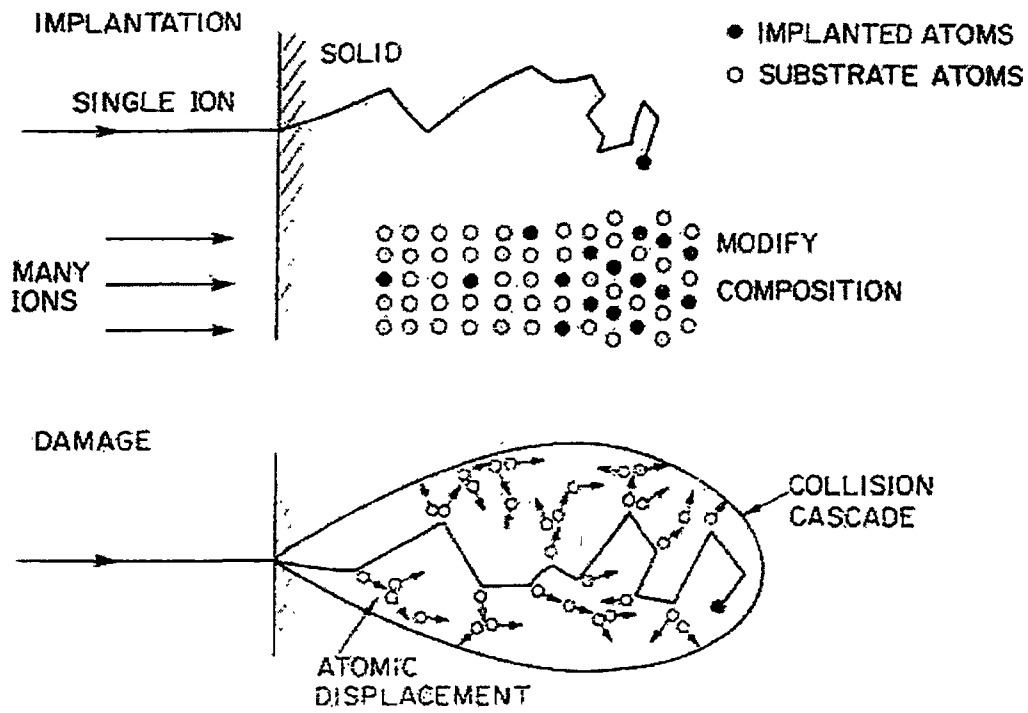


Figure 1.3: Schematic of the implantation and damage processes using energetic ion beams.[65]



Stage 1 (prompt stage): Part of the kinetic energy of the incoming ion is transferred to the target atoms in the solid through primary collisions. The target atoms that gain the energy recoil and lose some of their energy to other atoms through secondary collisions, thus evolving higher generations of collisions. The atoms colliding in a later generation produce low energy recoils that produce small displacements in almost random directions. Such a process is called a collision cascade, and the lifetime of such a cascade is about  $10^{-13}$  to  $10^{-11}$  s.

Stage 2 (thermal spike stage): Towards the end of the cascade the idea of temperature is re-established because the velocity of the atoms in motion assumes a Boltzmann distribution. During this stage, the atoms involved in a collision cascade lose their kinetic energy through both lattice and electron conduction. The lifetime of this stage is  $10^{-11}$  to  $10^{-10}$  s.

Stage 3 (relaxation stage): The solid assumes a uniform temperature. At this ambient temperature, processes, such as thermally activated motion of previously generated defects can continue for periods of time exceeding  $10^{-9}$  s.

Computer simulations have supported the existence of stages 1 and 2 [67-69], but problems associated with following the processes from the time of ion impact to the time of uniform temperature establishment, limit these simulations. Such a task requires monitoring both long and short lifetime processes, and that is expensive and time consuming with today's computer technology. Computer simulations cannot solely determine which of the three stages dominates under certain experimental parameters.

Two criteria have been used for the onset of amorphization in covalently bonded materials such as silicon and diamond. Morehead and Crowder [70] developed a model that predicts the collapse of the crystal lattice into the disordered (amorphous) state at a critical vacancy concentration; about 10% for silicon. The other criterion is based on experimental observations that an observable amount of the amorphous phase appears at a critical damage energy density. This latter criterion was used in the current study.

The critical energy density for amorphization of silicon has been reported to be about  $10^{24}$  eV/cm<sup>3</sup> [71,72]. Values of  $4.56 \times 10^{24}$  eV/cm<sup>3</sup> for implantation at 300 K and  $2.1 \times 10^{24}$  eV/cm<sup>3</sup> (42 eV/atom) at 77 K were reported by Washburn *et al.* [73]. The value of  $2.1 \times 10^{24}$  eV/cm<sup>3</sup> (42 eV/atom) was used in this study since the implantation was performed with a substrate temperature of 77 K.

The critical energy density for amorphization of single crystal diamond has been reported to be 5.5 eV/atom by several groups [74-76], and was used in this study.

## CHAPTER 2

### LITERATURE REVIEW OF NUCLEATION OF CVD DIAMOND

In this chapter, a general introduction to nucleation and growth will be followed by a discussion of the various views proposed for diamond nucleation from hydrocarbon-hydrogen vapor phase. This section will include a literature review of prior studies of surface modification effects.

#### 2.1 Nucleation Mechanisms:

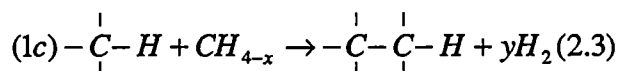
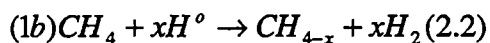
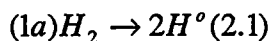
In a sense diamond deposition during the CVD process involves heterogeneous nucleation since the chemical reactions produce a new phase on a free surface rather than homogeneous nucleation which would result in clusters of diamond forming in the gas phase. In the CVD process for depositing diamond at least three nucleation process have been proposed [77]:

- A. **“Homogeneous”** nucleation on a non-reacting surface;
- B. **“Homogeneous-heterogeneous”** nucleation on a reactive surface in which an intermediate phase is first formed and the diamond nucleates on that intermediate phase; and
- C. **Heterogeneous** nucleation on surface defects and/or impurities.

#### A. “Homogeneous Nucleation”:

A critical factor in diamond nucleation is the attainment of sufficient carbon in the correct atomic configuration (diamond-cubic) of sufficient size to be stable. Thus, the formation of diamond nucleation from the interaction of the reactant gas with a non-reacting surface resembles classical homogeneous nucleation. Lux and Haubner [77] have summarized the nucleation and growth of diamond in this case by Figure 2.1. In this model, there is no carbon diffusion into the substrate and the critical size of diamond nucleus is reached by surface diffusion of the gaseous species that "stick" to the surface during the random encounters with it.

For CVD diamond deposition the reactant gas is composed of hydrocarbon radicals ( $CH_x$ ) and atomic ( $H^\circ$ ) and molecular ( $H_2$ ) hydrogen. The chemical reactions are:



As shown schematically in Figure 2.1, some atomic hydrogen ( $H^\circ$ ) and hydrocarbon radicals ( $CH_x$ ) stick to the substrate surface and by surface diffusion migrate to form clusters. The continued reaction with the activated gas, removes the hydrogen as  $H_2$  and some of the  $CH_x$  combines with  $H^\circ$  to form  $CH_4$  which goes back into the gas. A carbon-rich radical  $\begin{array}{c} | \\ -C- \\ | \end{array} \begin{array}{c} | \\ -C- \\ | \end{array} - H$  is left on the surface. If this cluster reaches a critical size with the correct atomic configuration (diamond-cubic), the nucleus can continue to grow as diamond.

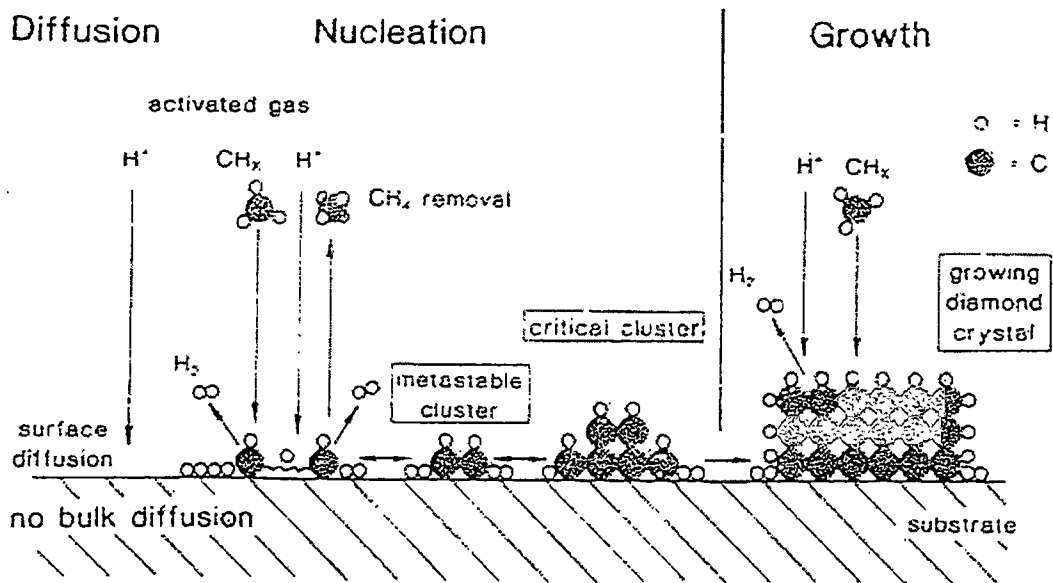


Figure 2.1: Nucleation and growth kinetics of low-pressure diamond deposition on a non-reacting surface.

Since there is a competition between the deposition and dissolution of carbon, the overall kinetics must favor the deposition in order for diamond growth to occur.

The critical size for a diamond nucleus formed in such a manner has been estimated to be about 3 nm [78]. However, the nucleation rate may be extremely slow because of limitations due to (a) the sticking-factor for gases impinging on a defect-free, clean surface; (b) surface diffusion; (c) dissolution of the metastable clusters by the reactant gases (e.g.,  $C_{\text{solid}} + 4H^{\circ} \rightarrow CH_4$ ). It has been observed that very long incubation periods (days or weeks) are required for diamond deposition on clean, highly polished silicon single crystals [77].

### **B. Homogeneous-Heterogeneous Nucleation After Intermediate Phase Formation**

The observation that incubation times vary by orders of magnitude for different substrate materials suggests that chemical reactions between the gases and substrate play an important role in the nucleation process. This has led to the postulate that the first step for diamond nucleation on carbide-forming elements is the formation of a carbide phase. For example, Williams and co-workers [79,80] claim that SiC must form on the surface of Si before diamond nucleation can occur. On the other hand, Abraham [81] found that diamond nucleation was a rare event on pure, highly polished SiC single crystals.

The reactions in a CVD process may be dominated either by atomic and molecular hydrogen or by carbon/substrate reactions.

### B.1 Reactions involving hydrogen

The gases may react with compound substrate materials in two competing ways: carbon deposition and hydrogen reduction of the substrate. Schematic representations of reactions for  $\text{SiO}_2$  and  $\text{SiC}$  given in Figure 2.2 indicate the competition between the reactions. In the case of the  $\text{SiO}_2$ , the  $\text{SiO}_2$  will react with the incoming  $\text{CH}_4$  and  $\text{H}_2$  to form  $\text{SiH}_4$ ,  $\text{H}_2\text{O}$  and  $\text{CO}$  in gaseous form without any carbon deposition. In the  $\text{SiC}$  case, the  $\text{Si}$  reacts with the  $\text{CH}_4$  and  $\text{H}_2$  to form the  $\text{SiH}_4$  gas leaving a carbon rich phase on the surface.

### B.2 Carbon/Substrate Reactions

Since a critical carbon concentration must be achieved in a local area, any process that reduces the local carbon concentration can decrease the rate of nucleation. Such processes include solution of carbon in the substrate material and the subsequent diffusion into the bulk, and compound (carbide) formation. Metals, alloys and pure elements can be categorized as:

- a. Little or no solubility or reaction: Cu, Ag, Au, Sn, Pb
- b. Solution of carbon and diffusion: Pt, Pd, Rh
- c. Carbide formation:
  - Metallic-bonded elements: Ti, Zr, Hf, V, Nb, Ta, Cr, Mo, W, Fe, Co, Ni
  - Covalent-bonded elements: B, Si
  - Ionic-bonded elements: Al, Y, rare earth metals.

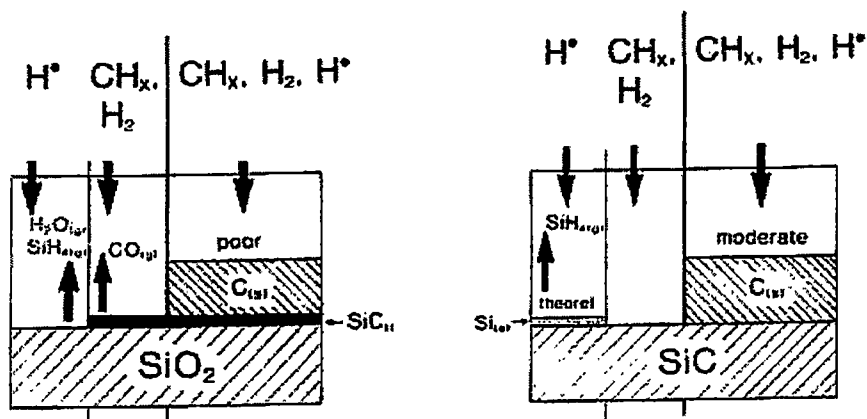


Figure 2.2: Chemical interactions between different substrates and the gas phase containing CH<sub>x</sub>, H<sub>2</sub>, H<sup>•</sup> [77].



Nucleation on pure, smooth substrates that have little or no solubility or reaction should proceed by the "homogeneous" process described above (section A). In the second category, the relative rates of carbon arrival at the surface and the diffusion of carbon from the surface into the substrate will determine the length of the incubation period for nucleation.

A model for nucleation on carbide-forming substrate was proposed by Lux and Haubner [77] and is schematically illustrated in Figure 2.3. Initially, carbon forms an interstitial solid solution in the near-surface region and diffuses into the substrate. Potential nuclei with sizes below the critical size may dissociate either by reaction with the gases or by the carbon being drained from the surface by rapid diffusion into the substrate. At some point the carbon concentration in the near-surface region reaches that necessary for compound formation. The compound may "lock up" the carbon at the surface and promote nucleation.

A continuous carbide film is formed by the lateral growth of the carbide particles. Thus, at an early stage, there are particles of carbides embedded in a metal-carbon solid solution, which then extend laterally to form a continuous film.

The effectiveness of the carbide particles in promoting nucleation depends on the rate of carbon diffusion through the carbide. The diffusion coefficient for carbon in refractory metals varies (high to low) in the following order: Cr, Ti, Mo, Nb, Hf, W, Ta [82].

The diffusion of carbon into the substrate continues to affect diamond nucleation and growth. The carbon concentration at the diamond-substrate interface is 100%. If

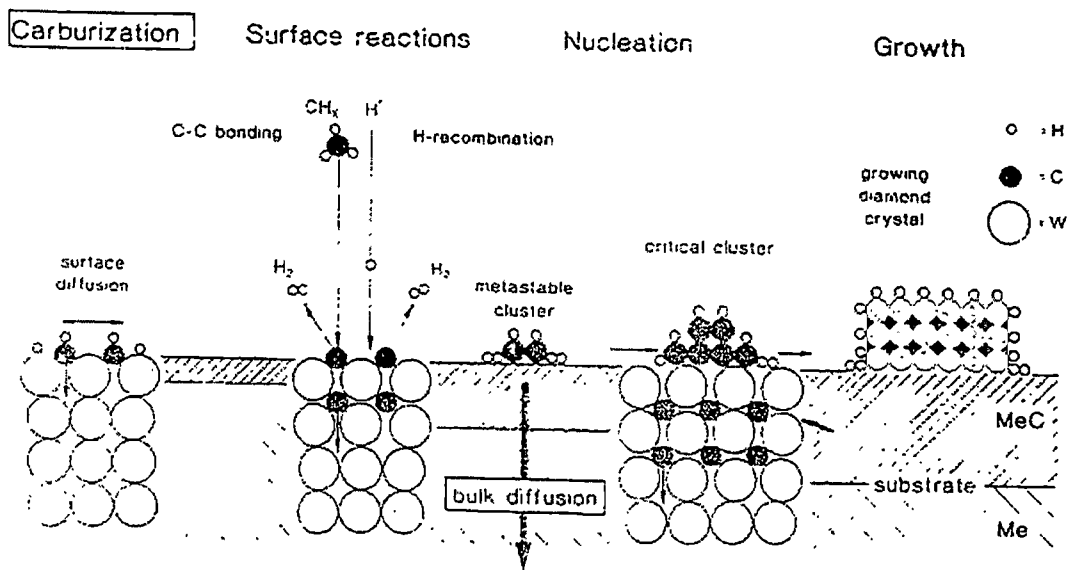


Figure 2.3: Nucleation and growth kinetics during low-pressure diamond deposition on a carbide-forming substrate surface.

the solubility of carbon in the substrate is high and the diffusion rate is high, dissolution of the diamond nuclei by the substrate may occur.

The nucleation of diamond by the carbide particles is heterogeneous as schematically described by Figure 2.4. After the hydrogen/hydrocarbon gases interact with the metal substrate, a metal-carbon solid solution is formed. Then, some metal-carbides form on the substrate on which diamond nuclei might form and grow.

### **C. Heterogeneous Nucleation on Surface Defects and Impurities**

Using the hot filament chemical vapor deposition process, the nucleation density of diamond on a polished surface of an untreated substrate is very low. For example, using an untreated silicon substrate the nucleation density, using 0.5% methane concentration and substrate temperature of 750<sup>o</sup> C, was found to be about 10<sup>4</sup> cm<sup>-2</sup> [83]. As a consequence of such low nucleation densities, it is difficult to achieve a continuous diamond film within a reasonable time, since the deposition rate is slow (about 1 μm per hour) in the HFCVD method. There are several ways a substrate can be treated prior to the deposition process that have been observed to increase the nucleation density. Based on experimental observations on treated substrates, several hypotheses for heterogeneous heteroepitaxial diamond nucleation have been made. One of the most widely used methods to enhance diamond nucleation density is the scratching of the substrate.

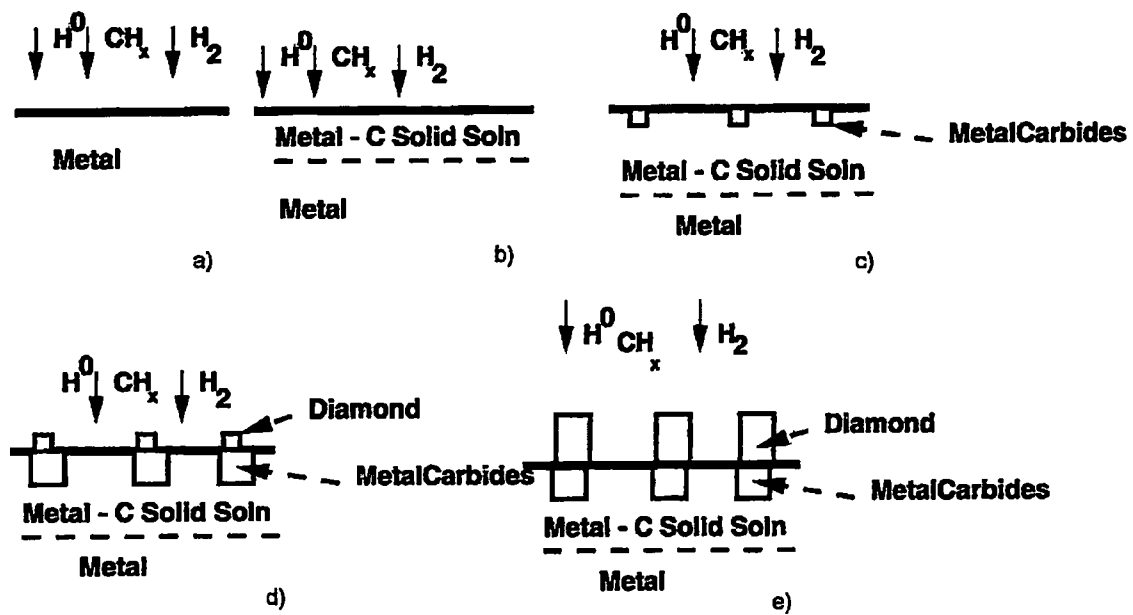


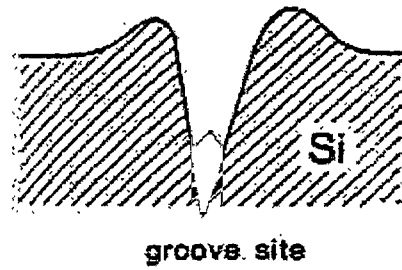
Figure 2.4: A schematic showing nucleation by the carbide particles being heterogeneous.

### Scratching the substrate:

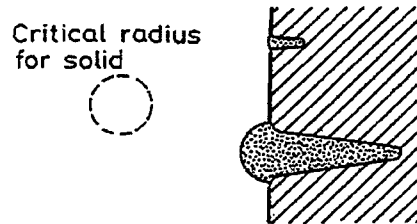
Nucleation on highly polished, defect-free, pure single crystal wafers of silicon, is very slow. Early in the study of CVD synthesis of diamond it was found that scratching or roughening of the silicon surface with a variety of abrasive methods increased the nucleation rate by orders of magnitude [84-87]. Scratching or polishing with diamond grits or by other hard particles such as SiC, B<sub>4</sub>C, B-N, Al<sub>2</sub>O<sub>3</sub>, etc [51,78,88-91], is effective in enhancing nucleation. Observations by scanning electron microscopy (SEM) sometimes suggest that the sharp edges of scratches act as nucleation sites [92,93], whereas, other studies concluded that nucleation occurs at the bottom of scratches [78].

Arguments to support nucleation at the bottom of scratches are analogous to nucleation of a pure solid from its liquid in the crevices and pores of a mold [94]. A schematic drawing showing this condition is given in Figure 2.5 a and b. In the figure, the upper nucleus cannot grow out of the crack cause it did not achieve the critical radius while the lower one can.

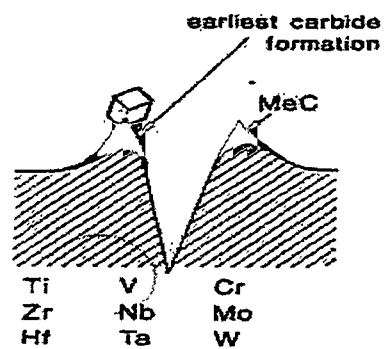
Other nucleation sites that have been proposed are the prominent features of a substrate surface. Those can be surface morphologies that protrude with sharp edges or points, instead of valleys or flats. Such features can be the result of scratching the substrate using the diamond slurry in an ultra sonic bath process. Observations of selected growth on prominent features of chemically etched surfaces have been made by Dennig and Stevenson [95,96]. Yugo *et. al.* [97] in their studies on diamond growth using plasma CVD, investigated the correlation between the shape of the scratches and



a)



b)



c)

Figure 2.5: Different mechanisms for diamond nucleation on scratches.

generation of nuclei. Using STM images to compare between untreated mirror polished silicon substrate, and ultrasonically treated silicon surface, they concluded that scratches with depth of about 10 nm acted as effective nucleation sites, while randomly using distributed small scratches with depth less than 5 nm suppressed the generation of nuclei.

Researchers who claim sharp corners act as nucleation sites argue that these locations are the preferred sites for forming metal carbides which then nucleate the diamond growth, see Figure 2.5 part c. The reasoning for such claim is that at a sharp corner carbon can diffuse from all directions (sides and top) into the substrate and saturate much faster than diffusion into a flat surface from the top only( $\rightarrow\wedge\leftarrow$ ).

Williams *et al.* Proposed that these sharp corners promoted the formation of SiC on silicon substrates and that this is a necessary first step to nucleation of diamond [79].

Despite the extensive TEM work that has been done, there is no proof that the enhancement of the nucleation density is due solely to the high surface-defect density.

A third view is that diamond debris or other carbonaceous material is collected in the scratches and act as pre-existing nuclei or carbon sources for easy nucleation [98-101]. During the bombardment of the diamond particles onto the substrate surface, small pieces of those particles could break off and attach to the surface as diamond or maybe as an ill-defined carbonaceous residue. Bachmann *et al.* [51] postulated that the nucleation sites were the residual diamond particles left on the surface from the scratching medium. This is based on the fact that diamond will prefer to nucleate on diamond seeds rather than any other nucleation site, thus resulting in homoepitaxy of

diamond. A direct observation of diamond nucleating on diamond nucleation sites was made by Iijima, Aikawa, and Baba [102,103], using high resolution transmission electron microscopy (HRTEM). However, there are other reports of high nucleation densities using abrasives other than diamond, such as cubic boron nitride (cBN), silicon carbide, and stainless steel [104-106].

Chakk *et al.* [99] report that for silicon surfaces treated with diamond, c-BN, and SiC slurries, the diamond CVD nucleation and growth takes place on the debris left on the surface during the abrasion process which, when damaged by ion irradiation at appropriate energies and doses, results in the suppression of diamond growth. Anger *et al.* [83] report that ultrasonic treatments of silicon wafers with various abrasive powders in different liquid phases lead to a mechanical alteration of the surface and to a chemical dissociation of both the hard particles and the liquid medium. They claim that the shock, friction, and cavitation induce very localized high increases of both the temperature and the pressure, which lead to the formation of SiC interface, in the presence of carbon-containing powder liquid. As a result of such treatments, very stressed and highly defective substrate surfaces and  $sp^2$  amorphous carbon phases are produced. According to Anger *et al.* there are three kinds of nucleation sites produced by varying the composition of both the powder and the liquid. Physical nucleation sites had a negligible effect compared to the chemical sites. Chemical nucleation sites composed of amorphous carbon phases and SiC, deposited in the defective regions, allow a significant improvement of the nucleation density. However, the very high



diamond crystal density obtained with the diamond powder is attributed to the diamond fragments embedded prior to the diamond deposition stage.

In principle, careful experiments using a variety of polishing compounds on the same substrate material should allow one to determine the relative importance of the various proposals. It is apparent that polishing with diamond grit provides the fastest nucleation but there may also be enhancement after polishing with other abrasives.

### Ion Bombardment Effects

There have been a number of studies that show that ion bombardment of substrate surfaces influence the subsequent nucleation and growth of CVD diamond [81,99,107-110]. As a result of these studies, four possible mechanisms were proposed to explain the suppression of nucleation by ion bombardment:

- 1) The amorphization of the diamond debris left from polishing.
- 2) The graphitization of diamond by the ion beam due to ion beam heating and/or displacements.
- 3) The amorphization of the substrate.
- 4) The smoothing of the surface due to amorphization or to sputtering by the bombarding ion beam.

The results of Abraham et al. [81] show that point defects created in the near-surface region of SiC substrates do not affect the nucleation rate. Implanted carbon ions also did not affect the nucleation. The latter observation suggests that a carbonaceous

particle must be larger than atomic dimensions in order to be an effective nucleating site.

One effect of ion implantation or ion bombardment of a solid is the displacement of lattice atoms from their normal lattice sites; creating a vacancy and an interstitial. Some of the interstitials (displaced atoms) recombine with nearby vacancies but some survive the “cooldown” stage and are trapped in the lattice. The usual model for calculating the number of displaced atoms (and thus vacancies) is that of Kinchin and Pease [65]. The number of displaced atoms,  $N(E)$ , due to deposited energy,  $E$ , is

$$N(E) = E/(2E_d) \quad (2.4)$$

Where  $E_d$  is the energy required to displace an atom from its lattice site. The factor of 2 is necessary in order for the bombarding ion (atom) to also escape the affected lattice site.

Values of  $E_d$  for metals are generally in the range of 20–40 eV [111]. For silicon the value of  $E_d$  is in the range of 10-30 eV [65], but compounds and tightly bound materials have higher values. In this study, a value of 20 eV was used for silicon and 80 eV was used for diamond [112] for calculations of lattice damage using the TRIM [113] code.

One output of TRIM calculations is the number of vacancies created for incident ion as a function of distance from the impacted surface. Using the value for number of

vacancies per ion, ion fluence and  $2 E_d$ , the deposited damage energy was calculated as a function of depth.

## CHAPTER 3

### CHARACTERIZATION TECHNIQUES

This section includes a brief explanation of the techniques used to characterize the results of each substrate used in this work.

#### **3.1 Scanning Electron Microscopy (SEM):**

In a scanning electron microscope, a small beam of electrons raster scans the specimen surface. Simultaneously, a square raster is traced out in synchronism on a cathode-ray tube (CRT) [114]. The incident electron beam causes low-energy electrons to be ejected from the surface of the specimen surface. The intensity of the ejected electrons depends on the angle between the incoming beam and the surface of the specimen at the specific raster. The number of electrons ejected from the specimen determines the intensity of the beam on the CRT. This results in an image of the topography of the specimen surface to be built up on the CRT as the raster is traced out.

The size of the electron beam incident on the specimen surface determines the resolution of the SEM. The minimum features that can be resolved are roughly the same as the beam. Thus, the smaller the size of the beam the smaller the features that can be resolved by the SEM

Another use of the SEM is to determine the crystallographic orientation of small surface areas. One can move the crossover point (where the beam crosses the column axis) to the specimen surface, by adjusting the scan coil current and lens. In this manner

the beam rocks about a fixed point on the specimen as illustrated in Figure 3.1. For planes (hkl) that are parallel or close to parallel to the beam axis, the beam will hit the specimen surface at the Bragg angle on each side of the column axis as shown in Figure 3.1. As this occurs, and due to a diffraction-related effect, the intensity of the ejected electrons changes. Consequently, the change at the two Bragg angles produces a band on the CRT. In this process, each (hkl) set that has the required Bragg angle will produce a band that is centered on the trace of the (hkl) plane on the image. Furthermore, the bandwidth is dependent on the Bragg angle. The change in the intensity of the ejected electrons that occurs at the Bragg angle, is similar to some channeling effects, and these patterns are called channeling patterns. This method is a quick way to determine whether a specimen has a crystalline surface or not.

### **3.2 Energy Dispersive Spectrometry (EDS):**

EDS is a technique by which one can determine the composition of a certain material. A detector is mounted inside the SEM chamber to collect characteristic x-rays produced by the electron bombardment of the sample. A spectrum of x-rays corresponding to each element in the material under study is produced and analyzed. Briefly, the principle behind EDS is that an x-ray photon is absorbed by an atom in the detector (Si or Ge) with emission of an energetic electron (photoelectron) which scatters inelastically, creating electron-hole pairs proportional in number to the photon energy. A bias across the detector separates the electrons and holes. An external circuit with a field effect transistor amplifier measures the charge.

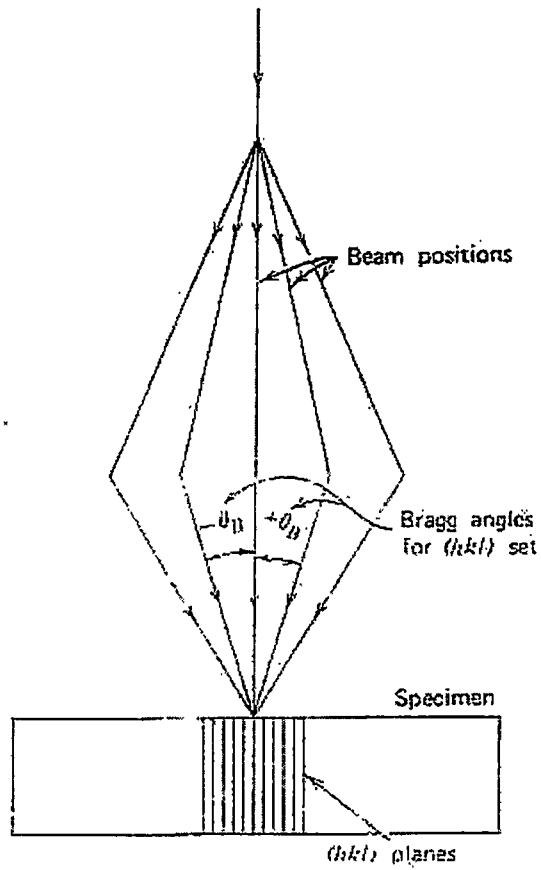


Figure 3.1: Scanning conditions for selected area channeling

### 3.3 Profilometry:

The roughness of the surface of the substrates can be measured by a mechanical stylus profilometer. The profilometer includes a position-sensitive opto-electrical transducer (pick up) that registers vertical displacements of the stylus tip as it scans along the surface of the substrate, which should be horizontal. The stylus has a diamond tip that has a semicircular configuration with a radius of 2.5  $\mu\text{m}$ . The size of the tip determines the resolution of the topography of the substrate surface. Keeping all other parameters the same, then the smaller the tip the better the resolution of the roughness details of the surface [115].

The waviness and the more widely spaced roughness irregularities are usually represented by a waveform. To electronically suppress the lower frequencies of such a waveform, a cut-off length (which is the same as the sampling length) is established. If one multiplies the number of cut-offs used by the cut-off length, the result will be the evaluation length of the trace. In this work, three cut-off lengths of 4 mm were used. The traverse speed of the scan and the load applied by the stylus on the substrate were preset by the manufacturer.

By selecting the ASME (ISO) mode on the instrument, the pick-up signals could be electronically filtered. Based on those pick-up signals the roughness parameters were determined. These parameters include the arithmetic roughness ( $R_a$ ), the root-mean-squared roughness ( $R_q$ ), and maximum peak to valley height ( $R_t$ ). The first two parameters were calculated according to the following equations:

$$R_a = (|y_1| + |y_2| \dots + |y_n|) / n \quad (3.1)$$

$$R_q = \left[ (|y_1|^2 + |y_2|^2 \dots + |y_n|^2) / n \right]^{1/2} \quad (3.2)$$

where  $y^n$  is the absolute deviation from a center line, and  $n$  is the total number of data points.

### 3.4 Atomic Force Microscopy (AFM):

The AFM was invented in 1986 by Binnig, Quate, and Gerber when they realized that the forces exerted by the tip on the substrate could be used to map the topography of a sample. They used a Scanning Tunneling Microscope (STM) tip placed in such a way so that its sharp end was parallel to the surface. The tip now acted as a cantilever. They used a STM to measure the small deflections of the tip that was acting as a cantilever. For the cantilever to be deflected by atoms as it is scanning, it should have a spring constant of about 10N/m. Some of the materials used for the cantilever are Si, SiO<sub>2</sub>, and commercially available cantilevers manufactured from CVD Si<sub>3</sub>N<sub>4</sub>.

An AFM can measure the long and the short range interatomic and intermolecular forces acting between the sample and the tip. A list of the more common forces encountered in AFM is available in Figure 3.2. If any of these forces acts between the substrate surface and the tip, the result is a deflection in the cantilever on which the tip is mounted. When the cantilever moves, the light beam from a small laser moves across the face of a four section photo detector, see Figure 3.3. From the difference in the light intensity on the sectors, one can calculate the displacement of the cantilever. The relationship between the cantilever's motion,  $x$ , and the force required to generate such motion is represented by Hooke's Law:



## Factors Involved in Force Measurement

- **Attractive Forces**

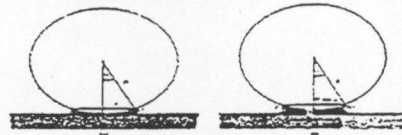
- Long Range

- van der Waals

- capillary condensation

- electrostatic

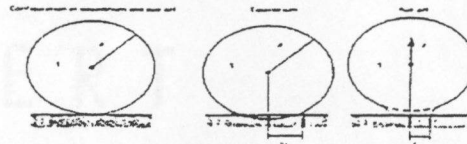
- magnetic



- Short Range

- hydration

- adhesion



- **Repulsive Forces**

- adhesion

- material properties, ie. Young's mod.

Figure 3.2: A list of common forces encountered in Atomic Force Microscopy

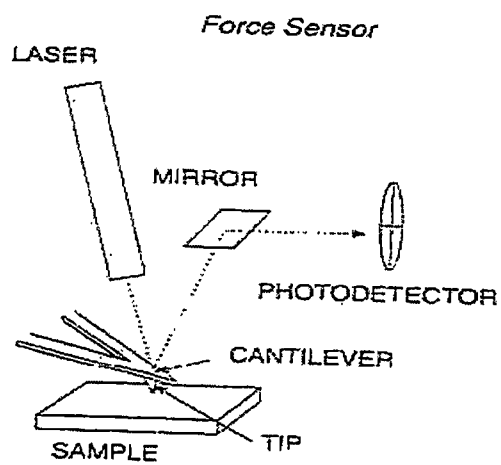
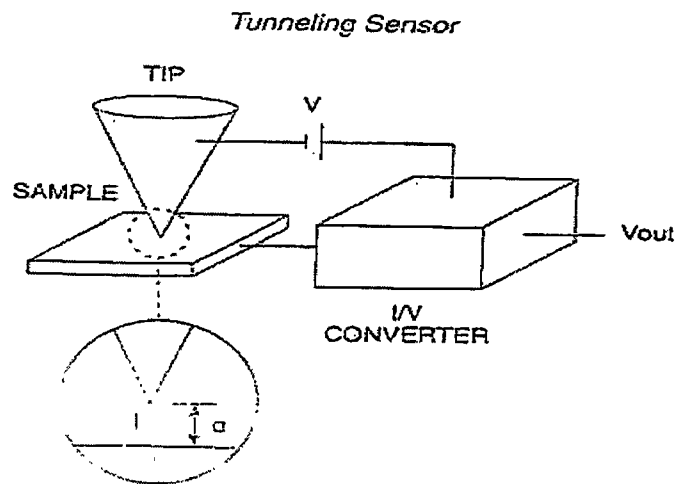


Figure 3.3: A schematic diagram showing the components of a tip on an AFM.

$$F = -kx \quad (3.3)$$

Cantilevers with a known force constant,  $k$ , of about 1 N/m can be made. Since a displacement of less than 1 angstrom can be measured, forces less than 0.1 nN are detectable. In general it is the Van der Waals and contact repulsion forces that reveal the topography of the sample.

### **3.5 Rutherford Back Scattering (RBS)/Channeling:**

One of the extensively used techniques for determining the elemental areal density, stoichiometry, and impurity distributions of thin films is backscattering spectrometry using ion beams with MeV energies. One way to identify the atomic masses and determine the distribution of target elements as a function of depth below the surface, is to measure the number and energy distribution of the ions that backscatter from the atoms that are in the near-surface region of a solid material.

In this technique, analysis ions scatter elastically from the target atoms with energy characteristic of the mass of the struck atom. Also, as these ions pass in and out of the material they lose some of their energy. A detection system, including a silicon barrier detector and a multi channel analyzer, is used for the energy analysis. The result of such analysis is a back scattering spectrum displayed in the form of counts per channel vs. channel number. Normally, there is a linear relation between the channel number and the backscattered ion energy. For an illustration of the above see Figure 3.4.

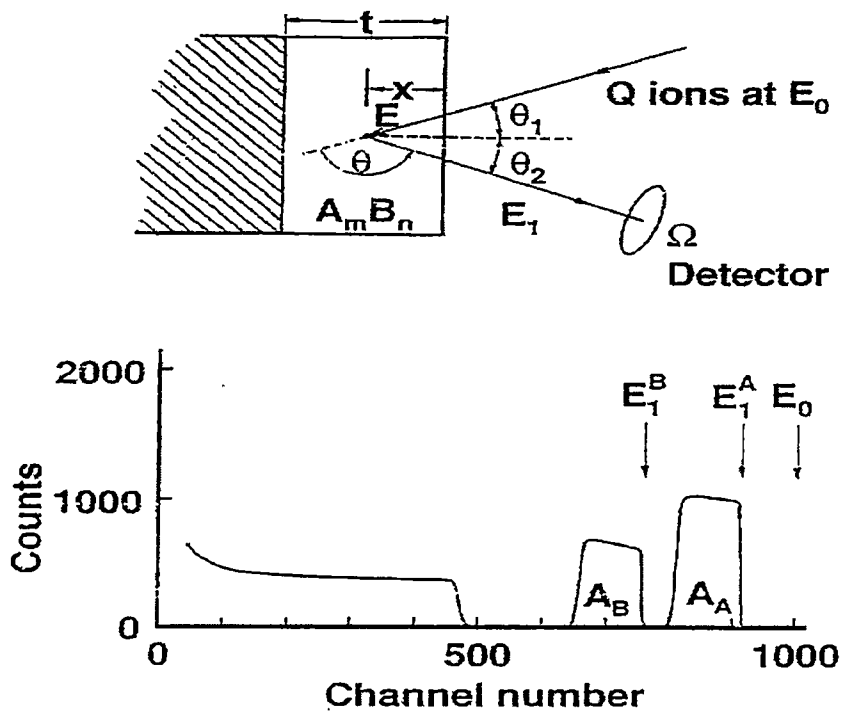


Figure 3.4: Basic backscattering spectrometry. Experimental geometry (upper figure), Backscattering spectrum (lower figure) for a two-element compound ( $A_m B_n$ ) film of uniform composition on a low-mass substrate.

Historically, most of the backscattering analyses have been performed using  $^4\text{He}$  analysis ions with 1-2 MeV energy range. The reasons for this are:

- The available accelerators produced beams with these energies.
- There was more data available about the energy loss of the  $^4\text{He}$  in the elements than any other ion.
- The energy resolution of the silicon surface barrier for the  $^4\text{He}$  is about 15 KeV
- When  $^4\text{He}$  ions are incident on all elements that are more massive than Be, the backscattering cross sections are nearly Rutherford in this energy region, i.e. they are pure coulomb scattering. This is the most important reason of all the above.
- The principal characteristics of Rutherford backscattering (RBS) that make it such a strong technique with the  $^4\text{He}$  ions are:
  - The use of standards is not required as it is an absolute method, and meaningful uncertainties can usually be assigned to the results.
  - It is a very easy and quick technique with typical data acquisition times of about ten minutes.
  - Most of the time it is a non-destructive method.
  - It may be used for depth profiling with 10-30 nm depth resolution.

Channeling was predicted in 1912, but was not detected until 1963 from the experimental studies of Davies and co-workers [117], and the computer simulations of ion trajectories by Robinson and Oen [118,119]. The steering of a beam of energetic ions

into open spaces or channels between close-packed rows or planes of atoms in a crystal is referred to as channeling. For an illustration see Figure 3.5. A diamond cubic structure such as the structure of both diamond and silicon crystals, is modeled using the ball and stick model in Figure 3.6. In this figure a random direction, a  $\{110\}$  planar channel, and a  $\langle 110 \rangle$  axial channel are shown. A correlated series of small-angle screened Coulomb collisions between the channeling ion and the atoms that surround the channel steers the ion in a channel. As a result, the channeling ion does not penetrate more than the screening distance of the vibrating atomic nuclei, and therefore the probability of Rutherford backscattering (large angle collisions), nuclear reactions, or inner-shell excitations occurring is much less than their probability of occurring with a random non-channeled beam of ions. Moreover, the yield of interactions with host atoms of an ion that finds a low angle  $\Psi$  channel into a close-packed direction is expected to be relatively low. The normalized yield  $\chi_h$  from the host atoms for such atoms is defined as the ratio of the yield of the channeled ions incident at an angle  $\Psi$  to the yield of a randomly incident beam of ions. For a highly perfect crystal and in the best axial channels,  $\chi_h$  is of the order of 0.01 at low temperatures. A possible way to make  $\chi_h$  even smaller is by aligning the detector and the incident beam with the channels. This is called "double alignment" and it causes the backscattered ions to be "blocked" by the rows of atoms surrounding the channel, and thus the detector does not see them.

Often, channeling is used to measure implantation damage, dislocation networks, strain in strained layer superlattices, and epitaxial layers quality. The reason for this is that the thermal vibration is what basically causes  $\chi_h$ , which increases even more by any

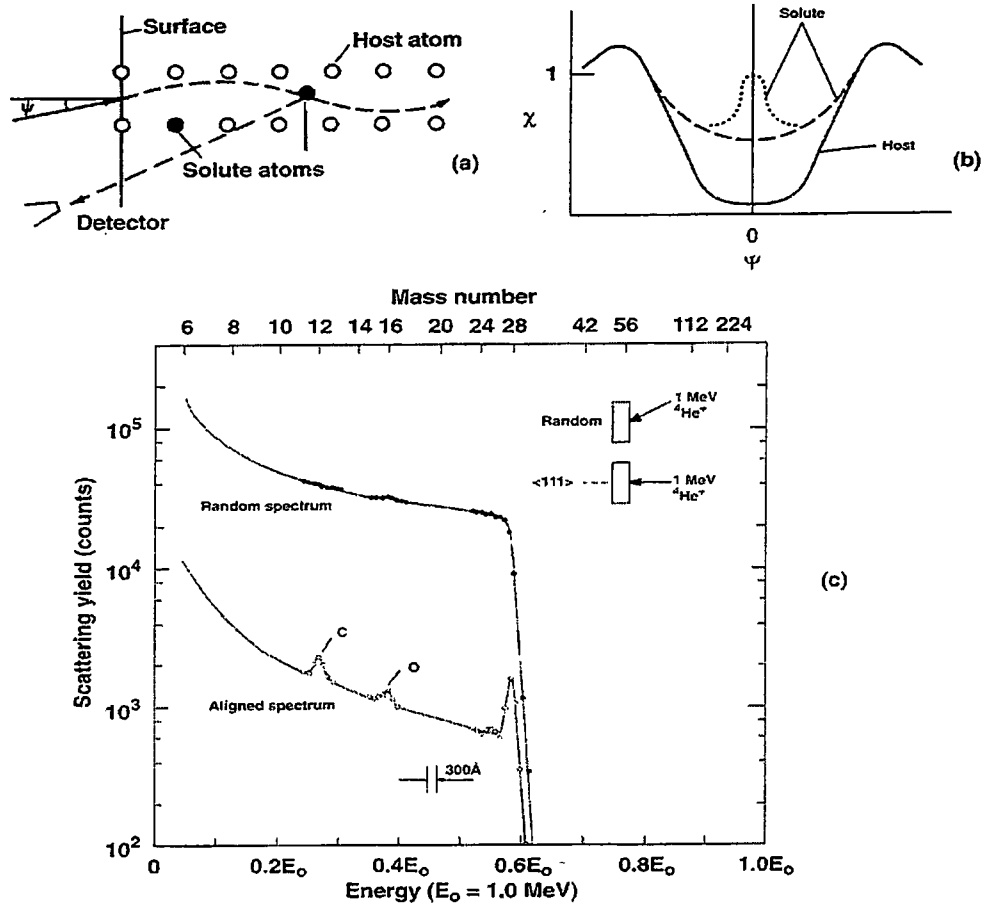


Figure 3.5: (a) Schematic view of the channeling of ions directed at an angle  $\psi$  to a close-packed row of atoms in a crystal. (b) The normalized yield  $\chi_h$  of ions that are backscattered from host atoms (the RBS yield) shows a strong dip at  $\psi = 0$ . If 50% of solute atoms are displaced into the channel, the normalized yield  $\chi_s$  of ions backscattered from the solute atoms is approximately half the random yield; i.e.,  $\chi_s = 0.5$  at  $\psi = 0$  (broken curve). If the displaced solute atoms are located near the center of the channel, a peak in yield may occur (dotted line). (c) The energy spectra of backscattered He ions from Si are shown for good  $\langle 111 \rangle$  alignment ( $\psi = 0$ ) and for random alignment. Small peaks caused by surface O and C atoms show up in the aligned spectrum.

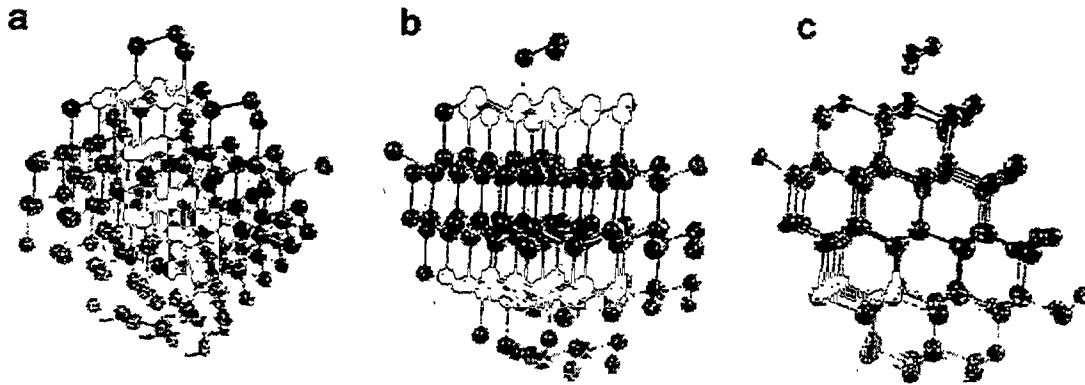


Figure 3.6: Model of lattice atoms, showing the atomic configuration in the diamond cubic structure, viewed along (a) random, (b)  $\{110\}$  planar, or (c)  $\langle 110 \rangle$  axial directions.



perturbation of the crystal lattice. Such perturbations include dislocations, stacking faults, point defects, mosaic structure, precipitates, and elastic strain.

Imperfections in a crystal can significantly affect the results of  $\chi_h$  in a channel. Suppose for example that due to some point defects or dislocations, a small concentration of host atoms in the channel are displaced. By multiple collisions with such displaced atoms, a channeled ion can scatter out of the channel as illustrated in Figure 3.7 (figure 10.3b). The fraction of dechanneled ions is measured by the normalized yield  $\chi_h$ , and the rate of change of  $\chi_h$  with depth is proportional to the concentration of the displaced host atoms. The probability of a single large-angle collision becomes important when the concentration of the displaced host atoms becomes larger than about 10%. If the near-surface layer is amorphous (completely disordered) as shown in Figure 3.7 (10.3c), then the value of  $\chi_h$  for that layer becomes unity. Because the ions lose energy as they pass through the crystal, the energy increment over which  $\chi_h = 1$  is an indicative of the thickness of the amorphous layer.

### **3.6 Transportation and Range of Ions in Matter (TRIM)**

TRIM is a computer code that calculates the stopping and range of ions (10 eV – 2 GeV) into matter using a full quantum mechanical treatment of ion-atom collisions.

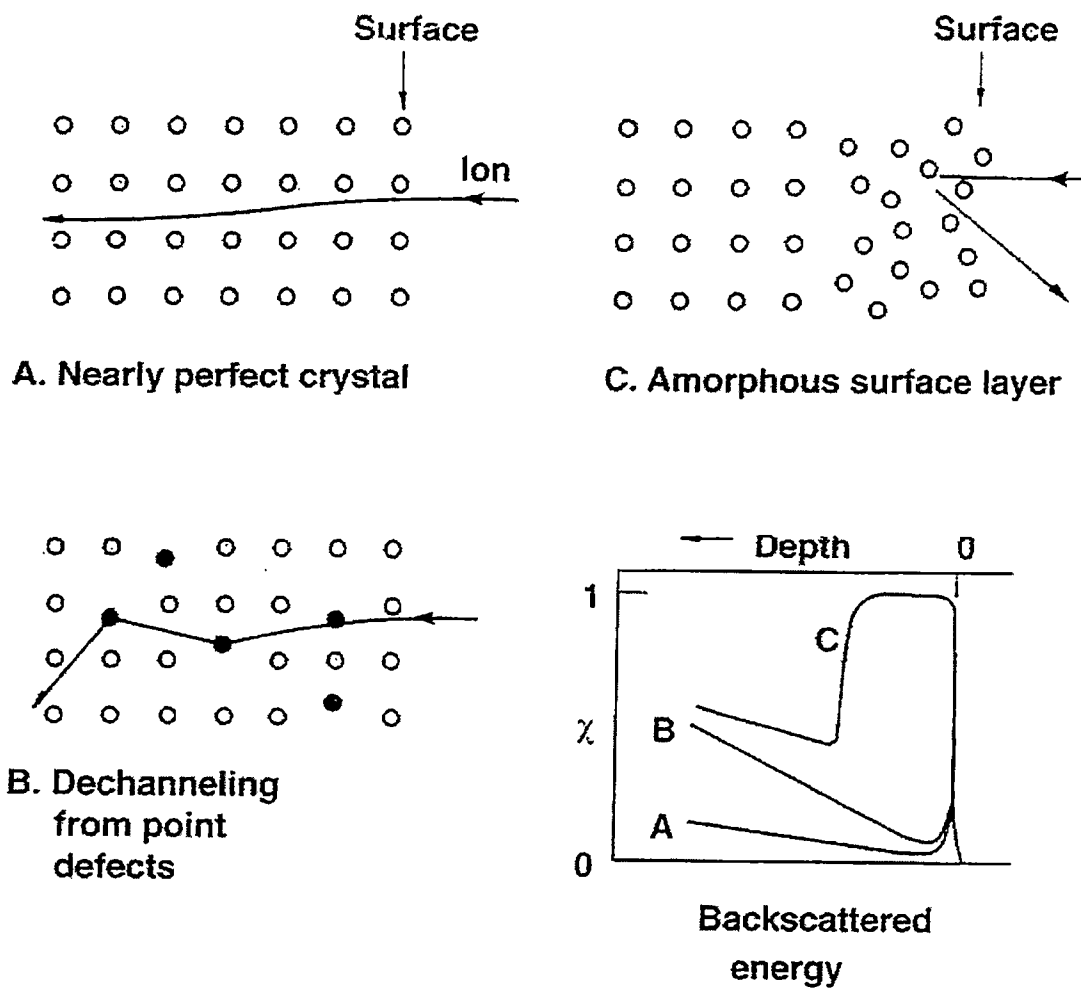


Figure 3.7: Schematic diagram illustrating ion scattering from defects: (a) little scattering for shallow depths in nearly perfect crystal, (b) dechanneling by multiple scattering from point defects, (c) direct backscattering from an amorphous surface layer.

## CHAPTER 4

### EXPERIMENTAL METHODS

#### 4.1 The Hot Filament Chemical Vapor Deposition apparatus (HFCVD):

The HFCVD apparatus consists of a CVD chamber, a gas source, mass flow controllers, a mechanical pump, and power supplies to heat the filament and the heater block, an optical pyrometer, and pressure gauge. For an illustration see Figure 4.1. The CVD assembly consists of a 4-way stainless steel high vacuum cross. On the 4-way cross, one end contained the electrical feedthroughs for the filament, the substrate heater element and gas inlet line. On the second end opposite to the first, a quartz tube slid over the filament and heater block assemblies into a Cajon O-ring seal, resulting in the "CVD chamber". The third end of the 4-way ports was connected to the mechanical pump (Varian direct drive, model # SD 200) that exhausts the system. Also connected to the third end was a quadrupole mass spectrometer, which samples the exhaust gases and serves as a residual gas analyzer. The means of connection of the mass spectrometer to the port was a leak valve (Varian ultra high vacuum leak valve, model # 951-5100). The last of the four ends included the feedthroughs for the thermocouple that was used to measure the heater block temperature. The gas inlet line was connected to the mass flow controllers (MKS, model # 1259B), a baratron (MKS pressure transducer type 627A, range 0-1000 torr), a safety switch, and a leak valve (Varian model # 951-5100).

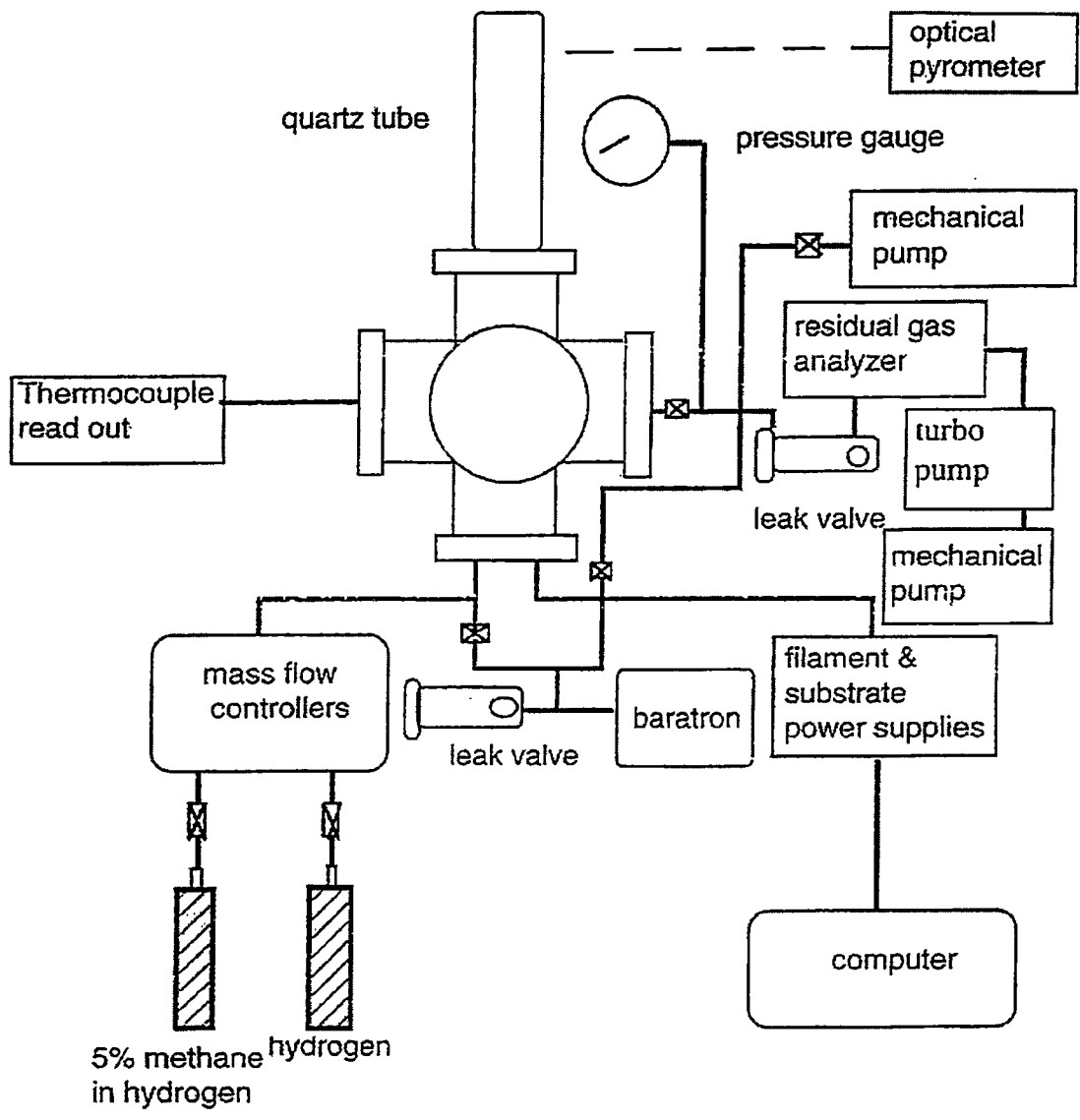


Figure 4.1: A schematic of the experimental set up used for growing polycrystalline diamond films.

#### 4.1.1 The CVD reactor:

The filament assembly inside the CVD chamber consisted of two molybdenum rods that were connected to electrical feedthroughs on a conflat flange. At the other end of these two rods are two small holes where the two ends of the tightly wound filament are inserted and held with two molybdenum screws, see Figures 4.2-4.3. A block made of machinable glass (maycor) was slid over the molybdenum rods. The substrate heater assembly consisted of a molybdenum heater block that also acted as the substrate holder, and a heater element. The heater block was mounted on two rods that were inserted on their other end into the machinable glass block, thus, isolating the heater block from the filament connections while holding it directly under the filament. The machinable glass acted as a means to secure both the filament and heater block assemblies in place inside the quartz tube. The substrate holder was heated using a rhenium wire (0.5mm diameter) surrounded by ceramic tubing and turned back and forth inside the block. A Pt-Pt 10% Rh (type S) thermocouple placed inside this block was used to measure the block temperature. The substrate was directly placed on top of the heater block exactly under the filament, thus, it was gaining its heat both through radiation from the filament and through conduction from the heater block. The temperature of the substrate was measured using an optical pyrometer (disappearing filament type) without taking into consideration any correction factors for emissivity or reflections. The substrate was viewed in the pyrometer through a hole in the center of the heater block and the use of a mirror.

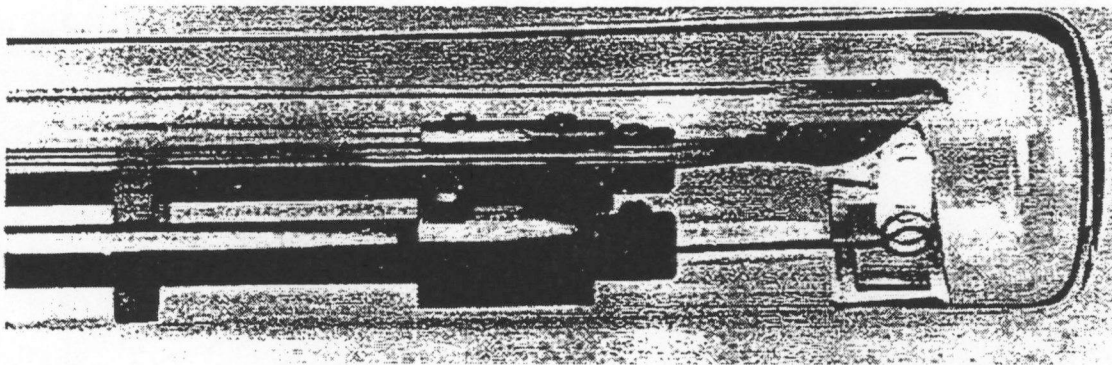


Figure 4.2: A HFCVD reactor during film growth (ORNL photograph YP-5852). The substrate is placed directly underneath the filament for indirect heating. The modified reactor has the capability of controlling the substrate temperature independent of the filament by providing conductive heating from the substrate holder equipped with a heater element.

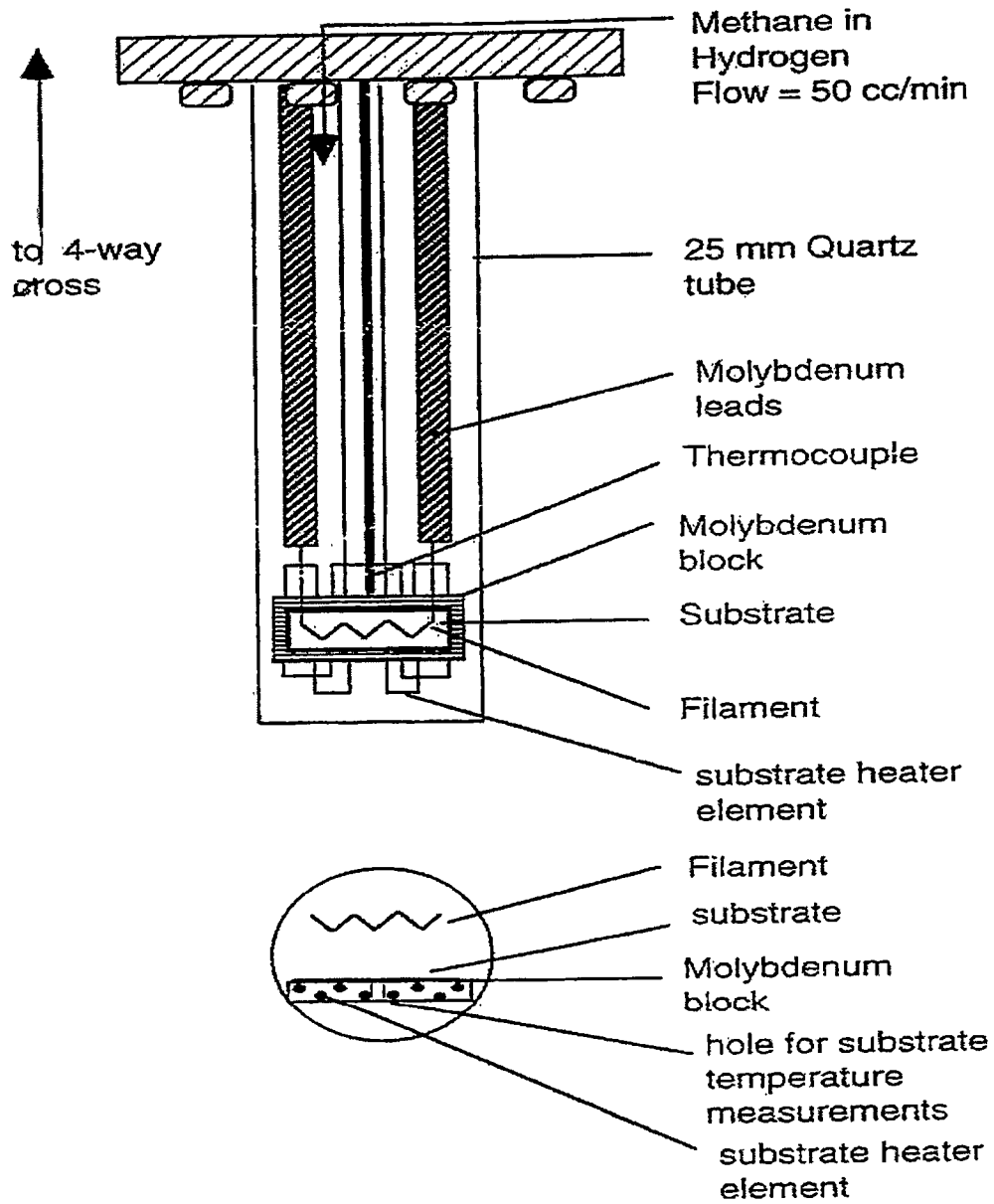


Figure 4.3: A schematic of the quartz tube reactor used for hot filament CVD depositions of diamond films.

#### 4.1.2 Mass Spectrometer

The mass spectrometer in this apparatus has sensitivity better than  $10^{-10}$  torr, mass range of 0-300 amu, and a resolving power better than 1 amu. The purpose of the mass spectrometer was to analyze the gases being exhausted from the HFCVD chamber during and after film growth. It was also used to monitor the system and detect any leaks present. Whenever there are any changes in the experimental growth parameters, the peak intensities varied. A commercially available differentially pumped UTI model 100 C quadrupole mass spectrometer with a closed ion source was used to record the mass spectra.

#### **4.2 Experimental Procedures:**

The substrates used in this study were polished single crystal (100) silicon. The silicon was purchased as wafers that were about 10 cm in diameter and 0.5 mm thick. Using a diamond scribe the wafers were cut into 12x8 mm pieces that were to be used as the experimental substrates.

The experimental procedure undertaken in this work can be divided into three stages:

- 1) Pre-deposition stage
- 2) During deposition stage
- 3) Post deposition stage



#### 4.2.1 Pre-deposition stage:

In this stage different pretreatment of the substrate were done depending on the goal of the experiment. The pretreatment included a) polishing the substrate with different powders, b) ion implantation of the substrate, and c) annealing the substrate.

##### a) Polishing the substrate

A sample was immersed in powder-ethanol slurry, which was then put in an ultra sonic vibrator for 10-15 minutes. A few substrates were abraded for longer times to see if that makes a difference on the nucleation density. To study the effects of different abrading materials on the nucleation of diamond, the powders used were diamond, SiC, Al<sub>2</sub>O<sub>3</sub>, and TiB<sub>2</sub>. All the powders had 20 μm average particle size. After polishing the substrates were cleaned using ethanol to remove any impurities left on the sample.

After the polishing treatment, there were five different types of substrates- 1) as received "virgin", 2) diamond abraded, 3) silicon carbide abraded, 4) alumina abraded, and 5) titanium diboride abraded.

##### b) Ion Implantation

Ion implantation in this work was done using the 20 kV Extrion accelerator in the Surface Modification and Characterization (SMAC) facility at the ORNL.

Only samples abraded with diamond powder were used in the implantation process, since the other powders did not seem to enhance nucleation (see results and discussion chapter). Part of each sample was masked before the implantation to enable

a comparative study of the nucleation between the implanted region and the non-implanted region. Silicon ions ( $\text{Si}^{29}$ ) were used in all implantation runs. The samples were implanted at 77 K in order to prevent diffusion of vacancies and interstitial atoms during implantation. To prevent any channeling, implantation was done at a tilt of  $7^\circ$ . All samples were implanted using ion energy of 150 KeV. A list of the doses used in the implantation process is given in Table 4.1:

The higher the dose the more damage introduced to the silicon surface. The purpose of using a range of ion doses was:

- 1) To destroy the crystallinity of any residual diamond particles, that might be on the surface of the silicon, without destroying that of the silicon.
- 2) To destroy the crystallinity of both the diamond debris and the silicon surface.

c) Annealing

Annealing of the substrates took place in two different furnaces. The first furnace was the HFCVD reactor used for diamond deposition, where the filament has already been carburized (see carburization section). This furnace will be referred to as the “carburized filament” furnace. The second furnace was another HFCVD reactor, where the filament had not been carburized and will be referred to as the “clean filament” furnace from this point on.

All anneals were done under hydrogen environment. The temperatures used for all the anneals was  $1000^\circ\text{C}$ , and the times of annealing varied according to the sample

**Table 4.1: Doses used in the implantation process.**

---

$5 \times 10^{14} \text{ Si}^+/\text{cm}^3$
$1 \times 10^{15} \text{ Si}^+/\text{cm}^3$
$2 \times 10^{15} \text{ Si}^+/\text{cm}^3$
$1 \times 10^{16} \text{ Si}^+/\text{cm}^3$
$2 \times 10^{16} \text{ Si}^+/\text{cm}^3$
$1 \times 10^{17} \text{ Si}^+/\text{cm}^3$

---

but most of the annealed samples were in a furnace for two hours. Depending on the goal of each run some samples were annealed after the abrasion and implantation but before diamond deposition, and some were annealed after diamond deposition.

#### 4.2.2 During deposition stage:

In this stage the pretreated sample is centered on the substrate heater inside the CVD reactor. After the reactor is sealed and the mirror (used to measure the substrate temperature) is properly positioned, the mass flow controllers for the  $\text{H}_2$  and  $\text{CH}_4$  gas are opened and the gas mix is inserted into the CVD reactor at a rate of  $50 \text{ std. cm}^3 \text{ min}^{-1}$ . The gas mix was set to either 0.5% or 1.0% methane in hydrogen. Then the pressure in the CVD chamber was set to 5.3 KPa (40 Torr). After that, stable current-controlled direct current power supply, operated via computer, was used to heat the filament to

2100° C. Using a similar power supply, the heater block was heated to give the substrate a temperature of 1000° C.

Diamond deposition times varied from 1hr to about 58hrs. The results of such depositions gave diamond as separate particles and also as complete continuous films. The deposition parameters for the CVD process used in this study are given in Table 4.2:

**Table 4.2: Deposition parameters for the CVD process.**

Substrate material	Silicon single crystal (100)
Substrate to filament distance	8 mm
Filament material	Tungsten (W)
Filament temperature	2100 °C
Substrate temperature	1000 °C
Hydrogen gas flow rate	40 or 45 sccm
5% methane in hydrogen flow rate	5 or 10 sccm
Chamber pressure	40 torr

#### 4.2.3 Post deposition stage:

In this stage the characterization techniques were used to detect and analyze the substrate surface after deposition.

The nucleation density of the CVD diamond on the silicon substrates was determined using an ISI 40 and a Hitachi S 800 high resolution scanning electron microscope equipped with a field emission gun. The ISI 40 was operated at 15 kV while the Hitachi S 800 was operated at 20 kV. Several images were taken for each sample in different areas including both implanted and non-implanted regions and any other significant observations. The diamond density on the substrates was estimated by counting the particles in a micrograph and dividing that number by the area of the micrograph. The Hitachi S 800 was also equipped with an x-ray detector for energy dispersion spectrometry, which was used to determine the composition of phases. The SEM was then operated at 50 kV for the EDS measurements.

To study the effect of mechanical treatments of the substrate, four samples were used. One was "virgin" silicon, and the other three were abraded in the ultra sonic vibrator each with either diamond, SiC, or Al<sub>2</sub>O<sub>3</sub> powder. The surface roughness of each sample was measured with the profilometer. Each sample was scanned three times in three different positions, and each scan was 4 mm long. The same samples were studied under atomic force microscopy where again each sample was scanned three different times. Two different types of surface roughness images were produced. One was a two dimensional (2-D) type photograph, and another was a three dimensional (3-D) type.

To study how the ion implantation and annealing affected the crystallinity of the substrate surface both RBS/channeling and SEM/channeling were used. The RBS/channeling was done using 2 MeV He<sup>+</sup> ions. The detector angle with the incoming beam was 160°. The beam angles were 0° for channeling and 4° for the random.

## CHAPTER 5

### RESULTS AND DISCUSSION

#### 5.1 Surface Mechanical Treatment

Observations by SEM on the as-received "virgin" silicon substrates after exposure to the reactant gases in the growth chamber for times of one hour found that there was essentially no nucleation on the surface of the silicon substrate in either the implanted or the unimplanted regions. Groups of diamond particles were occasionally observed in areas that appear to have been contaminated after the sample had been cleaned with ethanol, but before insertion into the CVD reactor. This result is in agreement with reports in the literature that the nucleation density in a CVD process on a clean, polished surface, is relatively low [83,85,120,121].

Surface roughness profiles were determined by profilometry and by AFM examinations. Samples were examined after ultrasonic abrasion by suspensions of diamond, SiC, and Al<sub>2</sub>O<sub>3</sub> powders in ethanol.

Profilometry studies showed no significant difference in roughness of all four samples (including the virgin). The arithmetic mean of the departures of the roughness profile from the mean line ( $R_a$ ), and the root mean square parameter corresponding to  $R_a$  ( $R_q$ ) values for each of three scans on each of the four samples are given in the Table 5.1. The average values taken over the three strikes for  $R_a$  and  $R_q$  respectively are given in Table 5.2.

**Table 5.1 Results of profilometer measurements on surface roughness of substrates:**

<u>R<sub>a</sub></u>				
Sample scratched with:	Virgin	Diamond	SiC	Al <sub>2</sub> O <sub>3</sub>
Strike 1	0.03 μm	0.02 μm	0.03 μm	0.01 μm
Strike 2	0.03 μm	0.02 μm	0.02 μm	0.01 μm
Strike 3	0.02 μm	0.02 μm	0.02 μm	0.02 μm

<u>R<sub>q</sub></u>				
Sample scratched with:	Virgin	Diamond	SiC	Al <sub>2</sub> O <sub>3</sub>
Strike 1	0.04 μm	0.02 μm	0.03 μm	0.02 μm
Strike 2	0.04 μm	0.02 μm	0.03 μm	0.02 μm
Strike 3	0.03 μm	0.02 μm	0.03 μm	0.02 μm

**Table 5.2 Average values for R<sub>a</sub> and R<sub>q</sub> based on the data in Table 5.1**

Substrate	Average R <sub>a</sub> (μm)	Average R <sub>q</sub> (μm)
Unpolished	0.0267	0.0367
Diamond polished	0.02	0.02
SiC polished	0.0233	0.03
Al <sub>2</sub> O <sub>3</sub> polished	0.013	0.02

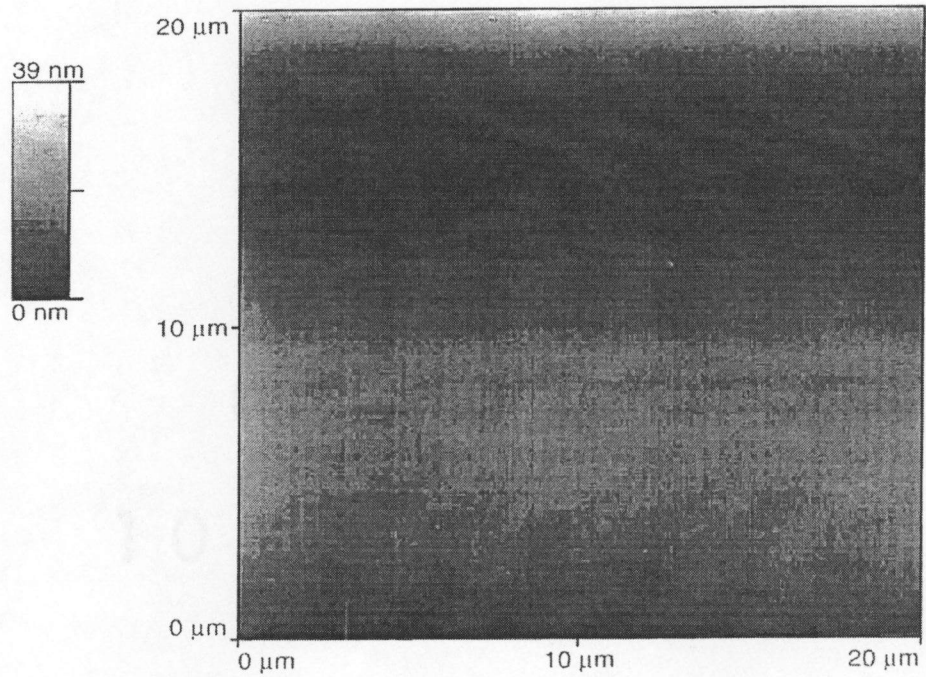


The mechanical profilometer gives the roughness on a scale of 10's of nm [122]. This indicates that the averages given in Table 5.2 are all on the order of the resolution of roughness of the profilometer, and none of the samples exceeds that value.

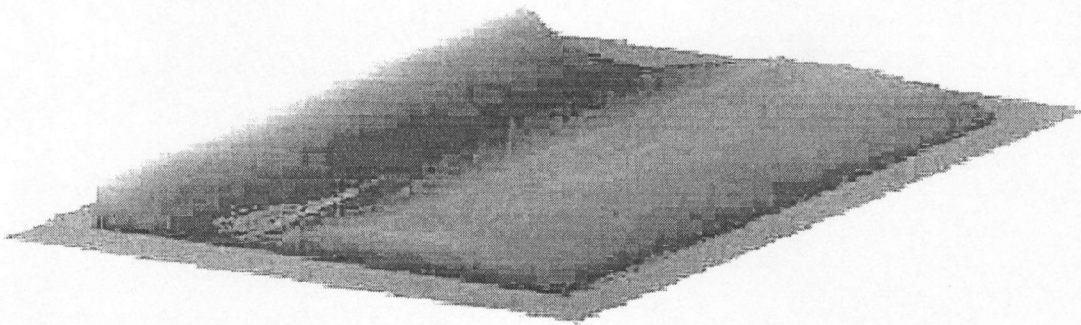
To measure the surface roughness on a finer scale, the same four samples were studied under AFM. The AFM can detect surface roughness on the order of a few tenths of a nanometer. The studies on the four samples also showed that there was no significant difference in the roughness between them, see Figures 5.1-5.4. In the 2-D images (part a of figures 5.1-5.4), the brighter the spot the higher its peak amplitude, and the darker the spot the higher its valley amplitude. In the 3-D images (part b of figures 5.1-5.4), the roughness of the surface is represented by spikes or valleys that protrude higher or lower in amplitude than the smooth regions. It appears that the substrate polished with the SiC powder may be slightly rougher than the substrates polished with diamond and Al<sub>2</sub>O<sub>3</sub>. Furthermore, all three abraded substrates appear to be rougher than the "virgin" one.

The density of nuclei for the samples abraded with diamond, SiC, Al<sub>2</sub>O<sub>3</sub> and TiB<sub>2</sub> was determined from SEM photographs. It is assumed that each diamond particle represents one nucleus. The density was determined by counting the number of particles in an area and dividing by that area. The range of densities for each condition is summarized in Table 5.3.

Nucleation was profuse only on the samples abraded 15 min with diamond, Figure 5.5. In order to determine any effect of CH<sub>4</sub>/H<sub>2</sub> ratio on nucleation density, samples exposed

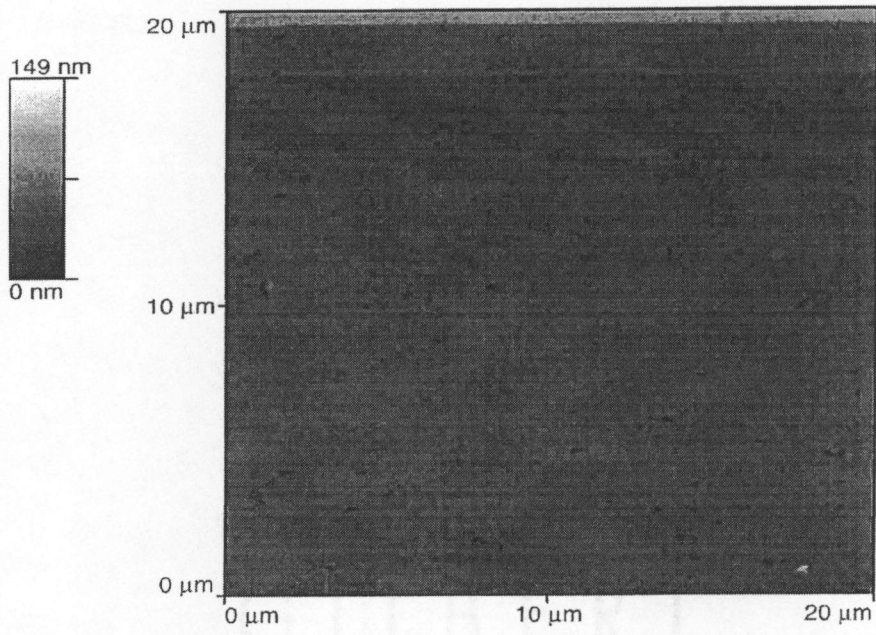


a)

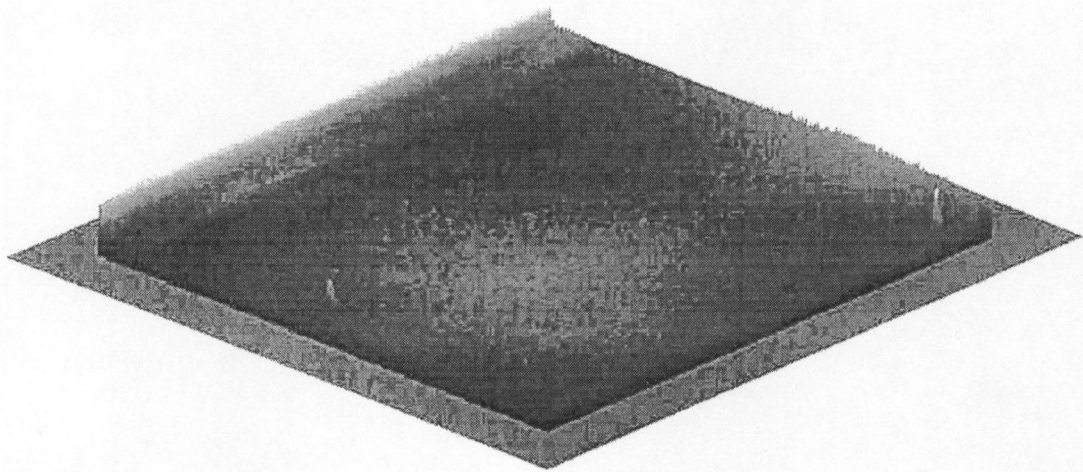


b)

Figure 5.1: AFM micrograph showing the roughness of a virgin silicon surface, a) 2-D, b) 3-D

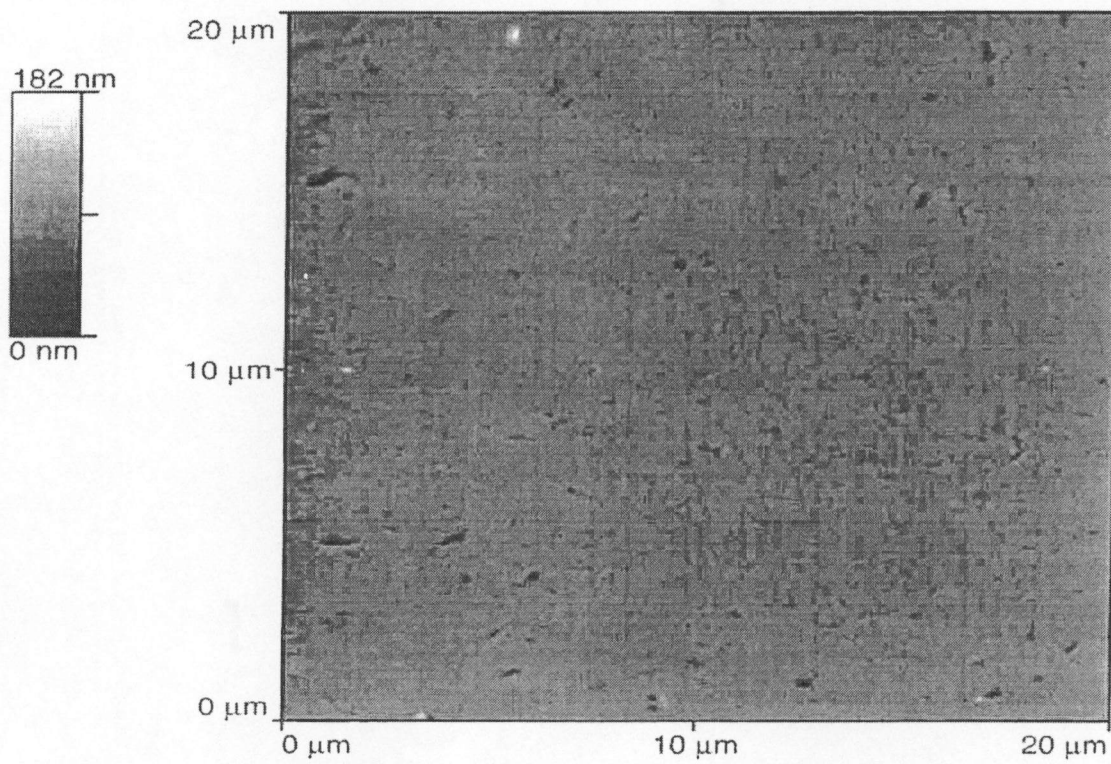


a)

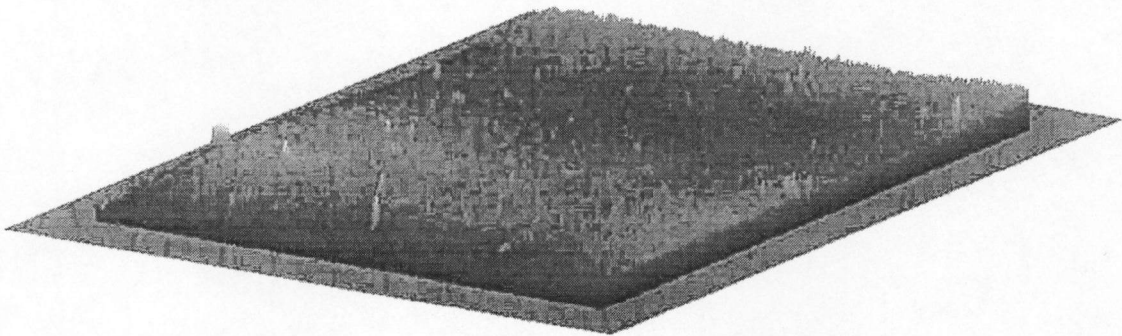


b)

Figure 5.2: AFM micrograph showing the roughness of a diamond polished silicon surface, a)2-D, b)3-D.

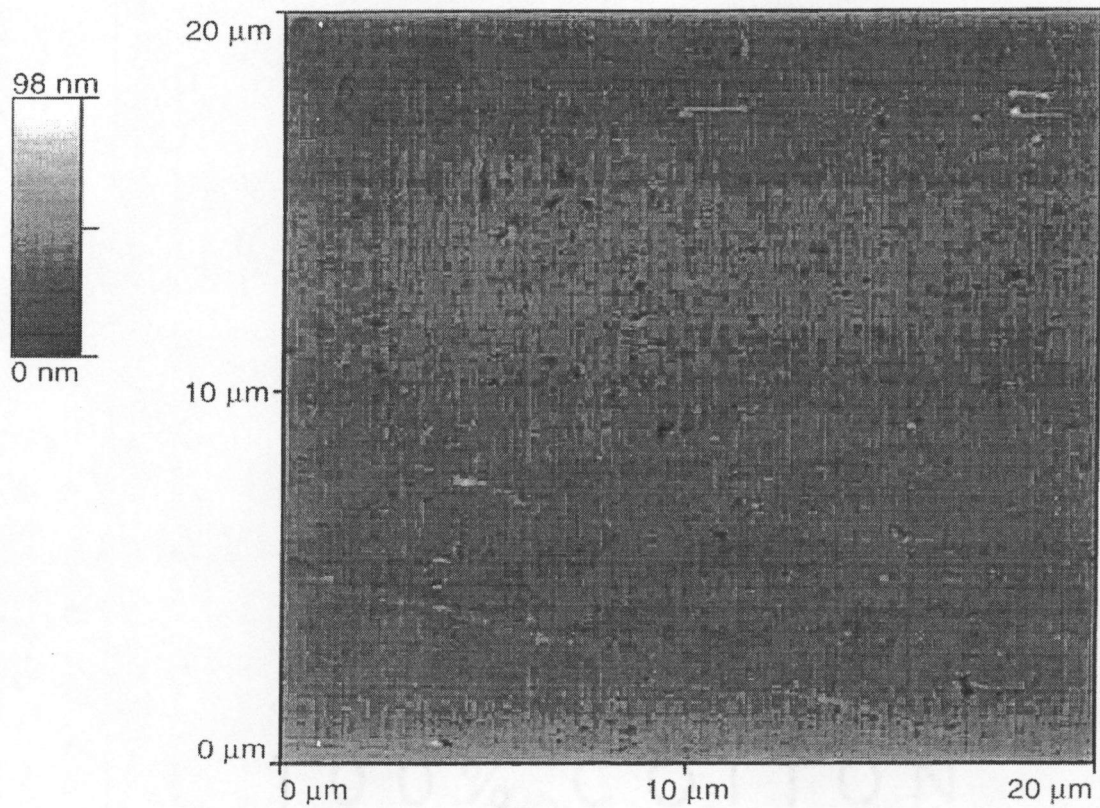


a)

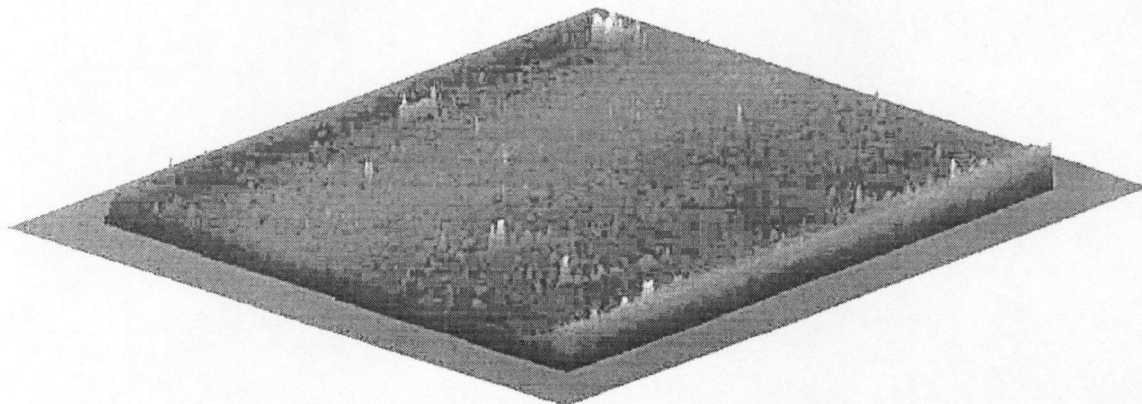


b)

Figure 5.3: AFM micrograph showing the roughness of a SiC polished silicon surface, a)2-D, b)3-D.



a)



b)

Figure 5.4: a) AFM micrograph showing the roughness of a  $\text{Al}_2\text{O}_3$  polished silicon surface, 2-D.

**Table 5.3 : Densities for samples abraded with diamond, SiC, Al<sub>2</sub>O<sub>3</sub>, and TiB<sub>2</sub> and their growth conditions**

Abrading-material/time (min)	CH <sub>4</sub> %/growth (min)	time	Nuclei-density Particles/cm <sup>2</sup>
Diamond / 15	0.5/75		1.7x10 <sup>7</sup> – 3x10 <sup>8</sup>
Diamond/15	1/60		2.2x10 <sup>8</sup>
SiC/15	0.5/75		6x10 <sup>4</sup>
SiC / 15	1/60		2.7x10 <sup>5</sup>
SiC/60	1/60		1-5.5x10 <sup>5</sup>
SiC/180	1/60		3.5-6.6x10 <sup>5</sup>
SiC/180	1/120		2x10 <sup>5</sup>
SiC/abrasive paper	1/60		3.15-4.8x10 <sup>6</sup>
Al <sub>2</sub> O <sub>3</sub> /15	0.5/75		4x10 <sup>4</sup>
Al <sub>2</sub> O <sub>3</sub> /180	1/60		4.3x10 <sup>5</sup> -1x10 <sup>6</sup>
Al <sub>2</sub> O <sub>3</sub> /180	1/120		3x10 <sup>5</sup>
TiB <sub>2</sub> /15	1/60		None

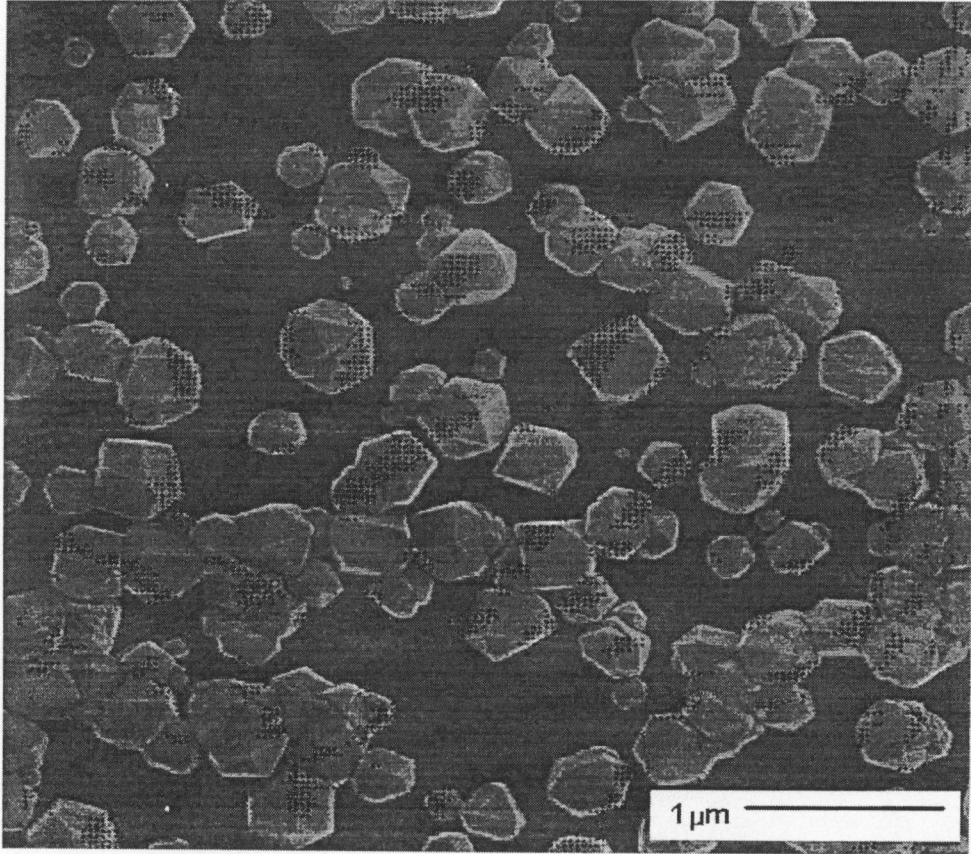


Figure 5.5: Scanning electron micrograph showing diamond nucleation density on a sample abraded with diamond slurry in the ultrasonic bath. Nucleation density of  $1.5 \times 10^8$  is the result of using  $\text{CH}_4$  concentration of 0.5% and is uniform across the entire sample. Magnification is 20K.

to 0.5 and 1.0 % CH<sub>4</sub> were examined. A comparison of Figure 5.5 (0.5% CH<sub>4</sub>) with a density of  $1.5 \times 10^8$  particles per cm<sup>2</sup> and Figure 5.6 (1% CH<sub>4</sub>) with a density of  $2.2 \times 10^8$  particles per cm<sup>2</sup> shows increasing the CH<sub>4</sub> concentration promoted growth without greatly affecting the density of nuclei. The density of nuclei on samples abraded for 15 min with Al<sub>2</sub>O<sub>3</sub>, SiC and TiB<sub>2</sub> was much lower. Figure 5.7 shows the density on sample abraded with Al<sub>2</sub>O<sub>3</sub> is  $4 \times 10^4$  particles per cm<sup>2</sup> after exposure to 0.5% CH<sub>4</sub> for 75 min. The sample abraded with SiC and exposed to the same conditions had a density of  $6 \times 10^4$  particles per cm<sup>2</sup>, Figure 5.8. Increasing the CH<sub>4</sub> concentration to 1% did not significantly change the density of particles on the sample abraded with SiC, Figure 5.9. No particles were found on the sample abraded with TiB<sub>2</sub>.

In order to determine if longer exposure to the abrasive slurries has an effect on the nucleation density, samples treated with SiC for 3 hours and 15 minutes were examined and compared, (Figures 5.10-5.11) after growth in 1% CH<sub>4</sub> for 1 hour. The density was  $3.5$  to  $6.6 \times 10^5$  particles per cm<sup>2</sup> for the 3hour treatment and  $2.7 \times 10^5$  particles per cm<sup>2</sup> for the 15minute sample. Thus increasing the abrasion time from 15 minutes to 180 minutes resulted in an increase in nucleation density by a factor of 1.5 to 2. As an alternate manner of treating the surface, a sample was polished on a felt pad using Al<sub>2</sub>O<sub>3</sub> water slurry. Figure 5.12 shows a density of  $2 \times 10^4$  particles per cm<sup>2</sup>, about the same as using the ultrasonic treatment for 15 minutes.

The results of the AFM and profilometry measurements indicate that the roughness (at the measured scale) of the substrate surface did not play a significant role



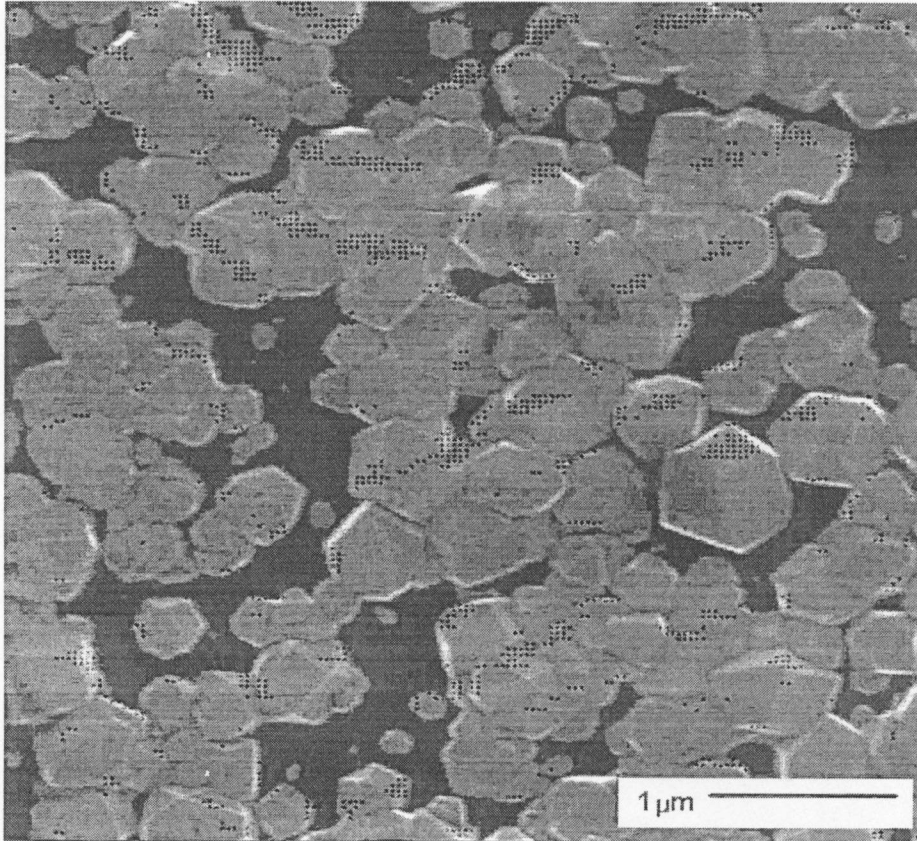


Figure 5.6: Scanning electron micrograph showing diamond nucleation density on a sample abraded with diamond slurry in the ultrasonic bath. Nucleation density of  $2.2 \times 10^8$  is the result of using  $\text{CH}_4$  concentration of 1.0% and is uniform across the entire sample. Magnification is 20K.

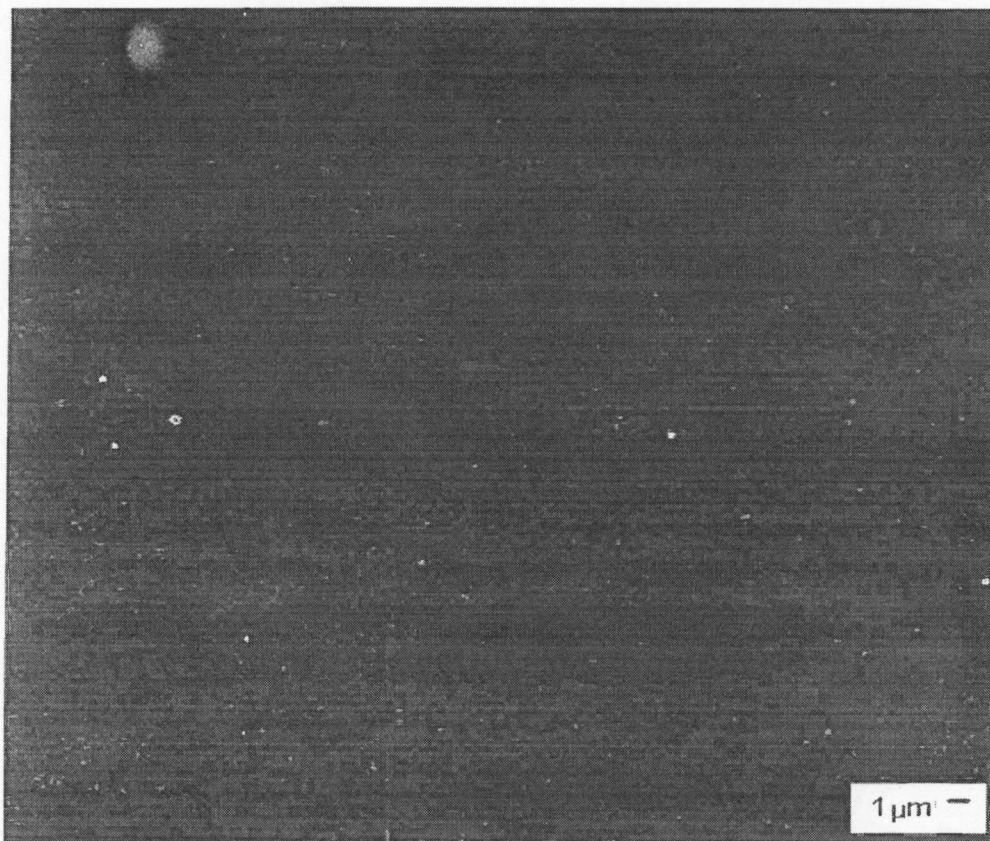


Figure 5.7: Scanning electron micrograph showing diamond nucleation density on a sample abraded with  $\text{Al}_2\text{O}_3$  slurry in the ultrasonic bath. Nucleation density of  $4 \times 10^4$  is the result of using  $\text{CH}_4$  concentration of 0.5%. Magnification is 2K.

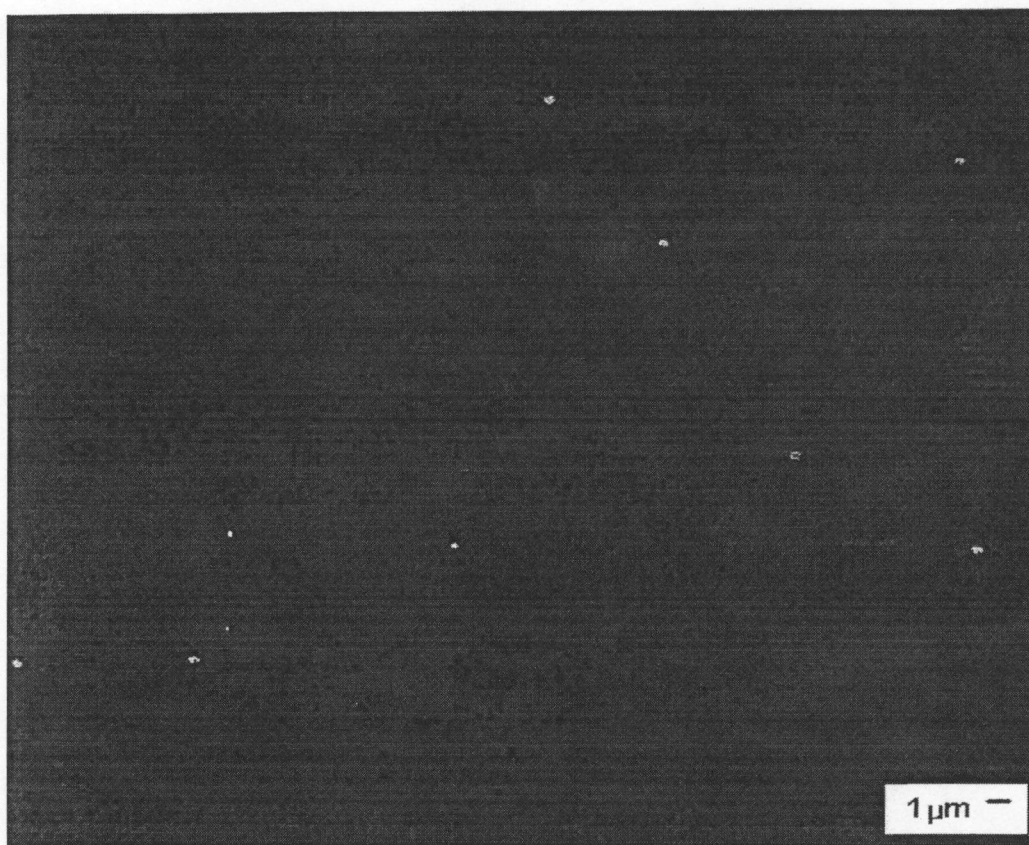


Figure 5.8: Scanning electron micrograph showing diamond nucleation density on a sample abraded with SiC slurry in the ultrasonic bath. Nucleation density of  $6 \times 10^4$  is the result of using  $\text{CH}_4$  concentration of 0.5%. Magnification is 2K.

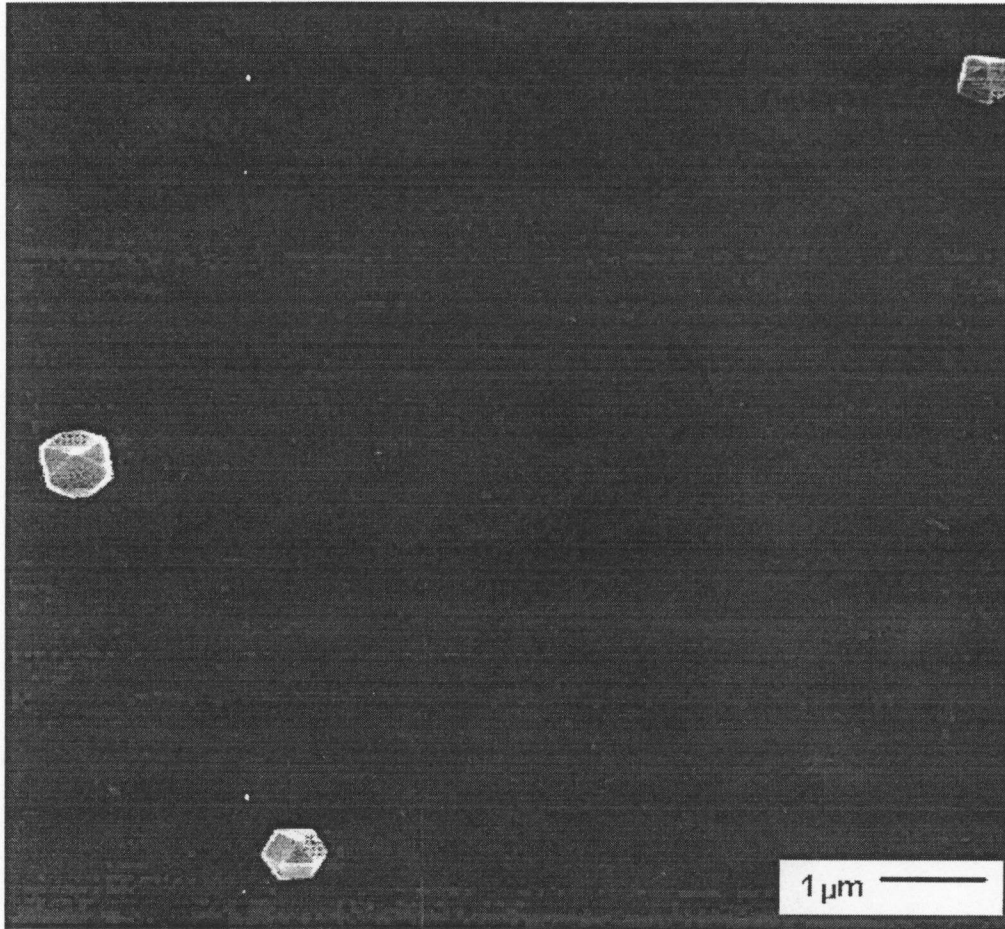


Figure 5.9: Scanning electron micrograph showing diamond nucleation density on a sample abraded with SiC slurry in the ultrasonic bath. Nucleation density did not increase as result of using CH<sub>4</sub> concentration of 1.0% (compare to Figure 5.8). Maginification is 10K.

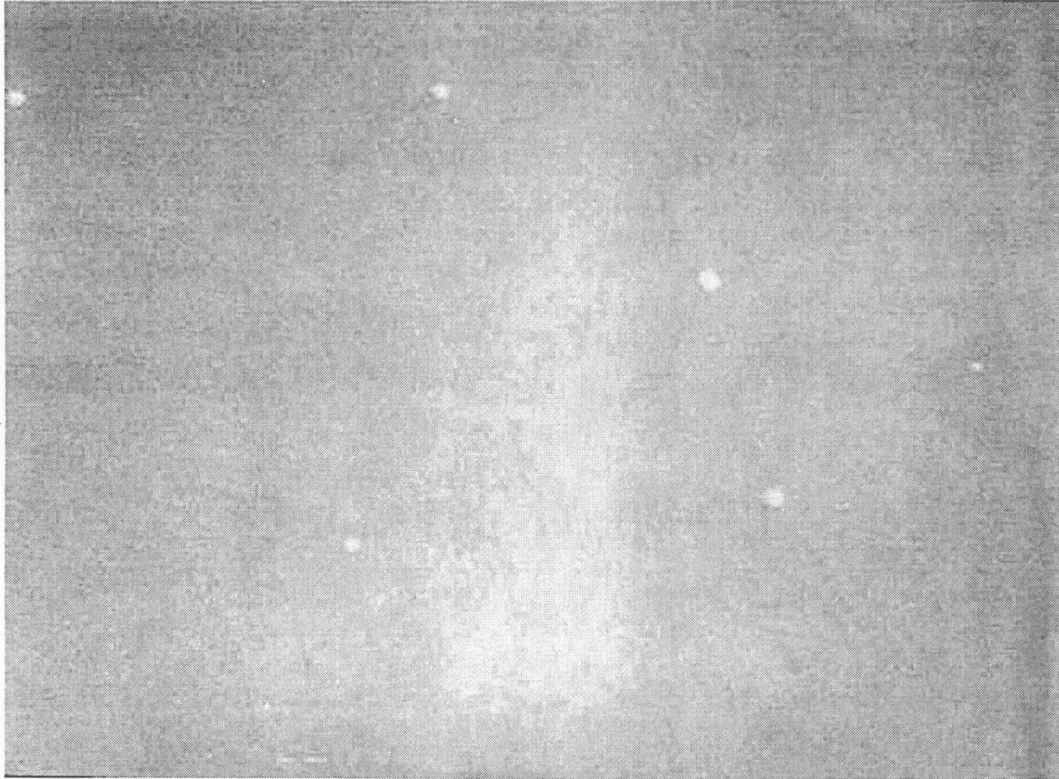


Figure 5.10: Scanning electron micrograph showing diamond nucleation density on a sample abraded with SiC in the ultrasonic bath for 15 minutes (compare to Figure 5-11). Nucleation density of  $2.7 \times 10^5$  particles per  $\text{cm}^2$  was achieved under 1%  $\text{CH}_4$  concentration. Magnification is 1.9K.

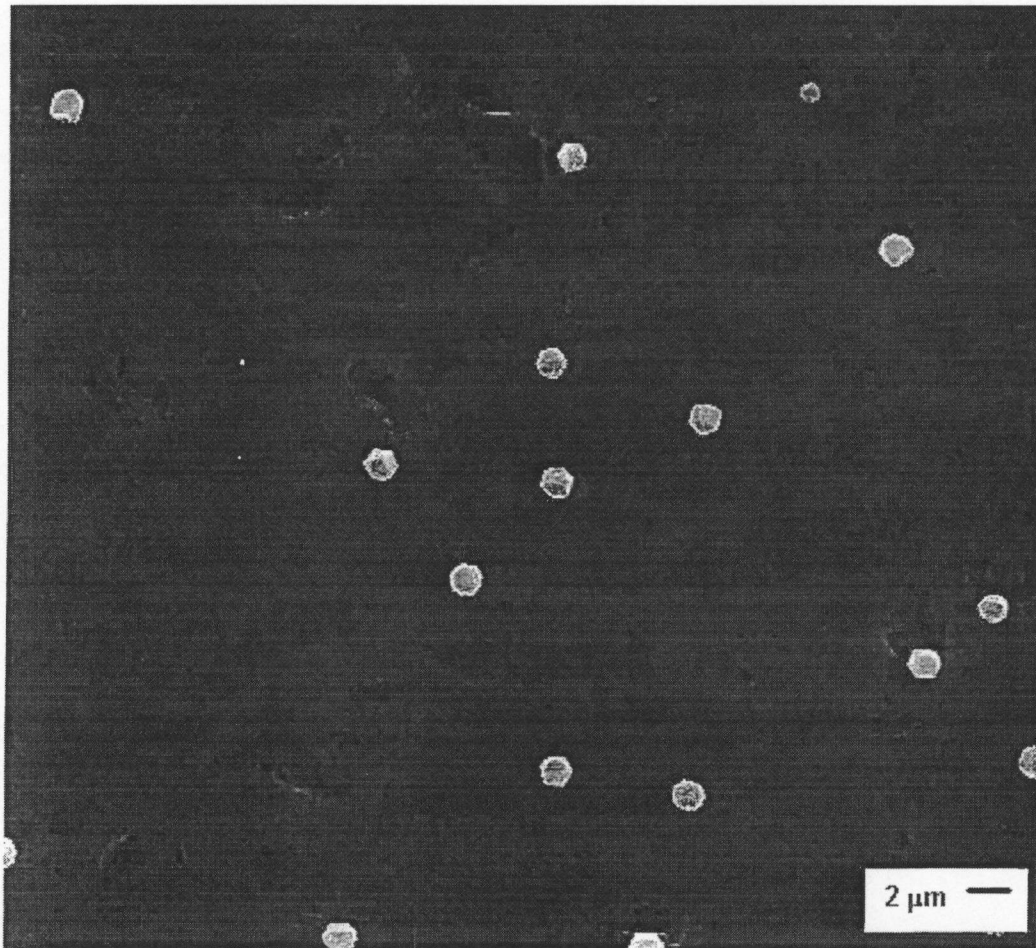


Figure 5.11: Scanning electron micrograph showing diamond nucleation density on a sample abraded with SiC slurry in the ultrasonic bath for 3 hours. Nucleation density of  $2 \times 10^5$  is the result of using  $\text{CH}_4$  concentration of 1.0% and is uniform across the entire sample. Magnification is 2K.

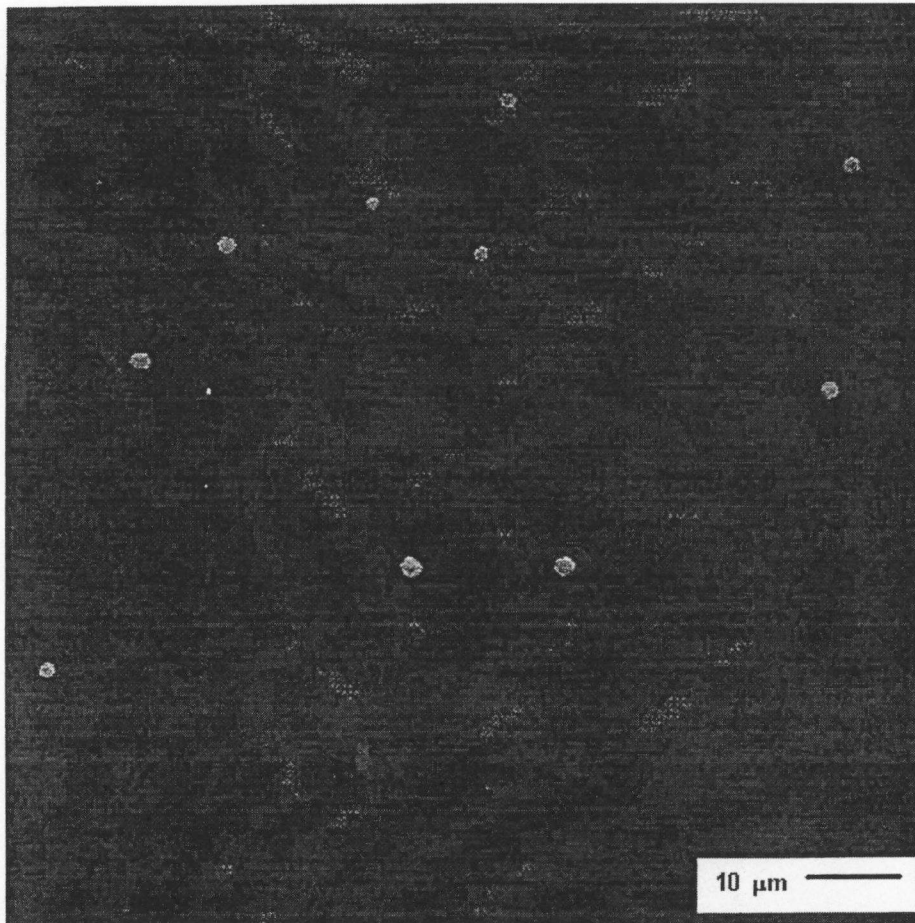


Figure 5.12: Scanning electron micrograph showing diamond nucleation on a sample that was polished on a felt pad using an  $\text{Al}_2\text{O}_3$  slurry. The density is about  $2 \times 10^4$  particles per  $\text{cm}^2$ . Magnification is 1K.

in the enhancement of the nucleation density of CVD diamond, since only the substrate scratched with diamond powder significantly increased the nucleation density.

A sample was partially scratched with SiC (400 grit) abrasive paper to study the effect of larger scale scratches on nucleation density. A SEM photograph of the nucleation density after the deposition process on that sample is given in Figure 5.13. The nucleation density in this photograph is  $3 \times 10^5$  particles per  $\text{cm}^2$ . Figure 5.13 also indicates that while some diamond particles may be trapped in some of the crevices created by the pretreatment, they do not appear to be associated with any particular features, such as edges or sides. This result is consistent with the results of the samples scratched ultrasonically, which confirms the conclusion that substrate surface roughness did not play a significant role in diamond nucleation enhancement.

This conclusion is consistent with the report of Anger *et al.* [83] who reported that the nucleation density on silicon substrates varied as listed in Table 5.4. Anger *et al.* attributed the modest increase for SiC abrasion to carbonaceous impurities left on the surface. The results contradict the conclusion that surface roughness alone causes enhanced nucleation [36,123,124].

In the current experiments, scratching at a much grosser scale also failed to enhance nucleation. In the one instance in which a diamond particle was detected in the AFM observation, it was associated with no obvious surface feature, see Figure 5.14. This observation is not consistent with the conclusion that diamond nucleation is favored on prominent surface features such as sharp edges or points [95,96]



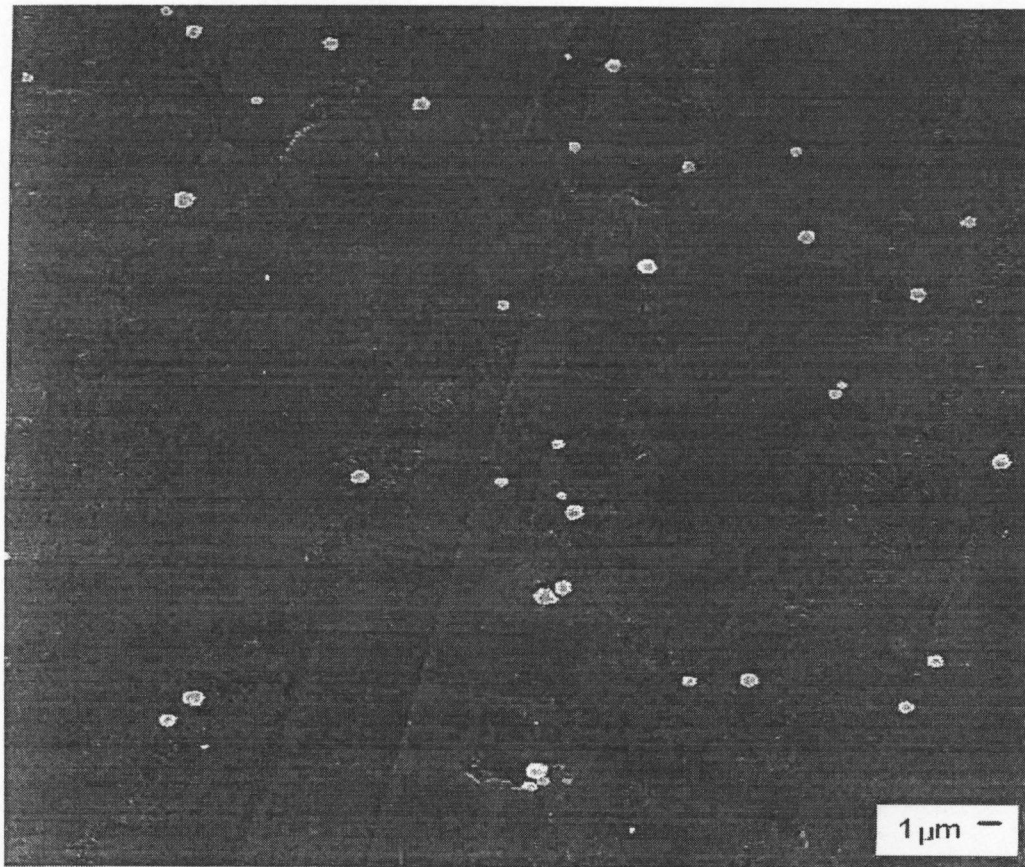


Figure 5.13: Scanning electron micrograph showing diamond nucleation on a sample scratched with SiC abrasive paper. Nucleation density is about  $3 \times 10^5$  particles per  $\text{cm}^2$ . Magnification is 2K.

**Table 5.4: Ratio of nucleation density on silicon substrates abraded with Al<sub>2</sub>O<sub>3</sub>, SiC, and Diamond.**

Substrate	Nucleation ration normalized to the virgin sample
Virgin	1
Al <sub>2</sub> O <sub>3</sub> abraded	5.6
SiC abraded	400
Diamond abraded	228000

These observations are consistent with the view that diamond debris is embedded in the substrate surface during the abrading and these very small diamond particles act as nuclei for the subsequent CVD growth [51,97,99].

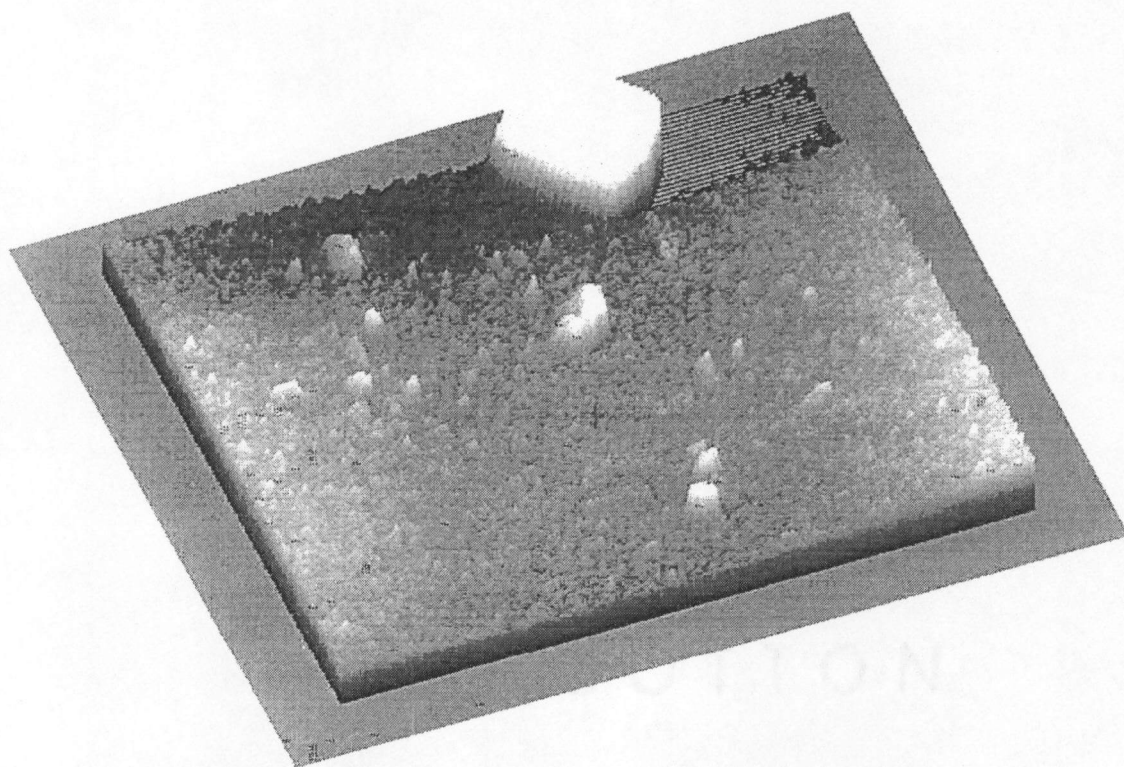


Figure 5.14: AFM micrograph showing a diamond particle which does not seem to be associated with any obvious surface features. The absence of the roughness on the right side of the particle is due to scanning defects in the AFM apparatus and is not part of the surface features. Magnification is 10K and 1K.

## 5.2 Ion beam Treatment

The estimates of nucleation densities of samples implanted with silicon and grown under various conditions are summarized in Table 5.5. The data indicates that essentially no suppression of nucleation for ion doses less than  $2 \times 10^{15}$  Si/cm<sup>2</sup> and a high degree of suppression after doses of  $1 \times 10^{16}$  Si/cm<sup>2</sup> and higher.

Figure 5.15 shows a SEM photograph for a typical area on the sample implanted with  $5 \times 10^{14}$  Si/cm<sup>2</sup> exposed to H<sub>2</sub> - 1% CH<sub>4</sub> for one hour. The boundary between the implanted and unimplanted region cannot be distinguished, indicating no detectable effect of implantation on nucleation.

Similarly, a sample implanted with  $1 \times 10^{15}$  Si/cm<sup>2</sup> and exposed for 12 hours to H<sub>2</sub>-0.5% CH<sub>4</sub> contained a continuous diamond film. This figure indicates little or no effect of the implantation on diamond nucleation. The RBS-ion channeling spectra for a sample implanted with  $1 \times 10^{15}$  Si/cm<sup>2</sup>, given in Fig 5.16, show that the silicon surface was highly damaged but not totally disordered (amorphous). The amorphous state would be indicated if the aligned spectrum (□) were completely coincident with the random spectrum (o) in the near surface region. Further evidence that the surface region was not amorphous is given by the high surface peak after annealing at 1000° C for 2 hours (x). Such a spectrum suggests either a polycrystalline or microcrystalline microstructure, or the retention of lattice disorder in the form of complex defect structures. If the surface had been amorphous, annealing under these conditions should produce a highly perfect single crystal due to epitaxial regrowth from the undamaged substrate. In that case the

**Table 5.5: Nucleation densities of samples implanted with silicon and grown under various conditions**

Substrate/pretreatment(polish material/time in min)	Implantation dose(per-cm <sup>2</sup> ) /energy (KeV)	Growth-Conditions CH <sub>4</sub> %/runtime (min)	Nucleation-density-(particles/cm <sup>2</sup> ) implanted/masked
SSA05 diamond/15	2x10 <sup>15</sup> /150	0.5/75	None/1.6x10 <sup>8</sup> – 2.9x10 <sup>8</sup>
SSA07diamond/10	2x10 <sup>15</sup> /150	0.5/15:40 hrs	6.6x10 <sup>6</sup> / continuous film
SSA26 diamond/10	5x10 <sup>14</sup> /150	1/60	1x10 <sup>8</sup> /continuous film
SSA27 diamond/10	5x10 <sup>14</sup> /150	1/60	1x10 <sup>8</sup> /continuous film
SSA29 diamond/10	1x10 <sup>15</sup> /150	1/120	Continuous film everywhere
SSA30 diamond/10	1x10 <sup>15</sup> /150	1/60	Continuous film everywhere
SSA31a diamond/10	1x10 <sup>15</sup> /150	1/60	3x10 <sup>8</sup> /continuous film
SSA31b diamond/10	1x10 <sup>15</sup> /150	1/60	4x10 <sup>8</sup> /continuous film
SSA41 diamond/10	2x10 <sup>15</sup> /150	1/15:40 hrs	Continuous film everywhere
SSA42 diamond/10	1x10 <sup>16</sup> /150	1/15:40 hrs	1x10 <sup>4</sup> /continuous film
SSA43 diamond/10	2x10 <sup>16</sup> /150	1/15:40 hrs	1x10 <sup>4</sup> /continuous film
SSA31B diamond/10	2x10 <sup>15</sup> /150	1/60	4x10 <sup>6</sup> /2x10 <sup>7</sup>
SSA31D diamond/10	2x10 <sup>15</sup> /150	1/60	7x10 <sup>7</sup> everywhere
SSA31G diamond/10	2x10 <sup>15</sup> /150	1/60	2x10 <sup>8</sup> everywhere
D diamond/10	1x10 <sup>15</sup> /150	1/60	Continuous film everywhere
E diamond/10	1x10 <sup>15</sup> /150	1/60	1x10 <sup>8</sup> everywhere
F diamond/10	1x10 <sup>15</sup> /150	1/60	1x10 <sup>8</sup> /2x10 <sup>8</sup>
G diamond/10	1x10 <sup>15</sup> /150	1/60	1.1x10 <sup>8</sup> /2.2x10 <sup>8</sup>
H diamond/10	1x10 <sup>15</sup> /150	0.5/12 hrs	1x10 <sup>7</sup> /continuous film
J diamond/10	1x10 <sup>17</sup> /150	0.5/54 hrs	7x10 <sup>3</sup> /continuous film

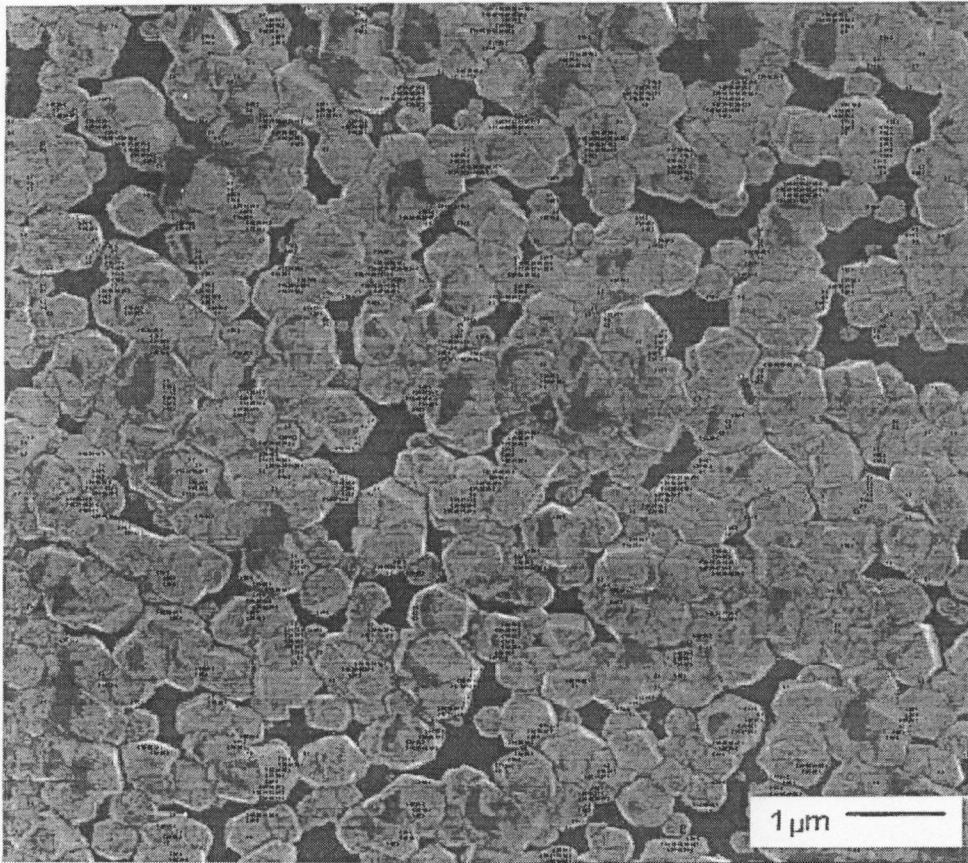


Figure 5.15: Scanning electron micrograph of a sample implanted with  $5 \times 10^{14} \text{ Si/cm}^2$  and exposed to 1.0%  $\text{CH}_4$  concentration. No boundary was detected between the implanted and non-implanted regions.

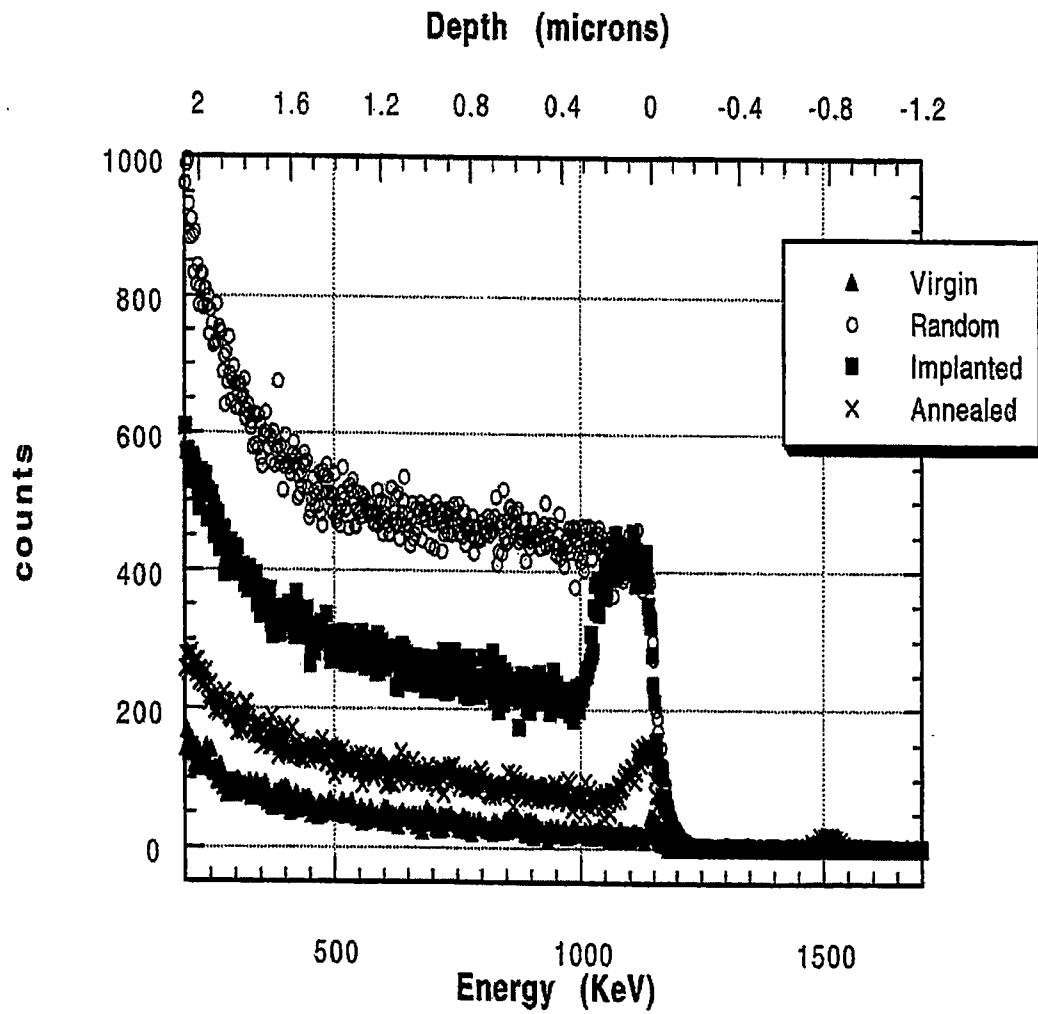


Figure 5.16: RBS/channeling spectra for a sample implanted with  $1 \times 10^{15} \text{ Si/cm}^2$

annealed aligned spectrums (x) would be coincident with the virgin aligned spectrum (▲).

The electron channeling pattern obtained in the SEM shows that the surface is a single crystal, Figure 5.17. Thus, the surface peak in the RBS-ion channeling spectrum appears to be due to retained lattice disorder.

The results for samples implanted with  $2 \times 10^{15}$  Si/cm<sup>2</sup> show almost complete suppression in sample SSA05, Nucleation densities obtained from Fig 5.18 were  $7 \times 10^2$  in the implanted region and  $10^7$  to  $10^8$  particles/cm<sup>2</sup> in the unimplanted region. On the other hand, Figure 5.19 shows only a slight suppression in the implanted area ( $\sim 10^7$ ) for a sample also implanted with  $2 \times 10^{15}$  Si<sup>+</sup>/cm<sup>2</sup> and exposed to H<sub>2</sub>-0.5% CH<sub>4</sub> for 15.67 hours and no suppression, i.e., a continuous film for the sample exposed to H<sub>2</sub>-1%CH<sub>4</sub> for 16 hours, Figure 5.20.

The dose of  $2 \times 10^{15}$  Si/cm<sup>2</sup> appears to be borderline for amorphizing the silicon substrate. Since the critical dose for amorphization increases with increasing implantation temperature, differences in the efficiency of the thermal bond between the sample and the liquid nitrogen-cooled sample holder could be responsible for differences in behavior of samples exposed to the same nominal dose. The total number of incident ions is determined by a Faraday cup in the beam line. The ion beam current during implantation is manually controlled. Temporary increases in the beam current during implantation could also increase beam heating of the sample.

Almost complete suppression of nucleation was found in all samples implanted with doses of  $1 \times 10^{16}$  Si/cm<sup>2</sup> and higher. The SEM photograph shown in Fig 5.21 for the



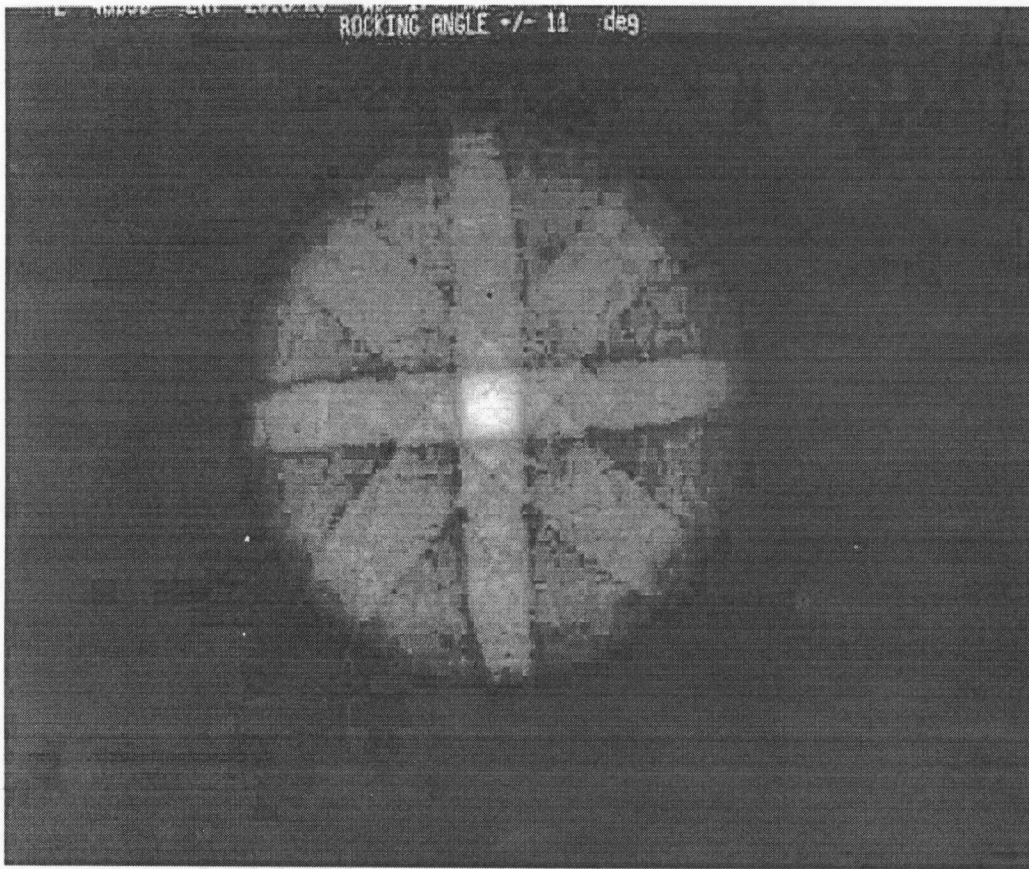


Figure 5.17: Scanning electron channeling pattern of an annealed silicon sample showing that surface to be a single crystal.

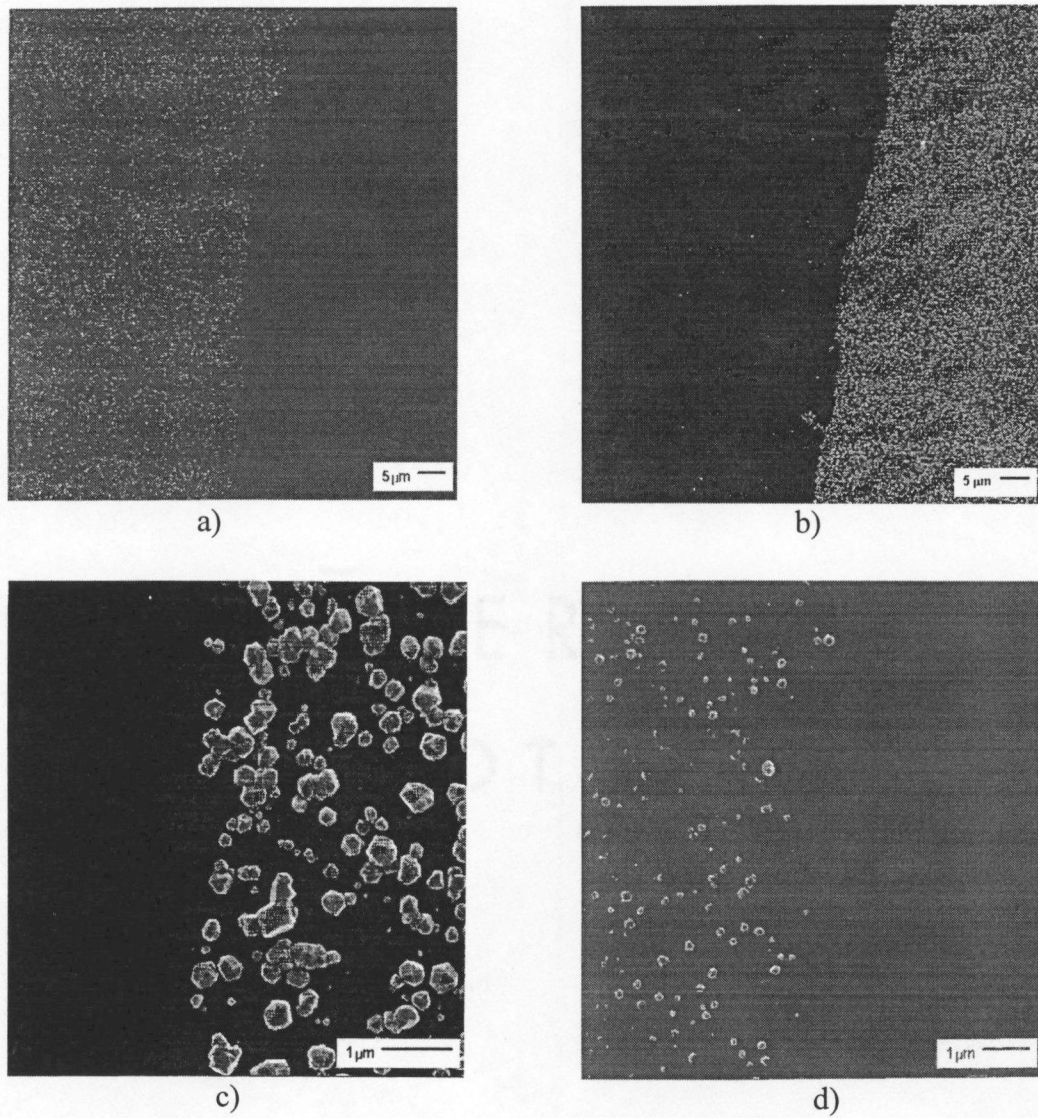
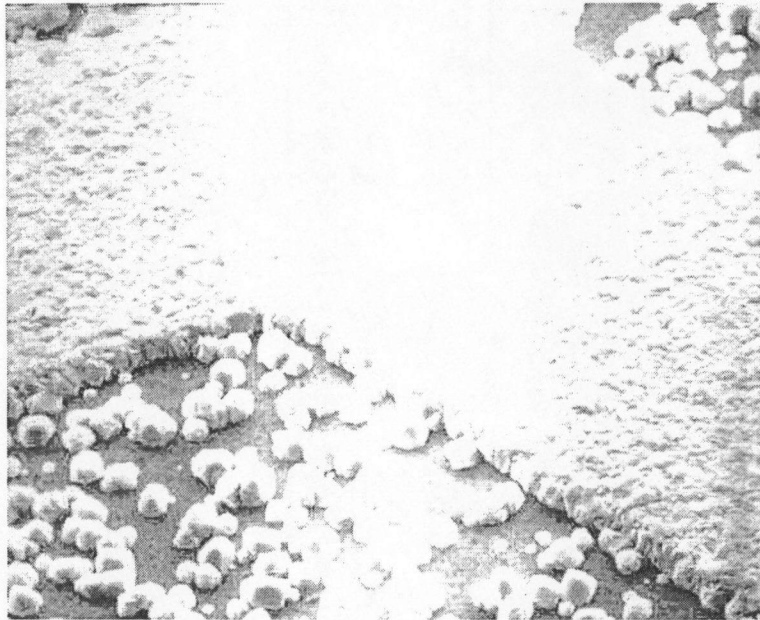
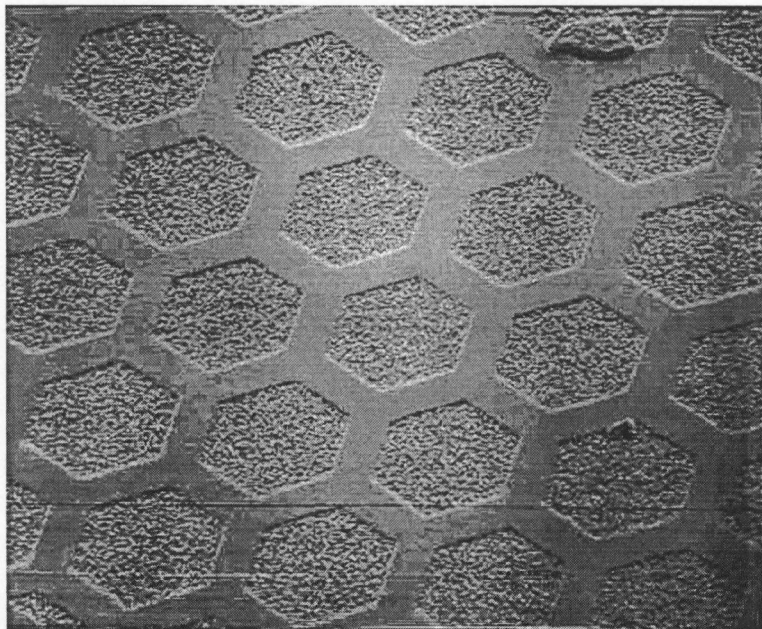


Figure 5.18: Scanning electron micrograph showing the difference in nucleation density between an implanted and non-implanted region of a silicon sample that was implanted with  $2 \times 10^{15}$  Si/cm<sup>2</sup>. The nucleation density in the implanted region is  $7 \times 10^2$  particles per cm<sup>2</sup>, and in the non-implanted region it is  $10^7$ - $10^8$  particles per cm<sup>2</sup>. a)1.2K, b)1.2K, c)15K, d)10K



a)



b)

Figure 5.19: Scanning electron micrograph showing slight suppression of nucleation in the implanted regions for a sample implanted with a dose of  $2 \times 10^{15} \text{ Si}^+/\text{cm}^2$ , and inserted into a 0.5%  $\text{CH}_4$  CVD reaction for 16.67 hours. The nucleation density in the implanted regions is about  $\sim 10^7$  particles per  $\text{cm}^2$ . a) 1.0 Kx, b) 0.1 Kx.

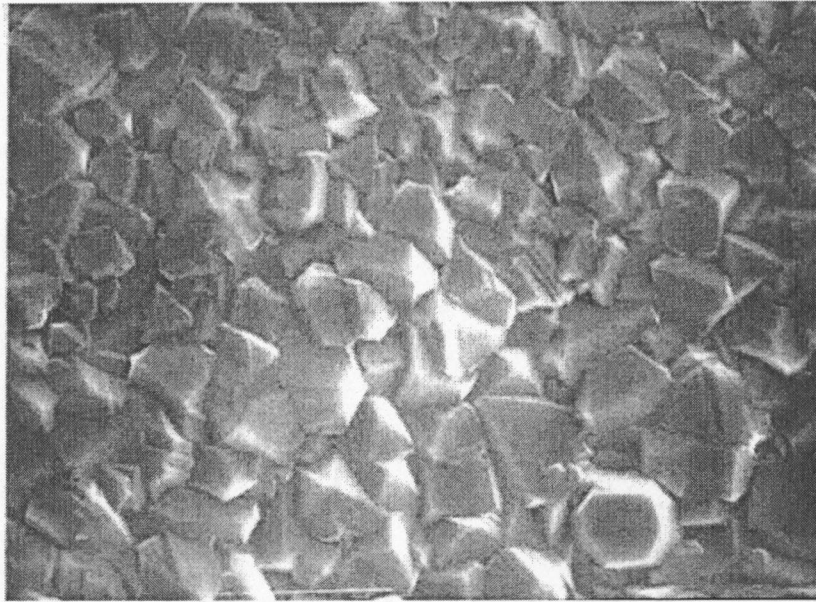
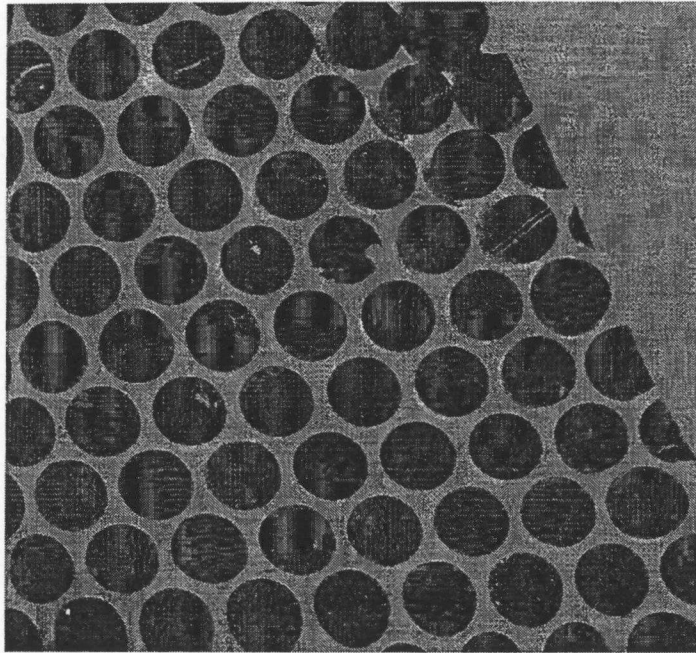
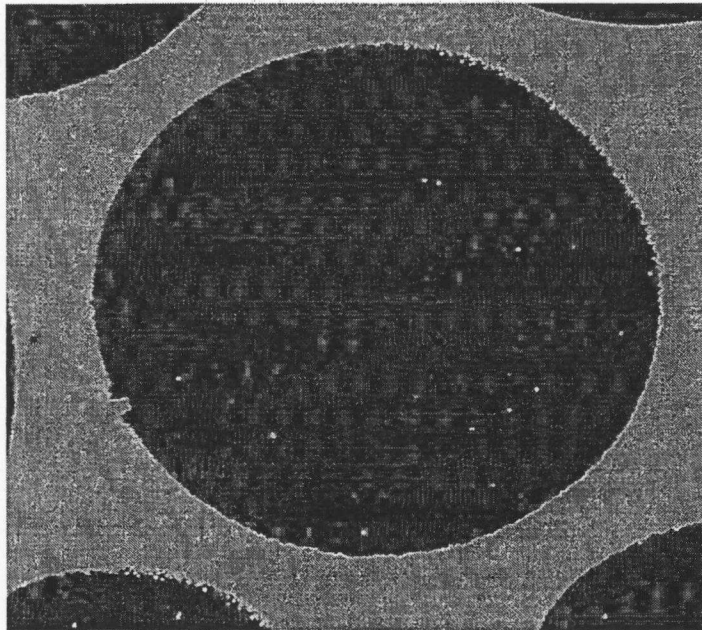


Figure 5.20: Scanning electron micrograph showing no suppression of diamond nucleation for a sample implanted with a dose of  $2 \times 10^{15} \text{ Si}^+/\text{cm}^2$ , and inserted into a 1.0%  $\text{CH}_4$  CVD reaction for 16 hours. Magnification is 1.85Kx.



a)



b)

Figure 5.21: Scanning electron micrograph showing almost complete suppression of nucleation. The sample was implanted with  $1 \times 10^{17}$   $\text{Si}^+/\text{cm}^2$  and run for 6 hours in a 0.5%  $\text{CH}_4$  concentration. a) 40x, b) 300x.

sample implanted with  $1 \times 10^{17}$  Si/cm<sup>2</sup> and grown for 6 hours in 0.5% CH<sub>4</sub> show a good, continuous diamond grid over the masked region (unimplanted) and only a few ( $\sim 10^4$  per cm<sup>2</sup>) diamond crystals on the implanted regions. The RBS-ion channeling spectra of Fig 5.22 indicate the surface to be amorphous to a distance of about 0.5  $\mu$ m from the surface. The spectra also shows a good quality epitaxial regrown surface after the annealing during growth (x). The energy of backscattering ions in the RBS process is directly related to the mass of the scattering ion. The spectra from diamond (C) appears at a lower energy than that from Si and is, therefore, hidden in the background of the Si-spectrum.

Since the deposited damage energy per atom required to amorphize single crystal diamond is reported to be less than that to amorphize silicon (5.5 eV/atom vs. 42 eV/atom), it was initially thought that an implantation condition might be found whereby the diamond debris would be amorphous but the silicon substrate would be crystalline.

Calculations of deposited damage energy in diamond and in silicon were performed using the TRIM code [113]. One output of TRIM is the number of vacancies created by primary and secondary elastic collisions as a function of depth from the free surface for each bombarding ion. Equation 2.4 can be rewritten as:

$$E = 2E_d * N(E),$$

where  $E_d$  is the displacement energy and  $N(E)$  is the number of vacancies (displaced atoms). The deposited damage energy per incident ion was calculated as a function of distance from the surface. Literature values were used for  $E_d$  for silicon (20 eV) [125] and diamond (80 eV) [126]. The number of vacancies was converted to vacancy

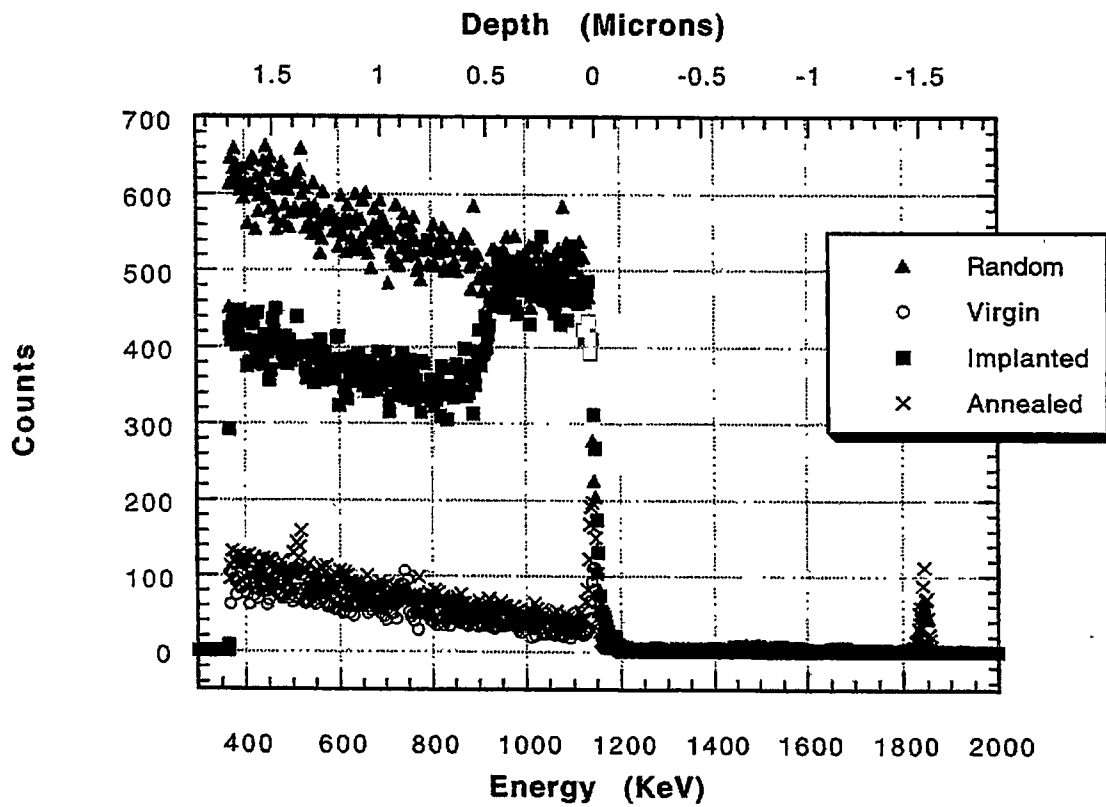


Figure 5.22: RBS/channeling for sample J. Note that the annealed spectrum coincides with the virgin one. The peak at about 1800 KeV, is W deposit.

concentration or per target atom by dividing by the atom density of silicon or diamond. The damage energy per atom was then calculated using the values of  $E_d$ .

Applying the TRIM results in the conventional manner for a dose of  $1 \times 10^{15}$  Si/cm<sup>2</sup> yields a value for deposited damage energy of 20 eV/atom at 5 nm into the silicon and a value of 39 eV/atom at 180 nm (the position of peak deposited energy). The critical value for amorphization of silicon is 42 eV/atom for implantation at 77K [127]. The calculation predicts that the surface of silicon would not be amorphous after this dose. The deposited energy approaches the critical value at 180 nm. The same calculation for diamond gives a value of 9.9 eV/atom at 3 nm and a peak value of 20 eV/atom at 90 nm. Thus, if each carbon atom were struck by an incident silicon ion, the diamond should be amorphous at the surface but the silicon would remain crystalline.

It was realized that the number of ions striking unit surface area of target might be less than the areal density of atoms at low doses. In this case, multiplying the vacancy (or damage energy) concentration by the total dose could overestimate the effect of ion bombardment.

The areal density of silicon is approximately  $1.369 \times 10^{15}$  atoms per cm<sup>2</sup>. For an ion dose of  $1 \times 10^{15}$  Si/cm<sup>2</sup>, only 1/1.37 of the silicon target atoms would be impacted by the ion beam. Thus the "effective" dose was approximately  $0.73 \times 10^{15}$  ions/cm<sup>2</sup> and the energy deposited was about 15 eV per atom. Again, this is less than the critical value.

Diamond has an areal density of  $3.136 \times 10^{15}$  atoms per cm<sup>2</sup>. Dividing the total dose of  $1 \times 10^{15}$  by this areal density indicates that approximately 1/3 of the carbon atoms will be hit by a bombarding ion. Thus the "effective" deposited damage energy is ~3.3



eV/atom rather than 9.9 eV/atom, and the diamond debris on the surface would not have amorphized.

An alternate method of estimating the deposited damage energy density for diamond is to consider the fraction of the sample surface exposed to the ion beam that is composed of diamond debris particles. The diamond debris left after ultrasonic abrasion has an average size of 10 nm or less, giving an area of about  $100 \text{ (nm)}^2$  per particle [99]. The number of diamond atoms on a surface of  $100 \text{ (nm)}^2$  is about 3136. An ion dose of  $1 \times 10^{15} \text{ ions/cm}^2$  corresponds to  $10^3 \text{ Si/(nm)}^2$ , or one ion per 3.14 diamond atoms, as above.

The deposited damage energy was scaled to ion dose and values at the surface and peak damage position are given in Table 5.6. These calculations indicate that the critical values for amorphization of both diamond and silicon was reached at a dose of about  $2 \times 10^{15} \text{ Si/cm}^2$ . This indicates that the dose of  $2 \times 10^{15} \text{ Si/cm}^2$  was indeed borderline, consistent with the experimental observations. The calculations also indicate that attempts to amorphize the diamond without amorphizing the silicon would not be successful.

The data given in Table 5.7 indicate that amorphization of diamond and/or silicon suppresses nucleation under some conditions used in this study. It was reported that amorphous silicon (due to ion implantation) is much more chemically reactive than crystalline silicon [128-130]. Therefore, reaction of Si with the hydrocarbon gas to form SiC should be faster for the amorphous Si than the crystalline Si. If formation of SiC

**Table 5.6: damage energy values at the surface and peak damage scaled to ion dose for both silicon and diamond targets.**

Target : Si

Dose( $\times 10^{15}$ ) ions/cm <sup>2</sup>	Surface damage energy (eV/atom) at 5nm	Effective damage energy (eV/atom) at 5nm	Peak damage energy (eV/atom) at 180nm
1	20.2	14.8	38.9
2	40.4	29.6	78.8
10	202	148	389
100	2020	1480	3890

Target : Diamond

Dose( $\times 10^{15}$ ) ions/cm <sup>2</sup>	Surface damage energy (eV/atom) at 3nm	Effective damage energy (eV/atom) at 3nm	Peak damage energy (eV/atom) at 90nm
1	9.9	3.2	19.7
2	19.8	6.4	39.4
10	99	32	197
100	990	320	1970

**Table 5.7: Nucleation on Ion Implanted Silicon Substrates.**

Sample	Dose Si/cm <sup>2</sup>	Growth conditions	Density of nuclei implanted	of nuclei unimplanted	Remarks
SSA02	-----	1%/1hr	-----	~ 10 <sup>8</sup>	Unimplanted reference
SSA26	5x10 <sup>14</sup>	1%/1hr	10 <sup>8</sup> to complete film		No suppression
SSA29	1x10 <sup>15</sup>	1%/1hr	Continuous film		No suppression
H	1x10 <sup>15</sup>	0.5%/12hr	10 <sup>7</sup>	continuous	Very little effect
SSA05	2x10 <sup>15</sup>	0.5%/1.25hr	>10 <sup>2</sup>	10 <sup>4</sup> - 10 <sup>8</sup>	Complete suppression
SSA07	2x10 <sup>15</sup> (TEM mask)	0.5%/15.67h	7x10 <sup>6</sup>	continuous	Some suppression
		r			
SSA41	2x10 <sup>15</sup>	1%/16hr	Continuous film		No suppression
SSA42	1x10 <sup>16</sup> (TEM mask)	1%/15.67hr	10 <sup>4</sup>	continuous	Good grid, suppression
SSA43	2x10 <sup>16</sup> (TEM mask)	1%/15.67hr	10 <sup>4</sup>	continuous	Good grid, suppression
J	1x10 <sup>17</sup> (TEM mask)	0.5%/6hr	10 <sup>4</sup>	continuous	Good grid, suppression

were a prerequisite for nucleation of diamond, then nucleation nuclei and the process is homoepitaxial rather than heteroepitaxial in nature.

Doses of  $5 \times 10^{14}$  and  $1 \times 10^{15}$  Si/cm<sup>2</sup> did not suppress nucleation. A nominal dose of  $2 \times 10^{15}$  is borderline between completely suppressing nucleation and having no effect. These observations suggest that the diamond debris remains highly effective as nucleating sites even at high levels of irradiation damages. Significant suppression occurred only in instances in which the diamond was undoubtedly amorphous. The observations also suggest that the carbonaceous material produced as a result of amorphization is not an effective nucleating agent.

### **5.3 Observations on Carbon Contamination – SiC**

Several reports [131-133] have claimed that a carbide phase such as SiC precedes the nucleation of diamond and that is a necessary condition for CVD of diamond. Other reports have concluded that this is not true, and that there are no carbide phases preceding diamond nucleation [134,135], while others have shown that SiC does not enhance the nucleation of diamond [81,136].

In order to determine the feasibility of growing diamond micro-components to near-net shape (part II of this dissertation), a sample implanted with  $1 \times 10^{17}$  Si<sup>+</sup>/cm<sup>2</sup> was exposed in the growth chamber for several sequential periods. After this implantation dose, the silicon substrate and the diamond debris were amorphous in the unmasked areas, i.e. in the ion-bombarded areas. The history of this sample is summarized in Table 5.8.

The etchant used was nitric-hydrofluoric acid, CP6-S. In order not to etch away

**Table 5.8 History of sample J implanted with  $1 \times 10^{17}$  Si<sup>+</sup>/cm<sup>2</sup> and exposed in the growth chamber for the indicated sequence.**

Time	Post-growth examination	Observations
6 hours	SEM	2.5 $\mu\text{m}$ thick diamond grid in unimplanted areas. Few particles on implanted areas, density $9 \times 10^3$ particles per $\text{cm}^2$
6 hours	SEM, RBS	Grid is 5.8 $\mu\text{m}$ thick. No new particles in implanted areas, density of $7 \times 10^3$ particles per $\text{cm}^2$ . Regrowth of amorphous Si to good quality single crystal.
Etched	SEM	Grid not attacked. Uneven attack of implanted areas.
6 hours	SEM, EDS	Grid is 9.7 $\mu\text{m}$ thick. New nuclei in unattacked areas ( $1.3 \times 10^5$ particles per $\text{cm}^2$ ). Very few nuclei on rough etched area ( $2.5 \times 10^4$ particles per $\text{cm}^2$ ). EDS indicates Si and C signals
12 hours	SEM	Grid is 23 $\mu\text{m}$ thick. New nuclei in unattacked areas ( $8 \times 10^4$ particles per $\text{cm}^2$ ). Very few nuclei in rough etched area ( $4 \times 10^3$ particles per $\text{cm}^2$ ).
24 hours	SEM	Grid is 45 $\mu\text{m}$ thick. Density in attacked area is $7 \times 10^3$ particles per $\text{cm}^2$ . Unattacked area developed a continuous film.

the entire silicon substrate from under the diamond film, a silicon test sample was first completely etched away, and the time taken for that to happen was recorded. It took about 8 minutes for the acid to eat through the entire thickness of the sample (0.5 mm). Taking into consideration the incubation period for the acid to start reacting with the silicon, the sample containing the diamond grid was initially immersed in the acid for 80 seconds. The acid appeared to have etched the silicon away in a non-uniform manner i.e. a certain area of the sample was not affected at all by the acid. The SEM photographs given in Figures 5.23-5.25 illustrate that observation.

Observations at higher magnification showed that there was a thin film on top of the silicon surface, see Figure 5.26. Energy Dispersion Spectroscopy (EDS) measurements showed that the thin film grown on top of the silicon is composed of Si and C as illustrated in Figure 5.27.

The observation that a film containing C and Si formed on this sample could be explained by either of two arguments. (a) Carbon deposition in the early stages of growth was absorbed on the surface and diffused into the near surface region and formed a film of SiC on the entire wafer (implanted and unimplanted regions). The residual diamond debris in the unimplanted region began to nucleate diamond growth very early during exposure to the reactant gases, and a continuous diamond film was grown before the SiC could act as effective nucleating sites. (b) Carbon contamination occurred after the initial growth stages and formed either a hard carbon or a SiC film only on the exposed silicon, i.e., implanted region. The EDS signal from a silicon substrate would show both C on the surface and the Si substrate for very thin C films.

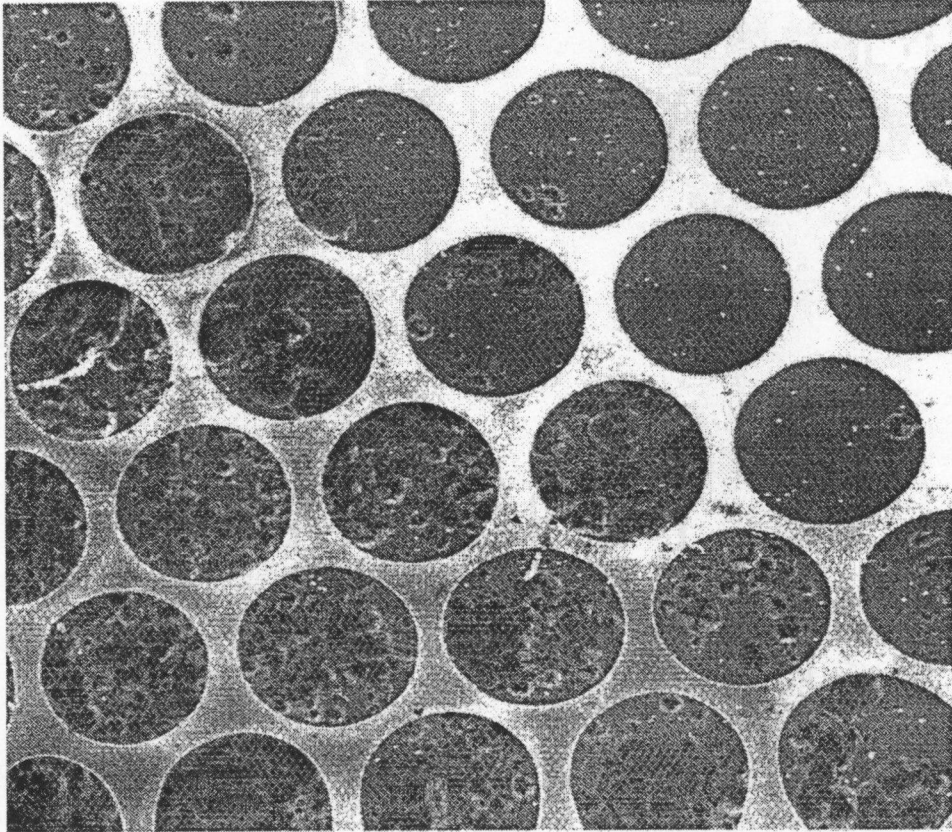


Figure 5.23: Scanning electron micrograph showing the boundary between the region that was affected by the etchant and the region that was unaffected. Note the upper right part of the graph still has diamond particles in the implanted region, while the lower left part has none since they were washed away due to the etchant. Magnification 70x.

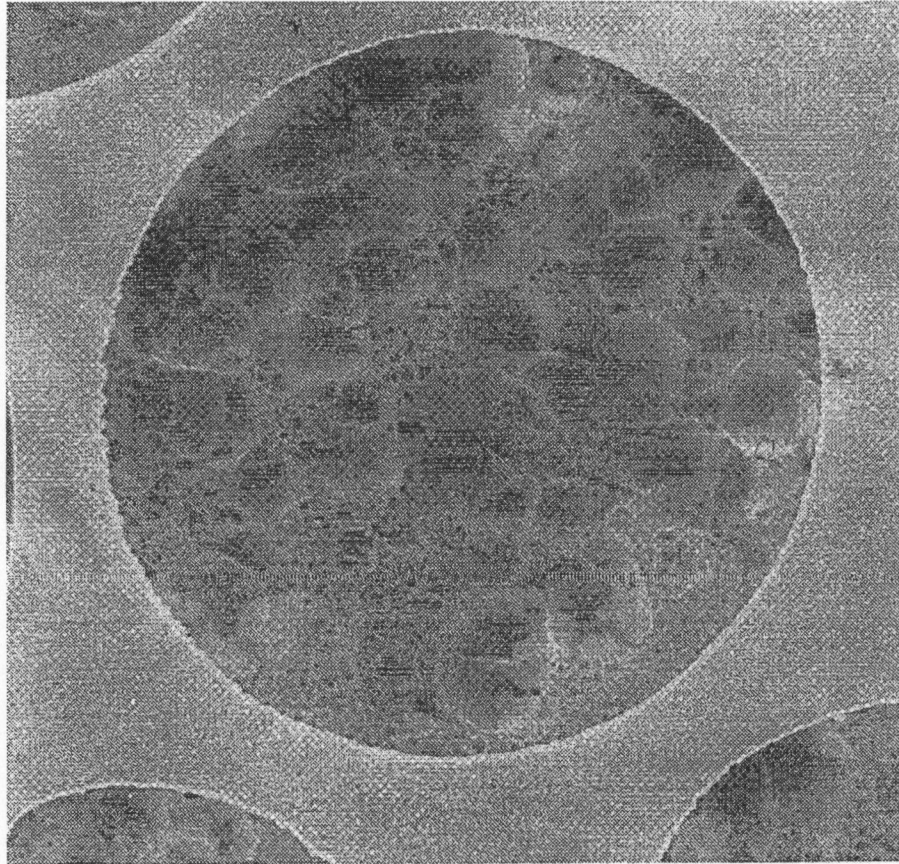


Figure 5.24: Scanning electron micrograph showing a high magnification (300x) of the region where the etchant was effective. No diamond particles left on the surface of the implanted region.



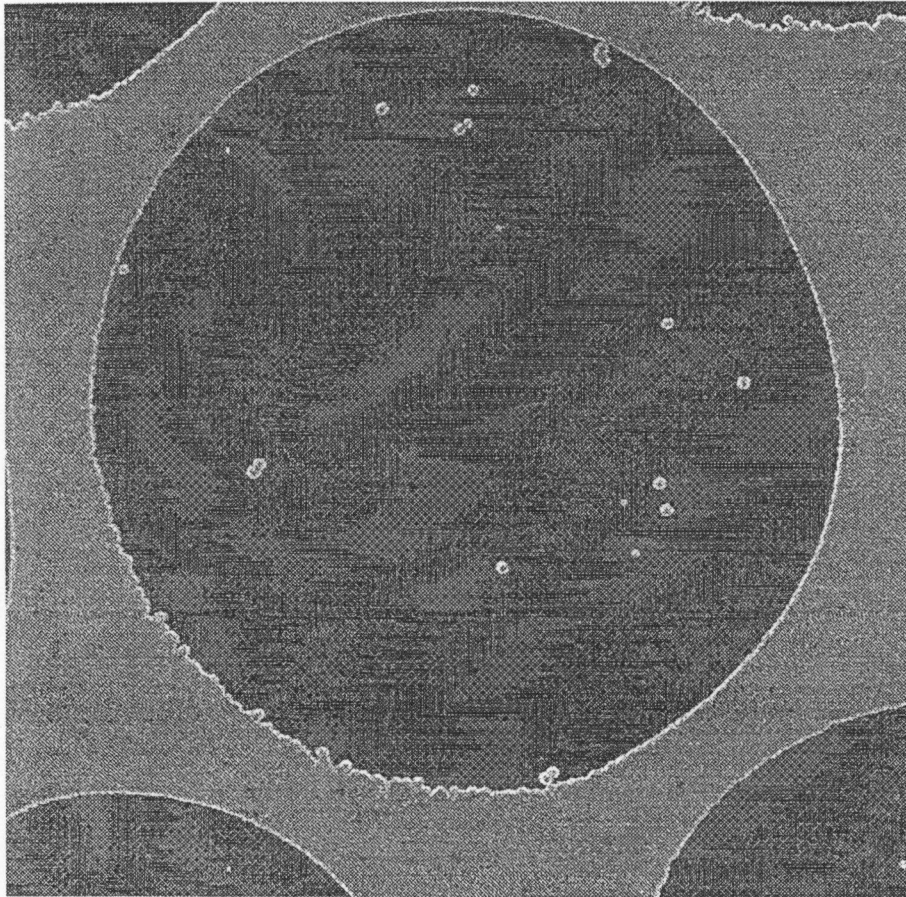
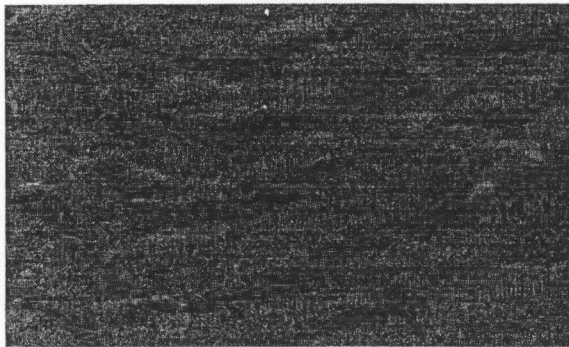
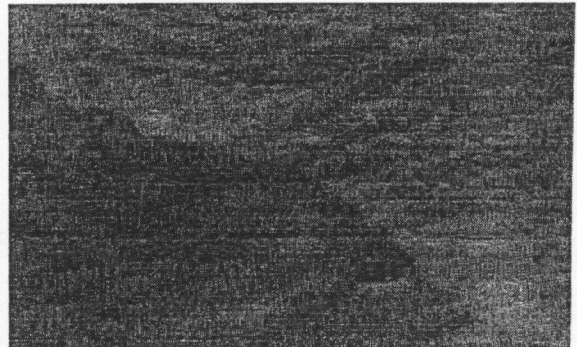


Figure 5.25: Scanning electron micrograph showing a high magnification (300x) of the part where the etchant was not effective. Note the diamond particles are still there.



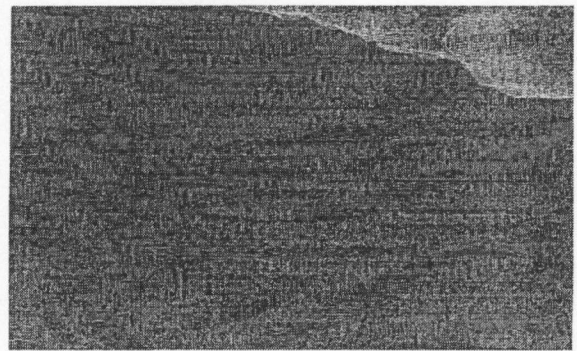
a)



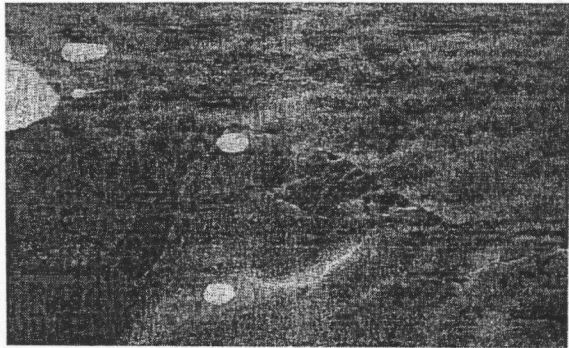
b)



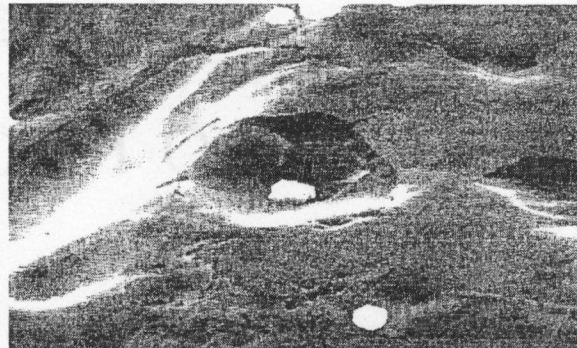
c)



d)

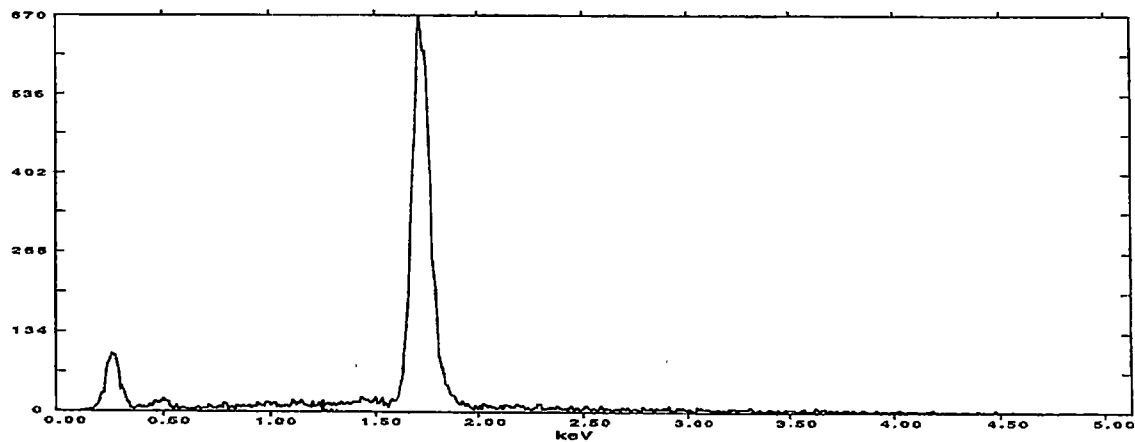


e)

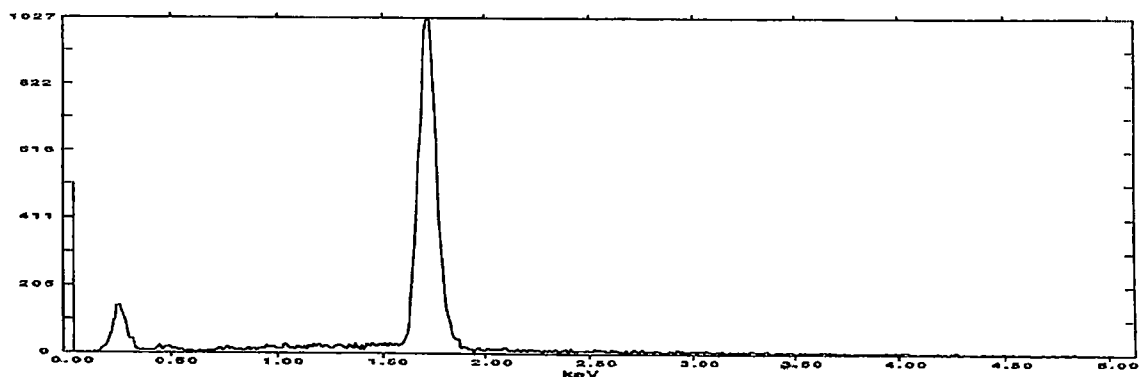


f)

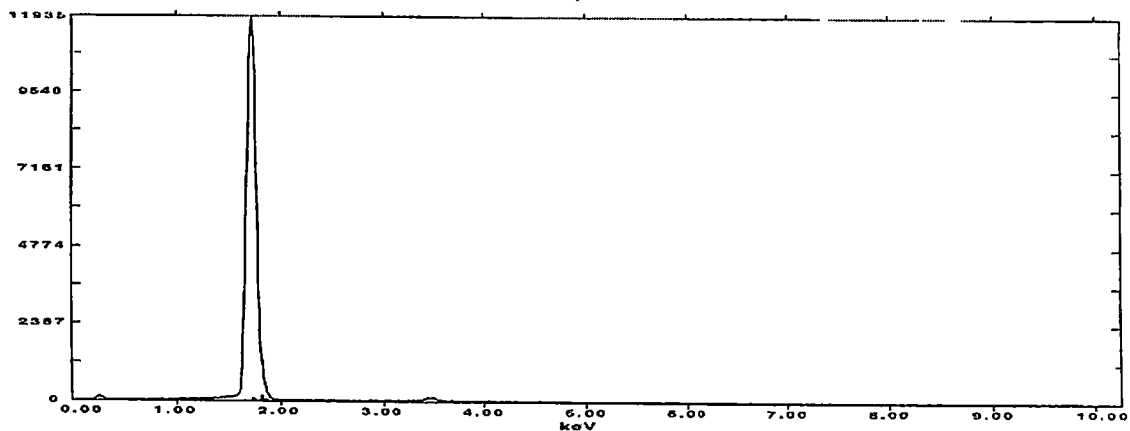
Figure 5.26: Scanning electron micrographs of different areas on J sample showing presence of a film between the silicon substrate and diamond particles.



a)



b)



c)

Figure 5.27: Energy dispersion spectrum on sample J. a) shows is a spectrum of the film on top of the silicon showing both a silicon peak and a carbon peak, b) shows a spectrum of an actual SiC sample, c) shows a spectrum taken on a silicon spot inside one of the implanted regions, at a 100K. Note in c) only the silicon peak shows.

The second explanation is favored by the following observations:

(a) Samples implanted with  $2 \times 10^{15} \text{ Si}^+/\text{cm}^2$  underwent deposition for times as long as 15.4 hours without evidence for formation of a contaminating film. The EDS examination of an implanted region detected only silicon, Figure 5.28.

(b) This film was detected only on a sample that had undergone a series of intermediate examinations and exposures in the growth chamber before the film was detected.

(i) The sample was examined in the SEM after 6 hours exposure. A continuous diamond film had formed over the unimplanted areas but only a very few stray diamond crystals were present in the implanted regions, see Figure 5.21.

(ii) The sample was replaced in the growth chamber for another 6 hours and examined by SEM again. The diamond film (grid) had become thicker but no new diamond crystals had formed on the implanted areas, see Figure 5.29.

(iii) The sample was then etched in nitric-hydrofluoric acid, rinsed in water and re-examined in the SEM. It was observed that the etching had been uneven across the sample face – some areas were apparently untouched and some were aggressively etched, leaving a rough Si surface. This suggests that the unattacked areas were protected by a

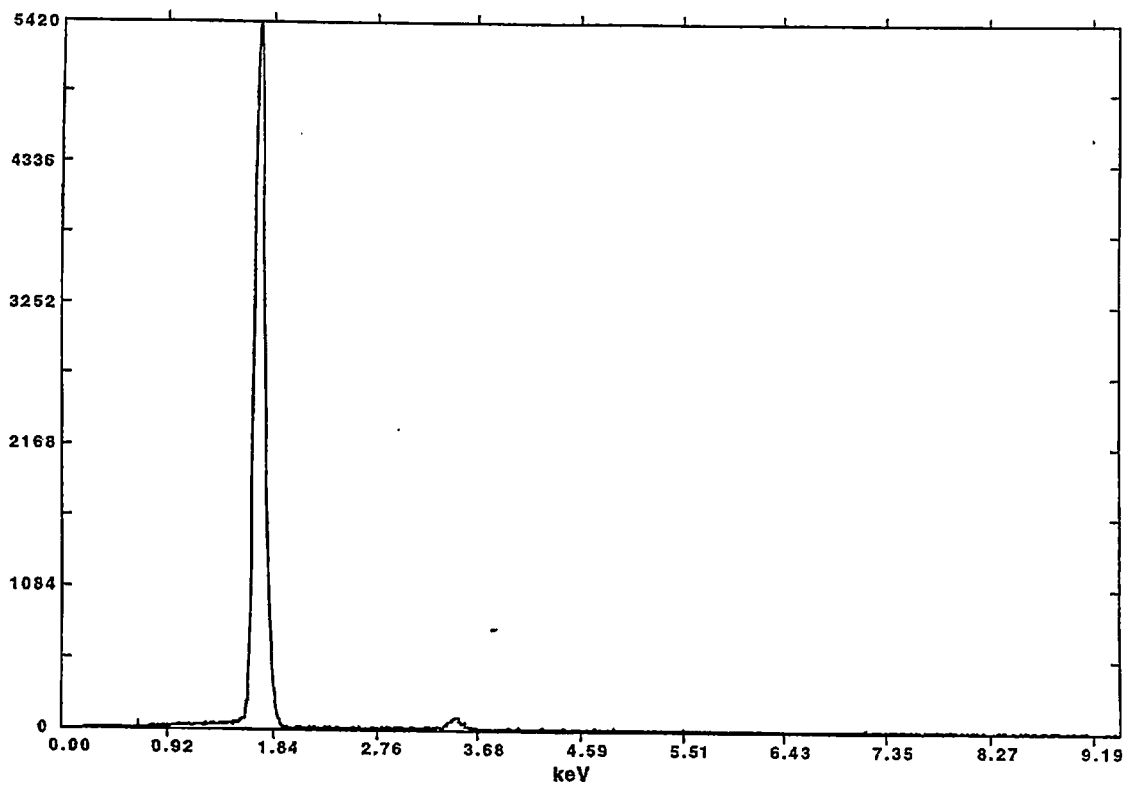
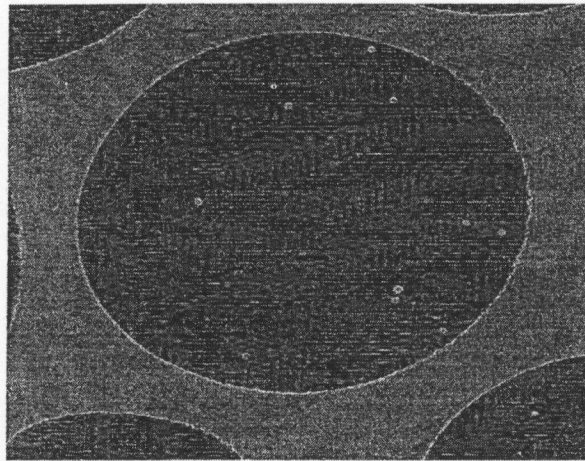
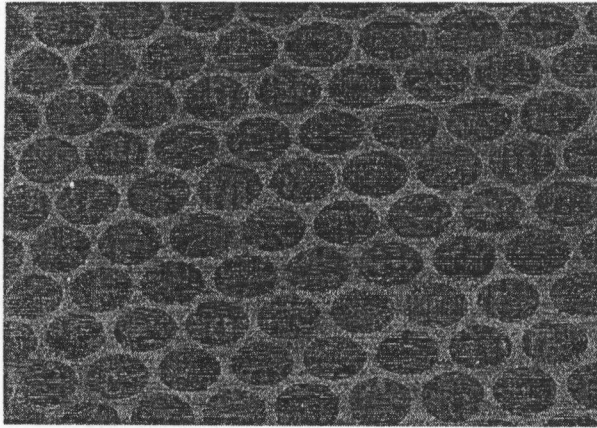


Figure 5.28: Energy dispersion spectrum for sample M, showing no carbon peak.



a)



b)



c)

Figure 5.29: Scanning electron micrographs for sample J, after the second run for six hours. Note that there are no new diamond nuclei in the implanted region. a) 300x, b)40x, c)10k taken for wall thickness.

film (C or SiC).

- (iv) The SEM examination after another 6 hours exposure to the reactant gases showed further growth of the diamond grid (over the unimplanted areas), no nucleation on the rough, etched implanted regions; and profuse nucleation on the unetched, implanted regions. The density of diamond particles was  $2.5 \times 10^4$  particles per  $\text{cm}^2$  in the etched areas and  $1.3 \times 10^5$  particles per  $\text{cm}^2$  in the unattacked areas. The results of the EDS examination (Figure 5.27) showed both C and Si to be present in the signal from the unetched, implanted areas.
- (v) The results after another 12 hours in the growth chamber were similar to those in (iv); very few nuclei ( $4 \times 10^3$  particles per  $\text{cm}^2$ ) on the rough, etched regions and a large number ( $7 \times 10^4$  particles per  $\text{cm}^2$ ) in the unetched, implanted regions. It was concluded from the observations (i) to (v) that carbonaceous contamination occurred during step (i) and/or (ii). This contamination resulted in formation of a very thin hard carbon or SiC film over the implanted regions. During further exposure in the growth chamber, diamond nucleation occurred in the regions containing this film. Very little nucleation occurred in the regions attacked by the etchant, i.e., the rough, clean silicon substrate.

It was noted in chapter 2, part A, that nucleation can occur on silicon carbide although it generally requires a long incubation period. Anger et al [83] reported that

amorphous carbon impurities on a silicon surface are active in promoting diamond nucleation but at a rate several orders of magnitude lower than surfaces abraded with diamond powder.

Longer times of etching with CP6-S on the same sample, resulted in breakage of some of the diamond film as a result of undercutting. SEM investigations of the area of the silicon surface where the diamond film broke off showed that the SiC carbide phase had indeed preceded the nucleation of diamond growth. Figures 5.30-5.31 show the silicon surface area where the diamond film broke off. The center of each three circles would have been the last point where the diamond breaks off. Such areas are shown to have SiC pieces still on the corners. Other SEM photographs given in Figures 5.32-5.33 show the SiC film extending from one ion-implanted region to another going through an unimplanted area where the diamond film had grown. Investigations of other substrates exposed to the same growth conditions indicated no such existence of any carbide phase. The conclusion drawn from such observations is that the existence of a SiC phase preceding diamond growth is a sufficient but not necessary condition for successful growth of CVD diamond.

#### **5.4 Annealing effects on the nucleation of CVD diamond**

Samples having several histories with respect to ion implantation were subjected to thermal anneals before they were inserted into the growth chamber. These treatments represented an attempt to separate the effect of damaged crystalline diamond debris, amorphous debris, and the crystalline to amorphous transformation of the silicon substrate on the nucleation process. Additional information was obtained on the effect of



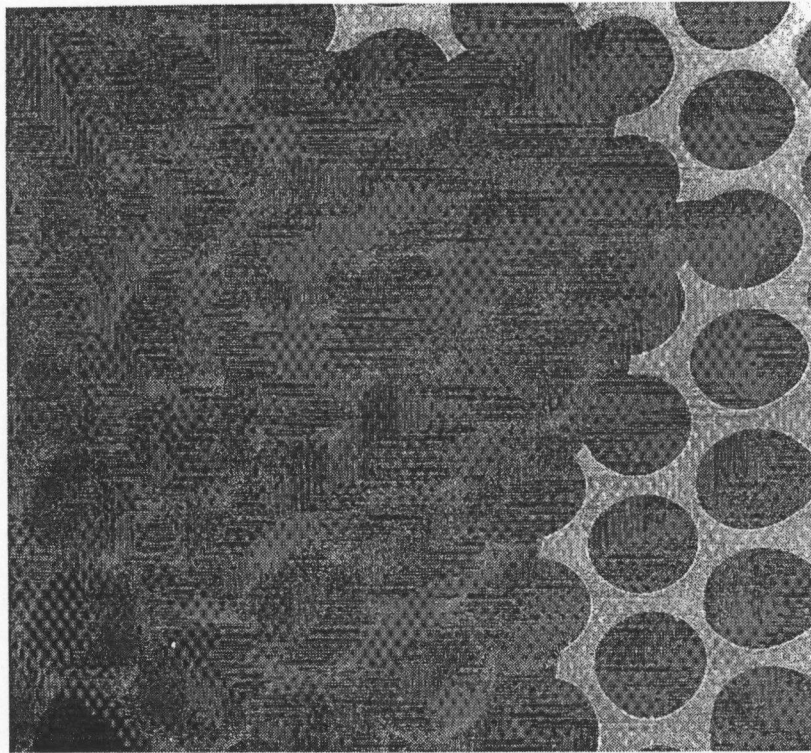


Figure 5.30: Scanning electron micrograph showing the area where part of the diamond grid fell off due to too much undercutting resulting from the etchant.

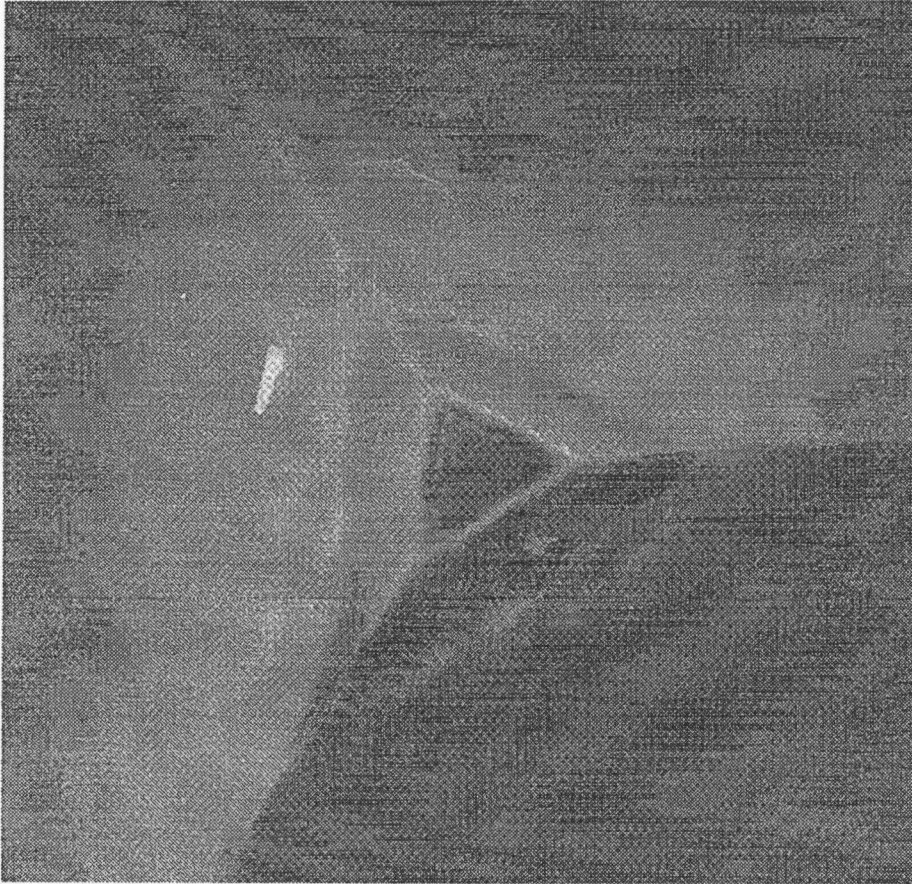


Figure 5.31: Scanning electron micrograph showing a center of three circles where diamond used to reside. Note the SiC on top of the silicon at that point.

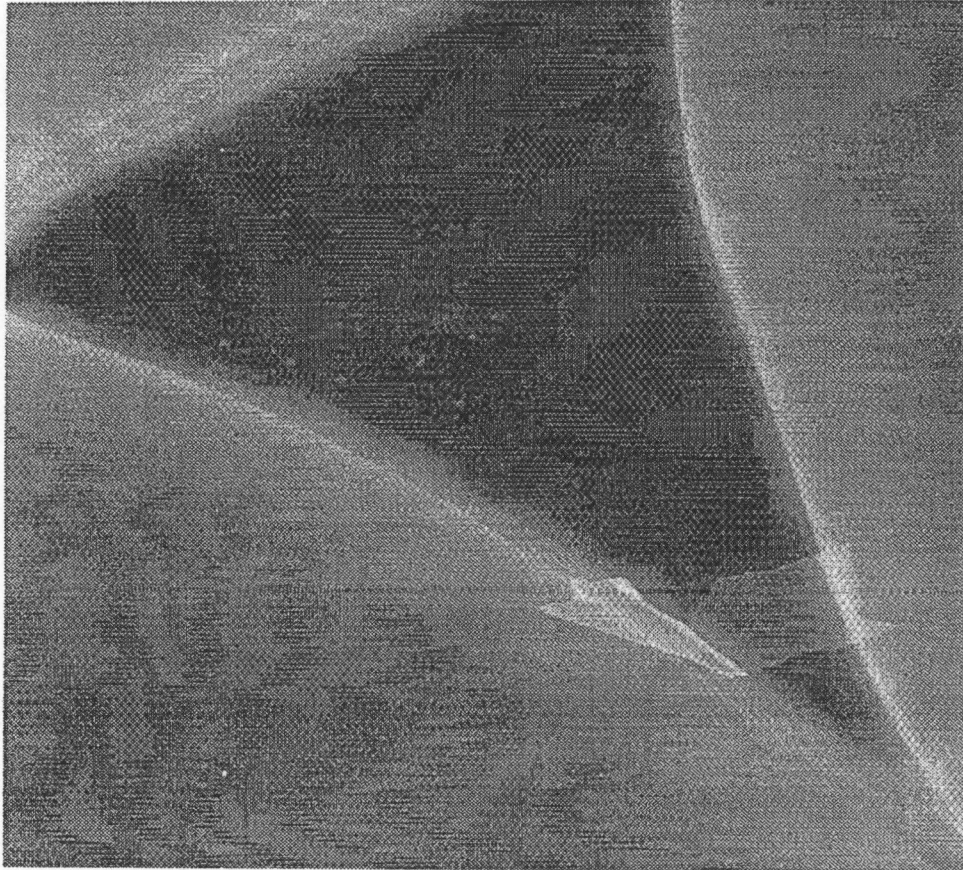


Figure 5.32: Scanning electron micrograph showing yet another center of three circles where diamond used to reside. Note the SiC film is stretched from one implanted area to another across a non-implanted area.

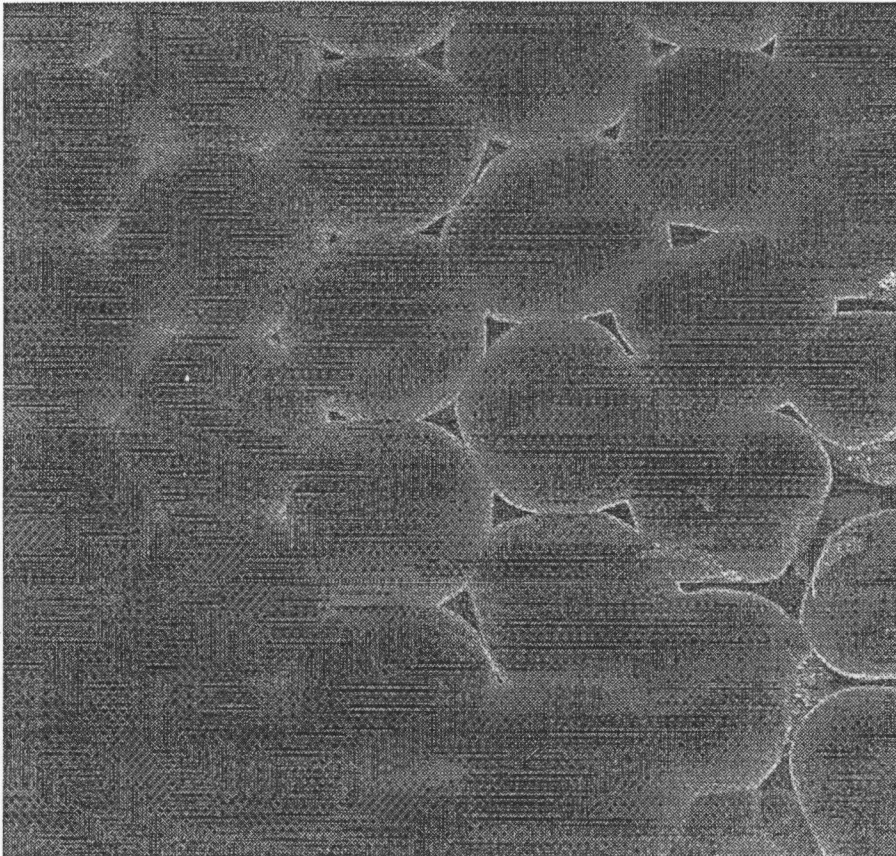


Figure 5.33: Scanning electron micrograph showing yet more areas where SiC is present under preexisting diamond.

annealing during the growth exposure by examining samples exposed to longer times during growth of micro-components.

The annealing experiments were designed using the following published information:

(a) Amorphous surface layers produced by ion bombardment undergo epitaxial regrowth from the undamaged substrate at temperatures in the range of 500° to 600° C [70] and times of a few minutes [137] (b) Diamond graphitizes in oxidizing atmospheres but the rate is slow and the incubation period is as long as 17 hours at 1450° C. Graphitization in vacuum of  $10^{-6}$  torr requires ~1h at 1675° C for the first detectable graphite to form [138];

(c) Small amounts of damage produced by low dose ion implantation of diamond can be recovered by annealing 1 hour at 1150° C in vacuum [139].

(d) Annealing diamond containing severe ion beam damage produces graphite in the damage region [140].

(e) Amorphous diamond produced by ion implantation does not revert to the diamond crystal structure during annealing at 1450°C in  $10^{-3}$  torr but turns to graphite [141].

(f) Graphite produced at diamond grain boundaries during CVD growth can be removed by exposure to hot hydrogen. The diamond is etched by the hydrogen-treatment but the reaction rate is extremely slow [142].

Because of the availability of annealing facilities, at the various stages of this investigation, four furnace configurations were used: (1) a growth chamber with an

uncarburized (W) filament; (2) a growth chamber with a carburized filament (WC); (3) the growth chamber itself during long exposures used for producing micro-components; and (4) a graphite furnace. Hydrogen was the environment for all configurations except (3) and a temperature of 1000° C was used for all anneals.

The results are analyzed in the form of a series of questions. They will be presented here as questions, results, and conclusions.

(1) Will annealing the diamond debris left by the slurry abrasion have an effect by graphitizing the diamond?

As-abraded (no implantation) samples were annealed for 2 hours: Specimens C, 44, and 31C in Table 5.9. A continuous diamond film was produced during subsequent exposure to growth conditions for 1 hour. A continuous film was also produced in 1 hour for specimen D that was annealed 2 hours before being implanted with  $1 \times 10^{15}$  Si/cm<sup>2</sup>.

The results indicate that annealing for 2 hours at 1000°C in hydrogen had no effect on nucleation and, thus, did not attack the diamond debris.

(2) Does annealing of lightly damaged diamond debris affect the nucleation efficiency of the debris?

A comparison of the observations for samples 26 and 27 indicate that no effect of annealing the lightly damaged diamond could be detected in this experiment. Both specimens were implanted with  $5 \times 10^{14}$  Si/cm<sup>2</sup> but only specimen 27 was annealed. Continuous films were formed in 1 hour growth time. This observation suggests that undamaged diamond and lightly damaged (by ion implantation) diamond debris are effective nucleating sites.

**Table 5.9: Annealing conditions and results.**

Specimen	Implantation (Si/cm <sup>2</sup> )	Pre-anneal time(h)	Growth Time(h)	Furnace No.	Nuclei Density in Implanted Region* (particles/cm <sup>2</sup> )
C	No	2	1	4	continuous film
44	No	2	1	2	continuous film
31C	No	2	1	1	continuous film
D	1x10 <sup>15</sup>	2(before Implantation)	1	4	continuous film
27	5x10 <sup>14</sup>	1	1	2	continuous film
26	5x10 <sup>14</sup>	0	1	2	>10 <sup>8</sup> to continuous film
E	1x10 <sup>15</sup>	2 before + 2 after	1	4	continuous film
G	1x10 <sup>15</sup>	2	1	4	continuous film
F	1x10 <sup>15</sup>	0	1	4	continuous film
30	1x10 <sup>15</sup>	2	1	4	continuous film
31a	1x10 <sup>15</sup>	2	1	4	3x10 <sup>8</sup> to continuous film
31b	0	2	1	4	4x10 <sup>8</sup> to continuous film
41	2x10 <sup>15</sup>	0	15.7	3	continuous film (anneal during growth)
07	2x10 <sup>15</sup>	0	15.7	3	6x10 <sup>6</sup> (anneal during growth)
31B	2x10 <sup>15</sup>	2	1	1	4x10 <sup>6</sup>
31D	2x10 <sup>15</sup>	4	1	1	3x10 <sup>6</sup>
43	2x10 <sup>16</sup>	0	15.7	3	10 <sup>4</sup> (anneal during growth)
J	1x10 <sup>17</sup>	0	6	3	9x10 <sup>3</sup> (anneal during growth)
J'	1x10 <sup>17</sup>	0	6+6	3	7x10 <sup>3</sup> (anneal during growth)

\* The reference state is the density on the unimplanted region. In all cases a continuous film or almost continuous film (density > 4x10<sup>8</sup> particles/cm<sup>2</sup>) formed.

(3) Does annealing of moderately damaged diamond debris have an effect on nucleation by graphitization or removal?

A comparison of data for specimens E and G with F indicate annealing had no detectable effect on nucleation. The three samples were implanted with  $1 \times 10^{15}$  Si/cm<sup>2</sup> and annealed (a) before and after implantation (E), (b) annealed after implantation (G), or (c) not annealed (F). No effect on the subsequently growth could be detected.

Specimens 30, 31a, and 31b were also implanted with  $1 \times 10^{15}$  Si/cm<sup>2</sup>. Numbers 30 and 31a were annealed after implantation, whereas, number 31b was not. Again there was no discernible effect of the annealing.

These observations indicate that the moderately damaged diamond debris is not graphitized or removed remains an effective nucleation site.

(4) Does annealing very heavily damaged or amorphous diamond debris affect nucleation?

It was noted in the Section B) "Ion implantation affect on the nucleation of CVD diamond" that a dose of  $2 \times 10^{15}$  Si/cm<sup>2</sup> was borderline for amorphizing both the diamond debris and the silicon substrate. Thus, some samples implanted with this dose showed suppressed nucleation while there was no effect in others, e.g., specimen 41. There was a decrease in nuclei density by two orders of magnitude ( $10^2$ ) in Specimens 07, 31B, and 31D which had been implanted with this fluence. There was no significant difference in the number of nuclei per unit area between the sample implanted and not annealed (07) and those implanted and annealed for two (31B) or four (31D) hours.



In this study, it has been assumed that all nucleating sites were present at the start of the growth process. The observation that a sample implanted and not annealed (07) had the same density of nuclei that samples implanted and annealed (31B and 31D) indicates that annealing had no effect on the nuclei density. The absence of crystallinity in the diamond debris, thus, appears to be the critical factor.

The reduction in nuclei density by only a factor of 100 is consistent with the conclusion that fluence of  $2 \times 10^{15}$  Si/cm<sup>2</sup> is borderline for amorphizing the debris. Some (the smaller) particles were rendered ineffective whereas some (the larger ones) were unaffected by either the implantation or the annealing.

(5) Does the regrowth of amorphous silicon into crystalline silicon and does the carbonaceous residue from annealed amorphous diamond have an effect on nucleation?

The RBS spectra (Figure 5.22) presented in an earlier section show that the amorphous silicon substrate of specimen J recrystallized into a high quality single crystal during 12 hours exposure in the growth chamber. The density of nuclei in the specimen irradiated with  $2 \times 10^{16}$  Si/cm<sup>2</sup> and that irradiated with  $1 \times 10^{17}$  Si/cm<sup>2</sup> was in the range  $10^3$  and  $10^4$  particles/cm<sup>2</sup>, i.e., a decrease by  $10^4$  to  $10^5$  from that of the unimplanted but annealed controls (C, 44, 31C) where continuous films formed in one hour. Thus, it is concluded that the recrystallization of amorphous silicon to the crystalline state had no effect on nuclei density. Likewise, any graphite or other carbonaceous material had no effect on nucleation.

The results for Specimen J strongly support this conclusion. The growth of a micro-grid was interpreted at several stages for examination of both the unimplanted

regions where the film was growing and the implanted areas. The density of nuclei in the implanted region was the same ( $7-9 \times 10^3$  per  $\text{cm}^2$ ) after 6 and 12 hours growth. No additional nucleation occurred between 6 and 12 hours, and the particles detected in the implanted regions after 12 hours were the same ones detected after 6 hours.

The following conclusions can be drawn from the annealing studies:

(1) Annealing for 2 hours at  $1000^\circ \text{C}$  in hydrogen does not change the effectiveness of diamond debris particles as nucleating sites for CVD diamond.

(2) Annealing the lightly damaged diamond debris particles does not affect the nucleation during subsequent growth. The damage is either recovered or light damage does not affect the debris particle ability to nucleate CVD diamond.

(3) Annealing of moderately damaged diamond does not graphitize or remove it, and it remains an effective nucleating site.

(4) The density of nuclei was reduced by 100 times by annealing of heavily damaged diamond debris particles suggesting that graphitization had occurred. The resultant graphite or other carbonaceous material is not an effective nucleating site.

(5) Amorphous diamond does not nucleate CVD diamond growth. Any other form of carbon produced by annealing, likewise, does not act as nuclei under the growth conditions used in this study.

(6) Whether the silicon substrate is amorphous or crystalline does not seem to play a role in nucleating CVD diamond growth.

These conclusions are consistent with the view that the primary nucleating sites are crystalline diamond particles that are embedded in the surface during the ultrasonic abrasion in diamond-ethanol slurry.

## CHAPTER 6

### SUMMARY PART I

#### 6.1 Surface Mechanical Treatments:

The nucleation rate on samples abraded with diamond-ethanol slurries was four to eight orders of magnitude higher than those abraded with slurries of  $\text{Al}_2\text{O}_3$ -ethanol, SiC-ethanol, or  $\text{TiB}_2$ -ethanol or than the as-received, polished substrates. Measurements of surface roughness using a mechanical profilometer and an atomic force microscope (AFM) showed no significant difference in the roughness of the various abraded samples.

Increasing the time of exposure to the SiC slurry from 15 minutes to 180 minutes caused a slight increase in nucleation density for samples exposed to the same growth conditions.

The nucleation densities on samples deformed by gross scratching of the surface by  $\text{Al}_2\text{O}_3$  or SiC was about the same as those for a 15minute abrasion by the slurry. Occasional rows of nuclei were found in or along the scratches but there was not obvious correlation between surface features and nuclei density.

#### 6.2 Ion Beam Treatments

The density of nuclei on samples implanted with doses of  $1 \times 10^{15}$   $\text{Si}/\text{cm}^2$  (50 KeV, 77 K) or less was similar to that on unimplanted samples that had received similar pretreatments. Nucleation was suppressed for doses of  $1 \times 10^{16}$   $\text{Si}/\text{cm}^2$  and higher. A dose

of  $2 \times 10^{15}$  Si/cm<sup>2</sup> was borderline for suppressing nucleation; suppression occurred for some samples but not others.

The RBS and electron channeling patterns indicated that the surface of samples implanted with doses less than  $2 \times 10^{15}$  Si/cm<sup>2</sup> were crystalline while those implanted with  $10^{16}$  Si/cm<sup>2</sup> and higher were amorphous.

Calculations with the TRIM code indicate that both diamond debris and the silicon surface should be crystalline at the lower doses and both amorphous at the higher fluences.

### **6.3 Effects of Carbon Contamination of Surfaces**

A SiC or some other carbon-containing film was detected between the silicon substrate and the diamond film in only one instance. In this case, a sample was subjected to several exposures in the growth chamber and was examined by various characterization techniques between exposures. This film was detected after three cycles of 6 hours growth followed by SEM examinations and etching. Further exposure in the growth chamber resulted in enhanced nucleation on the contaminant film. The observation suggests that the presence of a SiC or hard carbon film is a sufficient but not necessary condition for nucleation.

### **6.4 Annealing Studies**

Annealing for 2 hours at 1000° C in hydrogen does not change the effectiveness of diamond debris particles as nucleating sites for CVD diamond.

Annealing the lightly damaged diamond debris particles does not affect the nucleation during subsequent growth. The damage is either recovered or light damage does not affect the debris particle ability to nucleate CVD diamond.

Annealing of moderately damaged diamond does not graphitize or remove it, and it remains an effective nucleating site.

The density of nuclei was reduced by 100 times by annealing of heavily damaged diamond debris particles suggesting that graphitization had occurred. The resultant graphite or other carbonaceous material is not an effective nucleating site.

Amorphous diamond does not nucleate CVD diamond growth. Any other form of carbon produced by annealing, likewise, does not act as nuclei under the growth conditions used in this study.

Whether the silicon substrate is amorphous or crystalline does not seem to play a role in nucleating CVD diamond growth.

**PART II**

**Near Net Shape Micro Components**

# CHAPTER 1

## INTRODUCTION AND LITERATURE

Diamond would have no competitor in the field of micro-mechanical devices if an efficient way of fabricating the required components would be obtained. The field of micro-machines has grown rapidly over the past few decades [143]. Structures, with dimensions in the micron range, are being used as resonance devices, pressure sensors, electromechanical switches, etc. Free standing microstructures such as springs and gears that could be used for micro-dynamic devices have been demonstrated. Motors for use in micro-robotic applications are being designed. Possible micro-mechanical device applications range from micro-surgery to space travel.

Silicon and silicon-based compounds such as  $\text{Si}_3\text{N}_4$  have been for the most part the materials used for the fabrication of micro-mechanical devices. This is partially due to the advanced micro-fabrication technology used to produce silicon microprocessors based on semiconducting device technology. However, for many applications, the chemical and physical characteristics of silicon may limit the ultimate use of such micro-mechanical devices. Diamond on the other hand has many properties, such as its physical hardness, high Young's modulus, high tensile yield strength, chemical inertness, low coefficient of friction, high thermal conductivity, and low electrical conductivity, that make it an excellent material for micro-mechanical



device applications. Typically, the physical properties of diamond are an order of magnitude better than the physical properties of silicon. As an example of the advantages of diamond over silicon, micro-motors made from diamond would have less friction and would wear much less than those made from silicon. Unfortunately, the same properties that make diamond such a better candidate for micro-machines, are the ones that make it difficult to fabricate those devices [144]. The conventional approach of grinding, polishing and etching is slow and expensive. Progress toward applications of diamond components would be greatly accelerated if a process to grow components to near-net shape is developed.

John Hunn *et al* [145] developed a procedure to fabricate single-crystal diamond microcomponents. The technique uses a diamond single crystal as the substrate. This substrate is implanted at low temperature (-196° C) with high-energy ions (4- to 5- MeV carbon or oxygen with a minimum dose of  $10^{16}$  ions/cm<sup>2</sup>). This implantation produces a heavily damaged subsurface layer called the sacrificial layer, about 0.1  $\mu\text{m}$  thick and about 1-2  $\mu\text{m}$  below the surface. As the high-energy ions are implanted into the diamond substrate, initially they decelerate by giving energy to the electrons of the crystal's atoms. This ionization process does not perturb the nuclei at the surface because the ions are moving so fast and the probability of interaction between an incoming ion and a nucleus in the crystal is low. As the ions penetrate into the crystal and slow down, the probability of interaction increases significantly. The subsurface region changes its bond structure due to the displacement of atoms from their lattice sites that was caused by the energy transfer to them from the ions. Thus, the high-energy ion implantation produces an

amorphous subsurface layer below a lightly damaged diamond surface. Annealing this sample above 580° C allows the reduction of the surface damage as well as promotes the graphitization of the subsurface layer. The next step was to grow more diamond homoepitaxially, on the original diamond surface. The growth technique was the HFCVD with substrate temperature of about 900° C. The next step was to use laser ablation to cut a pattern into the diamond crystal. An ArF excimer laser was used due to the ability of this laser to cut and etch diamond. The excimer laser was shaped and collimated by a series of optics and delivered into a microscope equipped with UV-transparent objectives. The sample was attached to a computer driven stage. The stage motion was synchronized with the pulse of the laser. The final step was to lift off the microcomponent. The way this was done is by selective etching of the previously created sacrificial subsurface layer. Above 550° C graphite readily oxidizes, but temperatures above 585° C are required for significant oxidation of single-crystal diamond. Thus, if the sample is heated between these two temperatures in the presence of oxygen, the sacrificial subsurface layer can be etched without any significant effect to the crystalline diamond.

In this part of the dissertation, another promising method for fabricating near-net-shape micro components from diamond is discussed.

## CHAPTER 2

### EXPERIMENTAL SETUP AND PROCEDURE

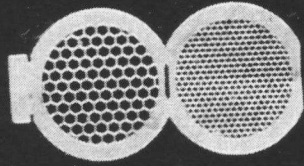
The experimental setup used here is the same as the one described in PART I of this dissertation.

The procedure used to grow freestanding near-net shape CVD diamond microcomponents can be divided into three stages:

- a) Ion implantation
- b) CVD growth
- c) Selective etching

#### a) Ion Implantation:

Using a patterned mask such as a TEM grid (see Figure 2.1), it is possible to implant the silicon substrate and achieve a patterned amorphous layer on the silicon surface. The results of PART I established the dose and energy are needed to obtain complete suppression of diamond nucleation on an abraded, implanted silicon substrate. Using 150 KeV energy and ion dose range of  $2 \times 10^{15}$  Si<sup>+</sup>/cm<sup>2</sup> to  $1 \times 10^{17}$  Si<sup>+</sup>/cm<sup>2</sup>, several samples masked with a pattern were implanted to allow selective CVD diamond growth.



b) CVD growth:

In this stage the implanted substrate was inserted into the Hot Filament CVD chamber and the selective diamond growth was achieved under the conditions given in Table 2.1.

**Table 2.1: CVD Growth parameters for patterned diamond**

Filament Temperature	2100 ° C
Substrate Temperature	1000 ° C
Pressure	40 Torr
Gas Mixture	0.5 % methane in Hydrogen
Deposition Time	Several Hours

The growth times were in the range of 5 hours to 54 hours. Characterization techniques such as, SEM imaging and channeling, RBS/Channeling, and AFM were also used on these substrates.

c) Selective Etching:

In order to obtain a free standing diamond pattern, the silicon substrate was etched from under the diamond pattern, by using a nitric hydrofluoric acid called CP6-S. The substrate with the diamond film attached to it was submerged into the CP6-S and within a matter of several minutes (about 15-20) minutes the silicon was etched away and the diamond pattern floated freely on the surface of the acid. The acid was then wasted in the proper manner and the container is diluted with water to prevent the

diamond from sticking to the walls of the container. The water and the diamond pattern were then placed onto a paper towel which soaks up the water leaving the free standing near-net-shape CVD diamond micro component.

## CHAPTER 3

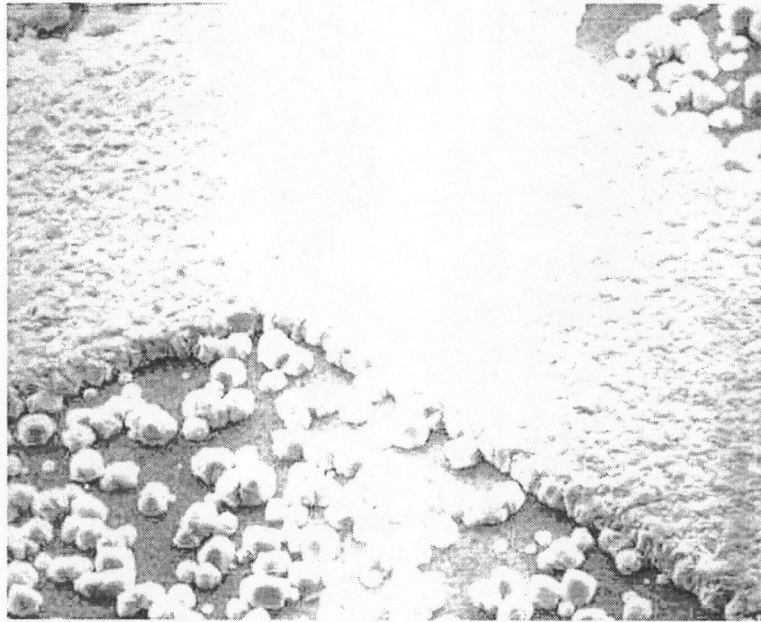
### RESULTS AND DISCUSSION

The near-net shape patterns grown using the above procedure are shown by the SEM images in Figures 3.1-3.5. A summary of the growth parameters for each of the samples is given in Table 3.1.

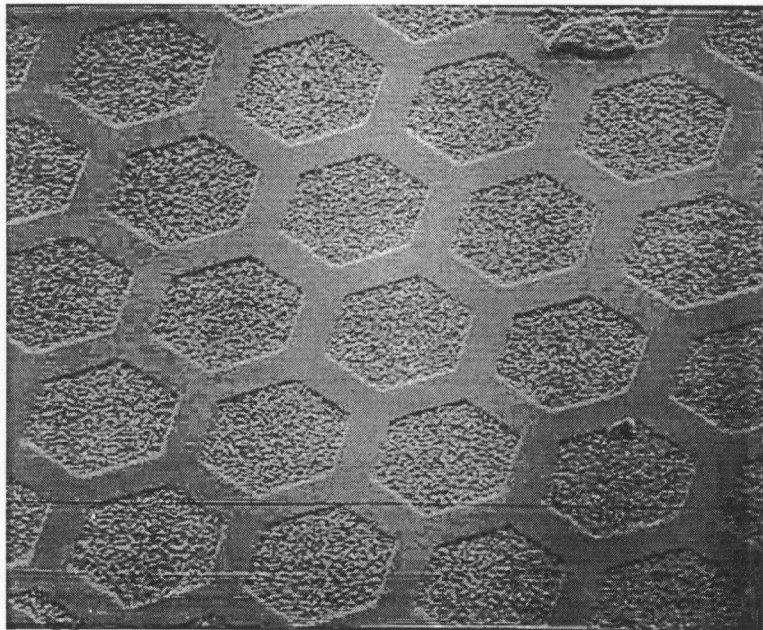
As can be seen from the figures, different patterns can be grown using this method. Samples SSA07, SSA42, and SSA43 have a hexagonal pattern. Sample J has a circular pattern, while sample M has square pattern. Furthermore, Samples SSA42 and SSA43 have two different sizes for the hexagonals i.e. the TEM grids that were used to mask the substrate contained regions of two different hole sizes.

**Table 3.1: Summary of growth parameters for the near-net-shape samples.**

Substrate	Ion dose (Si+/cm <sup>2</sup> )	Growth time (hrs:min)	Final net-shape
SSA07	$2 \times 10^{15}$	15:40	Hexagonal
SSA42	$1 \times 10^{16}$	15:20	Hexagonal
SSA43	$2 \times 10^{16}$	24:00	Hexagonal
J	$1 \times 10^{17}$	54:00	Circular
M	$1 \times 10^{17}$	05:00	Square



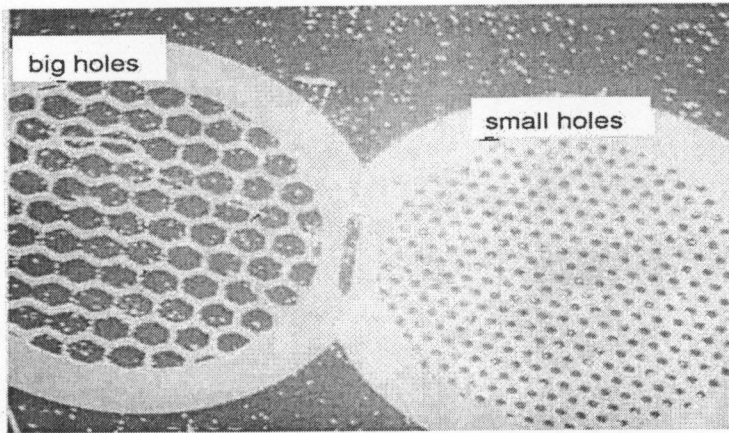
a)



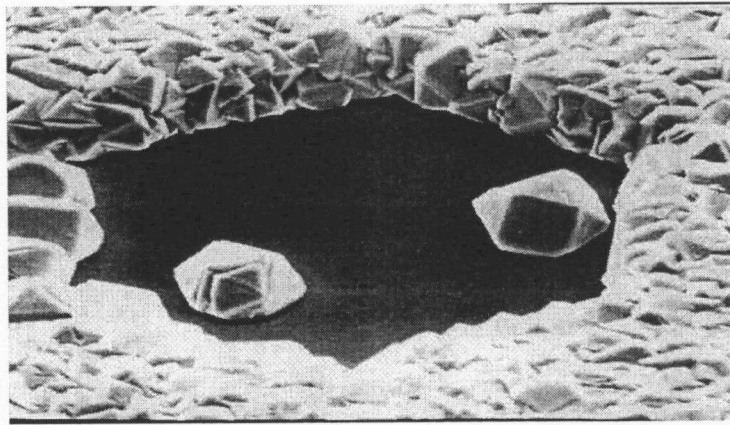
b)

Figure 3.1: Scanning electron micrographs showing the diamond pattern of sample SSA07. a) magnification is 1K, b) magnification is 0.1K.

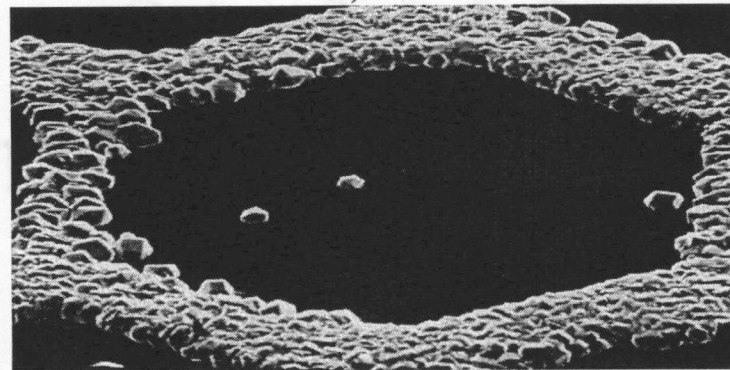




a)



b)



c)

Figure 3.2: Scanning electron micrographs showing the diamond pattern of sample SSA42. a) low magnification (23x) showing both the small and big hole regions, b) is 1.02 kx of the small hole region, and c) is 0.36 kx of the big hole region.

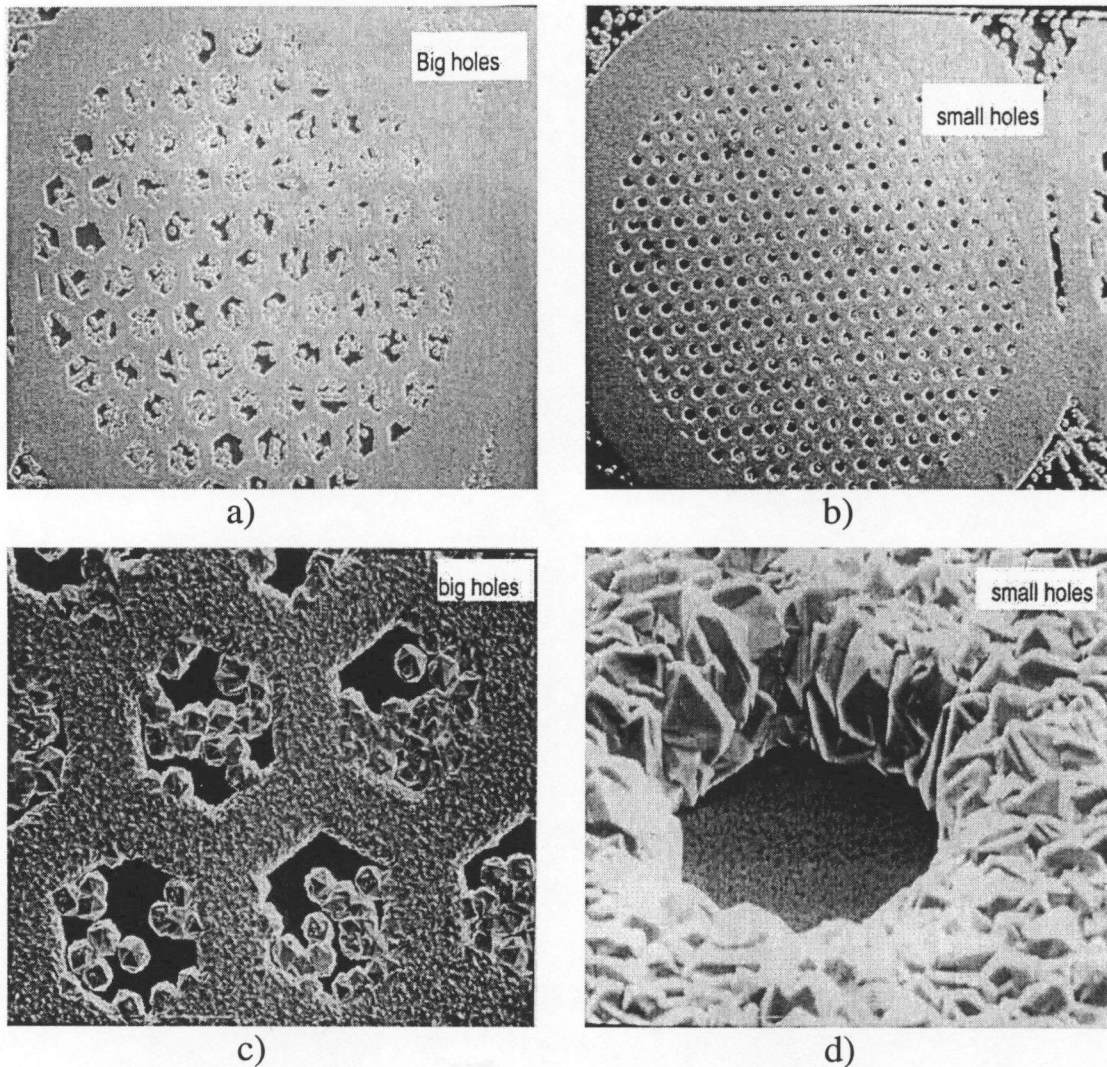
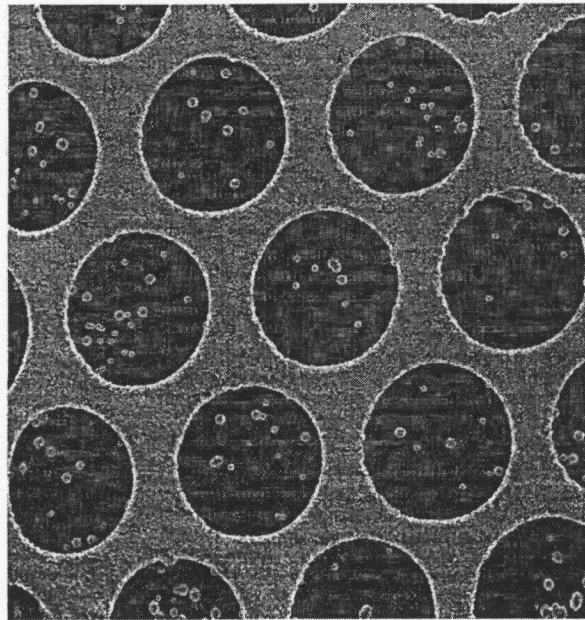
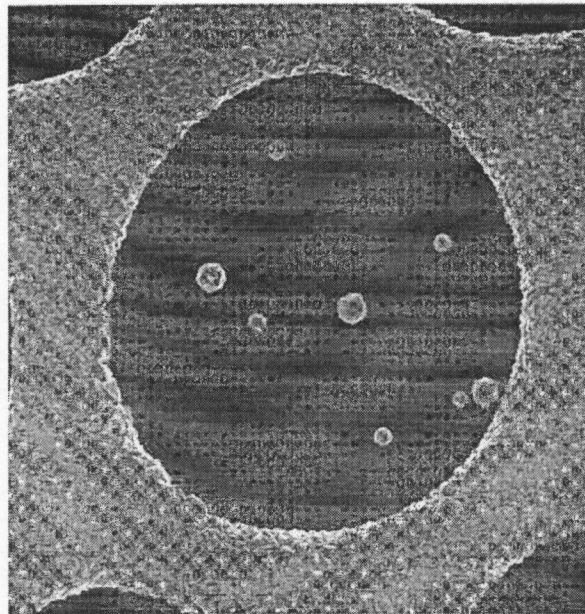


Figure 3.3: Scanning electron micrographs showing the diamond pattern of sample SSA43. a) shows the large hole region at 32 x, and b) shows the small hole region at 32x. c) shows the large hole region at 1.59 kx. Note that nucleation in the implanted regions is what seems to be closing the holes. d) shows a high magnification of the small holes region. In this case it appears that the side wall growth is what changed the hexagonal shape into almost a circular shape.

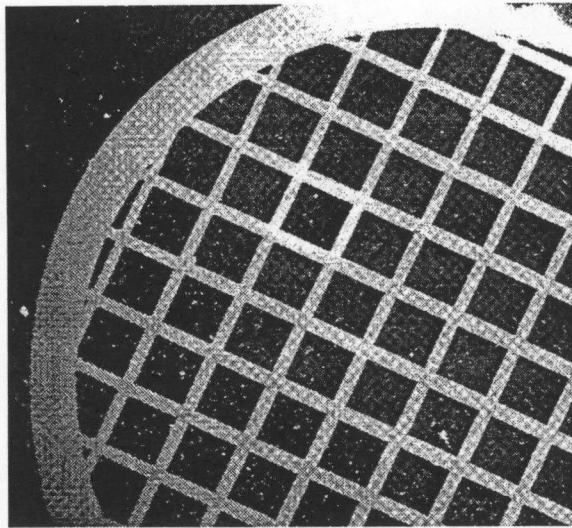


a)

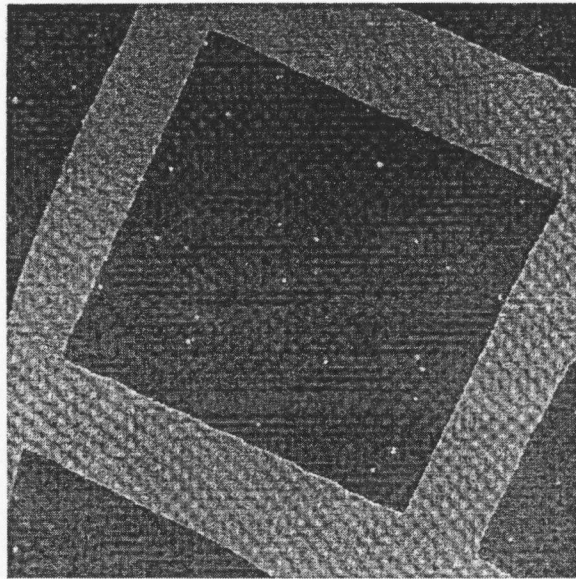


b)

Figure 3.4: Scanning electron micrographs showing the diamond pattern of sample J. a) low magnification, and b) high magnification.



a)



b)

Figure 3.5: Scanning electron micrograph showing the diamond pattern of sample M. a) low magnification, and b) high magnification.

The particles grown in the implanted regions were removed along with the silicon during the selective etching process. Thus, the final net-shape is not affected by stray nucleation in the implanted region so long as the diamond particles in that region stay separate and do not form a film that attached to the side walls of the pattern. A comparison of Figure 3.1 and Figure 3.7 below illustrates this observation. The limitation in this method comes in the fact that the side wall growth is not controlled and may cause the net-shape to lose its features after a long time of growth, see Figure 3.3b. A consequence of that is the thickness of the near-net-shape microcomponent is limited by the side wall growth of the diamond film.

Advantages of this technique over the Hunn procedure are:

- a) It is very economical and does not require a single crystal diamond substrate;
- b) A range of substrate materials (Si, SiC and more) can be used;
- c) Laser facilities are not required;
- d) Many components can be simultaneously fabricated.

The parameters of the diamond microparts produced in this study are given in Tables 3.2-3.6 below.

Figure 3.1 (sample SSA07) suggests that some side wall growth may have occurred due to additional nucleation on the continuous film. However, there is significant nucleation in the implanted regions during the 15 hour 40 minute exposure, suggesting that the holes might be filled by nucleation of additional continuous regions of diamond.

The results for sample SSA42 (Figure 3.2) are similar to sample SSA07 in as much as little side wall growth seems to have occurred. Only a small amount of nucleation in the implanted region occurred. As a consequence, the hexagonal shape was retained for both the small and large holes.

**Table 3.2: Parameters of the CVD near-net-shape microcomponent of sample SSA07 (Figure 3.1).**

Parameter	Value
Smallest hole dimension	90 $\mu\text{m}$
Largest hole dimension	130 $\mu\text{m}$
Film thickness	3.5 $\mu\text{m}$
Wall width 1 and 4	40 $\mu\text{m}$
Wall width 2 and 5	50 $\mu\text{m}$
Wall width 3 and 6	60 $\mu\text{m}$

**Table 3.3: Parameters of the CVD near-net-shape microcomponent of sample SSA42 (Figure 3.2).**

Large Hexagonals

Parameter	Value
Smallest diameter	163.9 $\mu\text{m}$
Largest diameter	250 $\mu\text{m}$
Film thickness	9.8 $\mu\text{m}$
Wall width	41.6 $\mu\text{m}$

Small Hexagonals

Parameter	Value
Smallest dimension	58.8 $\mu\text{m}$
Largest dimension	78.4 $\mu\text{m}$
Film thickness	13.7 $\mu\text{m}$
Wall width	65.2 $\mu\text{m}$

**Table 3.4: Parameters of the CVD near-net-shape microcomponent of sample SSA43 (Figure 3.3).**

Large Hexagonals

Parameter	Value
Smallest dimension	157 $\mu\text{m}$
Largest dimension	182 $\mu\text{m}$
Film thickness	No info
Wall width	81.7 $\mu\text{m}$ – 94.3 $\mu\text{m}$

Small Hexagonals

Parameter	Value
Smallest diameter	5 $\mu\text{m}$
Largest diameter	5 $\mu\text{m}$
Film thickness	20 $\mu\text{m}$
Wall width	93.8 $\mu\text{m}$



**Table 3.5: Parameters of the CVD near-net-shape microcomponent of sample J (Figure 3.4).**

Parameter	At hrs	6hrs	At 12 hrs	At 30 hrs	At 54 hrs
Average Diameter	463.3		450	435.5	415.5
( $\mu\text{m}$ )					
Film thickness ( $\mu\text{m}$ )	2.5		5.8	23	45

**Table 3.6: Parameters of the CVD near-net-shape microcomponent of sample M (Figure 3.5).**

Parameter	Value
Inside square dimensions	287.5 $\mu\text{m}$ x 267.5 $\mu\text{m}$
Wall width 1	77.5 $\mu\text{m}$
Wall width 2	57.5 $\mu\text{m}$
Wall width 3	75 $\mu\text{m}$
Wall width 4	62.5 $\mu\text{m}$
Film thickness	1.7 $\mu\text{m}$

On the other hand, side wall growth appears to have transformed the small hexagonal holes to an almost circular shape in sample SSA43 (24 hours), Figure 3.3d. Little side wall growth appears to have occurred for the large holes (Figure 3.3c) but additional nucleation in the implanted regions is closing the holes. A lower magnification view of the grids (Figure 3.3 a and b) indicated that the filling of the large holes is more complete than the smaller ones.

The data in Table 3.5 for sample J show that films as thick as 45  $\mu\text{m}$  can be grown in 54 hours with a reduction in hole diameter of approximately 12%. Figure 3.4 shows no evidence of uniform side wall growth. A few nuclei are present in the implanted region. The marked region shows a diamond particle that has nucleated on the substrate at the edge of the continuous film, suggesting that it is nucleation rather than growth that causes the holes to be closed.

Figure 3.5 shows the square grid at an early stage of growth (5 hours). There is not evidence for preferred nucleation or growth at the corners of the square diamond film.

Since the closing of the spaces of the grids by nucleation appears to dominate in the implanted region, it was postulated that the film could be removed from the substrate after an initial growth period and used as a "free-standing" template. Figure 3.6 shows the pattern for a sample exposed for 18 hours, removed from the substrate, and placed on a silicon substrate for an additional 36 hours exposure. The results of part I indicated that

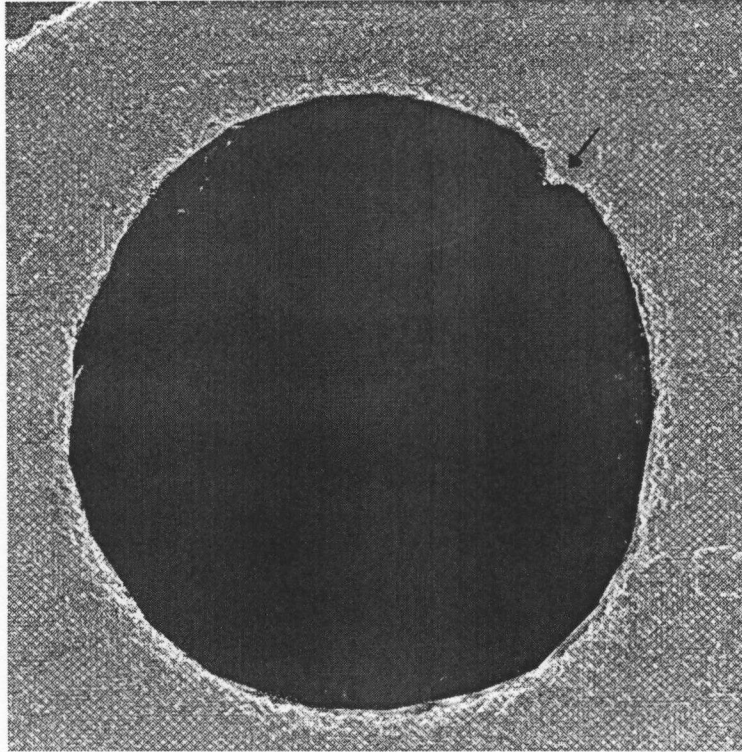


Figure 3.6: Scanning electron micrograph showing a diamond pattern of a sample that was grown for 18 hours on a pretreated substrate, then the diamond grid was removed and placed on a another substrate for another 36 of growth. During the growth on the last substrate the film grew from  $9.7 \mu\text{m}$  to  $40 \mu\text{m}$  thick.

no nucleation would occur on this new substrate. The film that was 9.7  $\mu\text{m}$  thick after the initial growth period of 18 hours grew to a total thickness of 40  $\mu\text{m}$ .

Examples of diamond microcomponents produced by this process are given in Figures 3.7-3.12.

On the following pages, Figures 3.7-3.12 show the near-net shape diamond microcomponents fabricated using the process in this study. The figures are listed in the following order:

Figure 3.7: Free standing microcomponent, sample SSA07 small holes.

Figure 3.8: Free standing microcomponent, sample SSA07 large holes.

Figure 3.9: Free standing microcomponent, sample SSA42 .

Figure 3.10: Free standing microcomponent, sample SSA43 small holes.

Figure 3.11: Free standing microcomponent, sample SSA43 large holes.

Figure 3.12: Free standing microcomponents, Samples SSA07, SSA42, SSA43 together.



GILBERT  
100% COTTON



GILBERT





GILBERT  
100% COTTON



GILBERT



100% COTTON



GILBERT

## CHAPTER 4

### SUMMARY OF PART II

A procedure for producing freestanding diamond structures was developed using ion implantation, the hot-filament CVD processes, and etching. Diamond films ranging in thickness from 1.7 to 45  $\mu\text{m}$  were prepared with a variety of grid patterns (circular, square, and hexagonal). Nucleation of diamond within the grid openings appeared to be the major limitation to increasing film thickness without closing the grid pattern. This limitation can be circumvented by removing the diamond shape from the substrate, at an early stage, via etching. Additional thickening can be accomplished by placing the film on a clean substrate and re-inserting into the growth chamber.

**PART III**  
**CONCLUSIONS**

## CHAPTER 1

### CONCLUSIONS FOR PART I

Mechanical deformation per se of silicon substrate surfaces plays a minor role in the nucleation of diamond in the hot-filament CVD process. The densities of nuclei on samples abraded with  $\text{Al}_2\text{O}_3$  and SiC were in the range of  $10^4$ - $10^5$  particles per  $\text{cm}^2$  for the growth condition used in this study. Abrasion with  $\text{TiB}_2$  produced no nucleation. On the other hand, similar treatments with diamond-ethanol slurries resulted in nucleation densities from  $10^7$  to greater than  $10^8$  particles per  $\text{cm}^2$ . Measurements of surface roughness showed no significant differences for the various mechanical treatments, leading to the conclusion that it is the residual diamond debris that produces the most effective nucleation sites rather than some surface physical features.

Ion beam treatments totally suppressed nucleation in instances where both any diamond debris and the silicon surface were amorphized. No suppression was found in samples where both debris and substrate were damaged but crystalline. These observations lead to the conclusion that crystalline diamond is the effective nucleating agent and "amorphous" diamond is ineffective.

The presence of a hard carbon or SiC film is a sufficient but not necessary condition to promote nucleation. The effectiveness of such a film, however, is orders of magnitude less than that of diamond debris particles.

The annealing studies also lead to the conclusion that the primary nucleating sites are crystalline diamond particles that are embedded in the surface during the ultrasonic

abrasion in diamond-ethanol slurry. The "amorphous" diamond or "graphite" produced by annealing ion-irradiated diamond does not promote nucleation.

These results indicate a procedure for preparing near-net shape micro mechanical components of diamond and are the basis for part II of this dissertation.

## CHAPTER 2

### CONCLUSIONS FOR PART II

The results of part I were used to grow diamond with a variety of geometric shapes. Extraneous nucleation of diamond crystals rather than side wall growth appears to determine how fine of a structure can be produced. One way to overcome this limitation is by removing the diamond film, at an early stage, from the treated substrate and placing it on a clean substrate surface for further growth. The overall results of this technique prove it to be a promising one for the fabrication of diamond microparts.

Several processes were used to pretreat the silicon substrates in order to study their effect on the nucleation of diamond via the CVD process.

The first treatment to alter the features of the silicon substrate surface used was to immerse the silicon samples in diamond-ethanol slurry and polish them using an ultrasonic bath. To study the effect of different scratching materials, other powders such as SiC, Al<sub>2</sub>O<sub>3</sub>, and TiB<sub>2</sub> were later used to scratch the samples and to study their effect on the nucleation of diamond.

Methods of scratching other than using the ultrasonic bath were used. Those included manually scratching the silicon substrates with powder slurry or by using abrasive paper.

Another way to alter the surface features of the silicon, was to ion implant the substrate with high energy silicon ions. That was done using several ion doses ranging



from  $5 \times 10^{14}$  ions/cm<sup>2</sup> to  $1 \times 10^{17}$  ion/cm<sup>2</sup>. TEM masks were used to implant the surface with certain patterns in order to grow near-net-shape microcomponents from diamond.

Another way to modify the surface features on the silicon surface was to anneal the substrates. Four different types of furnaces were used, a contaminated filament furnace, a clean filament furnace, a graphite wall furnace, and a CVD growth atmosphere under long times of growth.

In order to study the results of the pretreatments before and after the CVD process, several different analysis techniques were used, including SEM, AFM, profilometry, RBS/channeling, and SEM/channeling.

The growth method used for nucleation diamond was the hot filament chemical vapor deposition, and two different methane concentrations were used; 0.5% and 1% in hydrogen. The substrate temperatures were at an average of a 1000<sup>o</sup> C. The periods of growth varied from 1 hour to 54 hours.

In conclusion it has been possible to grow near-net shape components with features and dimensional control on the order of the film thickness.

**PART IV**  
**SUGGESTED FUTURE WORK**

## CHAPTER 1

### Recommendations

The majority of effort in this study was concentrated on the abrasion of the sample with the different powder-ethanol slurries. The importance of ethanol could be revealed by repeating the abrasion process using water instead of ethanol for the slurries.

Using the results of part I of this work, one can easily calculate the required doses and energies required to amorphize either the diamond or the silicon but not both. That would give an exact correlation between the crystallinity of the substrate and/or the diamond and the nucleation rate.

Further examination of the carbon contaminated specimen by XPS/x-ray photoemission spectroscopy, Auger spectroscopy and electron diffraction to determine if the film is SiC or just some form of carbon would be another immediate check point.

The control of unwanted nucleation in the implanted regions of the diamond microcomponents was only briefly studied in this project. More detailed studies of removing the diamond film from the substrate, at an early stage of growth, and placing it on another substrate for further growth is another important step. A way of controlling nucleation in the implanted regions would improve the development of such microcomponents and allow better resolution of their features.

The results of the current studies are consistent with the conclusion that crystalline diamond debris are the most effective nucleating sites. However, no direct evidence for the existence of diamond particles embedded in the substrate has been

obtained in this or other studies. A search for such particles should be made using the array of surface analytical tools now available.

## **REFERENCES**

1. Sunil Abraham "Effect of Surface Defects on The Nucleation of CVD Diamond on 6H Silicon Carbide", Master's thesis 1994, University of Tennessee.
2. Peter Gielisse "Mechanical Properties of Diamond, Diamond Films, Diamond-Like Carbon and Like-Diamond Materials", Handbook of Industrial Diamond and Diamond Films, pp49.
3. Alexander G. Gontar pp377 "Electrical and Electronic Properties", in *Handbook of Industrial Diamonds and Diamond films*, edited by Mark A Prelas, Galina Popovici, and Louis K. Bigelow, (1997).
4. Alexander M. Zaitsev "Optical properties" in *Handbook of Industrial Diamonds and Diamond films*, edited by Mark A Prelas, Galina Popovici, and Louis K. Bigelow, (1997).
5. Paul W. May "CVD diamond – a new technology for the future?", *Endeavour Magazine* **19**(3), (1995) pp101-106.
6. Max N. Yoder "Diamond Potential and Status" in *Diamond and Diamond-like films and coatings*, Edited by Robert E. Clausing, Linda L. Horton, John C Angus, and Peter Koidl, NATO ASI Series B **266**, 1 (1991).
7. Robert E. Clausing, "Diamond Morphology", *Industrial Handbook on diamonds and diamond films*, Edited by Mark A. Prelas, Galina Popovici, and Louis K. Bigelow, 19 (1997).
8. Wilks J. and Wilks E. M. (1979) in J. E. Field (ed), *The properties of Diamond*, Academic Press, 352.
9. Evans T. (1979) in J.E. Field (ed), *The properties of Diamond*, Academic Press, 405.

10. J. E. Field "Natural Diamond: The Standard", page 25, in *Diamond and Diamond-like films and coatings*, Edited by Robert E. Clausing, Linda L. Horton, John C Angus, and Peter Koidl, NATO ASI Series B 266, 17 (1991).
11. Ono, T. Baba, H Funamoto, and A. Nishikawa (1986) Japan. J. Appl. Phys. Vol 25, L808-810.
12. V. Spitsyn, L. L. Bouilov and B. V. Derjaguin "Diamond and Diamond-Like Films: Deposition From the Vapour Phase, Structure and Properties", 79, (1985).
13. Alberto Argoitia, Christopher S. Kovach and John C. Angus, "Hot-Filament CVD Methods", PP797, Handbook of industrial diamonds and diamond films.
14. Peter K. Bachmann, "Microwave Plasma Chemical Vapor Deposition of Diamond", PP821, Handbook of industrial diamonds and diamond films, 1997.
15. Steven L. Girshick, "Diamond CVD Using Radio-Frequency Plasmas", PP851, Handbook of industrial diamonds and diamond films.
16. Mark A. Cappelli "Arcjet Synthesis of Diamond", PP 865, in *Handbook of Industrial Diamonds and Diamond films*, edited by Mark A. Prelas, Galina Popovici, and Louis K. Bigelow, (1997).
17. Akimitsu Hatta and Akio Hiraki "Low Temperature CVD", PP887, in *Handbook of Industrial Diamonds and Diamond films*, edited by Mark A Prelas, Galina Popovici, and Louis K. Bigelow, (1997).
18. R. C. Devries, Ann. Rev. Mater. Sci. 17, 161 (1987)
19. K. E. Spear, J. Am. Ceram. Soc. 72, 171 (1989)
20. Thomas R. Anthony "Methods of Diamond Making", PP 556, *Diamond and Diamond-like films and coatings*, Edited by Robert E. Clausing, Linda L. Horton, John C Angus, and Peter Koidl, NATO ASI Series B 266, 555 (1991).

21. B.V. Spitsyn and B. V. Derjaguin, Author's certificate (patent application, July 10 (1956); USSR patent 339 134, May 5, (1980).
22. W. Eversole, US patents 3030187 and 3030188 (1962) (filed in 1959).
23. H. J. Hibshman, US patent 3371996 (1968) (filed in 1964).
24. S. Matsumoto, Y. Sato, M. Kamo, and N. Setaka, Jpn. J. of Appl. Phys. 21, L183 (1982).
25. Y. Hirose and Y. Terasaki, Jpn. J. of Appl. Phys. 25, L183 (1986).
26. Sawabe and T. Inuzuka, Appl. Phys. Letters, 46, 2, 146 (1985).
27. M. Sommer and F. W. Smith, presented at the "Diamond, Boron Nitride, Silicon Carbide and Related Wide Bandgap Semiconductors" Symposium, MRS Fall Meeting, Boston (1989), MRS Symposium Proceedings Vol. 162 (1990).
28. Y. Hirose and N. Kondo, Extended Abstracts, 35<sup>th</sup> Spring Meeting, Jpn. Appl. Phys. Soc. March 29, 434 (1988).
29. Y. Hirose, S. Ananuma, N. Okada, K. Komaki, Proceedings of the "First International Symposium on Diamond and Diamond-like Films", The Electrochemical Society, Pennington, NJ, Proceedings Vol. 89-12, 80 (1989).
30. Matsui, A. Yuuki, M. Sahara, and Y. Hirose, Japanese J. Appl Phys., Vol. 28, no. 9, 171 (1989).
31. Y. Hirose and S. Amanuma, Denshi Zairyo, Vol. 28, no.8, 45 (1989).
32. K. Snail, L. Hanssen, W. Carrington, D. Oakes, and J. Butler, Proceedings of the First International Conference New Diamond Science and Technology, Tokyo, Oct. 24-26, 38 (1988).



33. B. V. Derjaguin, L. L. Bouliov, and B. V. Spitsyn, *Arch Nauki Mater.*, 7, 2, 111 (1986).
34. J. M. Pinneo, 1<sup>st</sup> Diamond Technology Initiative Workshop, MIT Lincoln Laboratories, Boston, MA, Feb. 2, paper 4 (1987).
35. K. V. Ravi and M. I. Landstrass, Proceedings of the "First International Symposium on Diamond and Diamond-like Films", The Electrochemical Society, Pennington, NJ, Proceedings Vol. 89-12, 24 (1989).
36. K. Suzuki, A. Sawabe, H. Yasuda, and T. Inuzuka, *Appl. Phys. Letters*, 50, 12, 728 (1987).
37. K. Suzuki, A. Sawabe, H. Yasuda, and T. Inuzuka, *Appl. Phys. Letters*, (1990).
38. Singh, O. R. Mesker, A. W. Levine, and Y. Arie, *Appl. Phys. Letters*, 52, 1658 (1988).
39. N. Ohtake, H. Tokura, Y. Kuriyama, Y. Mashimo, and M. Yoshikawa, Proceedings of the "First International Symposium on Diamond and Diamond-like Films", The Electrochemical Society, Pennington, NJ, Proceedings Vol. 89-12, 93 (1989).
40. S. Matsumoto, M. Hino, Y. Moriyoshi, T. Nagashima, and M. Tsutsumi, US Patent No. 4 767 608, August 30, 1988 (filed Oct. 19, 1987).
41. K. Kurihara, K. Sasaki, M. Kawarada, and N. Koshino, *Apply. Phys. Lett.*, 52, 6, 437 (1988).
42. S. Matsumoto, in *Diamond and Diamond-like Materials Synthesis* edited by G.H. Johnson, A.R. Badzian, and M.W. Geis, *Mat. Res. Soc. Symp. Extended Abstracts*, EA-15, Pittsburgh, PA, 119, (1988).

43. P. K. Bachmann, H. Lydtin, D.u. Wiechert, J. J. Beulens, G. Kroesen, D.C. Schram, Proceedings of the "Third International Conference on Surface Modification Technologies", Neuchatel, Switzerland, The Minerals, Metals & Materials Society (TMS), Warrendale, PA, (1989) in press.
44. S. Matsumoto, J. Mat. Sci. Lett., 4, 600 (1985).
45. D.E. Meyer, R.O. Dillon, and J.A Woolham, J. Vac. Sci. Tech. 7,3, 2325 (1989).
46. P. Wood, T. Wydeven, and O. Tsuji, Abstracts of the 1<sup>st</sup> Int. Conference on the New Diamond Science and Technology, Oct. 24-26, Tokyo, P 100, Japanese New Diamond Forum (1988).
47. S. Matsumoto, M. Hino, and T. Kobayashi, Appl. Phys. Lett. , 51, 10, 737 (1987).
48. S. Miyake, W. Chen, A. Hoshino, and Y. Arata, Trans. JWRI, 17, 2, 323 (1988).
49. S. Matsumoto, Proceeding of the "First International Symposium on Diamond and Diamond-Like Films", The Electrochemical Society, Pennington, NJ, P Proceedings Vol. 89-12, 50 (1989).
50. R. Badzian, B. Simonton, T. Badzian, R. Messier, K.E. Spear and R. Roy, Proc. SPIE, 683, 127 (1986).
51. P.K. Bachmann, W. Drawl, D. Knight, R. Weimer, and R. F. Messier, in "Diamond and Diamond- Like Materials" (edited by A. Badzian, M. Geis, and G.Johnson), Materials Research Society, Pittsburgh, PA, Extended Abstracts Vol. EA-15, (1988) 99.
52. P.K. Bachmann, R. Weimer, and R. Messier, Diamond Technology Initiative Symposium, July 12-14, 1988, Crystal City, Arlington, Va. Technical Digest, Paper T 2.

53. K. Ishibori and Y. Ohira, Abstracts of the 1<sup>st</sup> Int. Conference on the New Diamond Sci. and Tech., Oct. 24-26, Tokyo, p104, Japanese New Diamond Forum (1988).
54. D. M. Tung, W. L. Hsu, K. F. McCarty, Proceedings of the "First International symposium on Diamond and Diamond-Like Films", The Electrochemical Society, Pennington, NJ, Proceedings Vol. 89-12, 500 (1989).
55. Y. Mitsuda, T. Yoshida, and K. Akashi, Rev. Sci. Instrum. , 60, 2, 249 (1989).
56. H. Kawarada, K.S. Mar, and A. Hiraki, Jpn. Appl. Phys. 26, 6, L1032 (1987).
57. J. Suzuki, Jpn. J. Appl. Phys. 28, 2, L 281 (1989).
58. M. Aklufi and D. Brock, Proceedings of the " First International Symposium on Diamond and Diamond-Like Films", The Electrochemical Society, Pennigton, NJ, Proceedings Vol. 89-12, 114 (1989).
59. Michael W. Geis and John C. Angus. Scientific American, October 92, p.84
60. V. Spitsyn, L. L. Bouilov and B. V. Derjaguin, Prog. Crystal. Growth and Charact. 1988, Vol. 17, pp. 79-170.
61. F. G. Celii and J. E. Butler, Appl. Phys. Lett., 54 (1989), 1031-1033
62. David G. Goodwin and James E. Butler, Industrial Handbook on diamonds and diamond films, Edited by Mark A. Prelas, Galina Popovici, and Louis K. Bigelow, 19 (1997), 527.
63. R. E. Clausing personal discussion
64. D. Joslin, Ion Mixing in Oside-Sapphire Systems, Doctoral Dissertation, University of Tennessee, 1993.

65. J. S. Williams and J. M. Poate "Introduction to Ion and Beam Processing" in *Ion Implantation and Beam Processing*, edited by J. S. Williams and J. M. Poate, p6 figure 3, 1984
66. S. Matteson, and M. A. Nicolet, *Ann. ReV. Mater. Sci.* **13** (1983) 339.
67. V. I. Protasov and V. G. Chudinov, *Radiation Effects* **66** (1982) 1.
68. W. L. Johnson, Y. T. Cheng, M. van Rossum, and M.A. Nicloet, *Nucl. Instr. Meth. Phys. Res. B7/8* (1985) 657.
69. R. S. Averback, D. N. Seidman, *Mater. Sci. Forum* **15-18** (1987) 963.
70. F. F. Morehead and B. L. Crowder, *Radiat. Effects*, **6** (1970) 27.
71. J. F. Gibbons, *Proc. IEEE*, **60** (1972)
72. F. L. Vook, *Radiation Damage and Defects in Semiconductors* (London Institute of Physics, 1972) p60.
73. J. Washburn, C. S. Murty, D. Sadana, P. Byrne, R. Gronsky, N. Cheung and R. Kilaas, *Nuclear Instruments and Methods* **209/210** (1983) 345-350.
74. J. D. Hunn, M. L. Swanson, E. A. Hill, N. R. Parikh, and G Hudson, *New Diamond Science and Technology MRS Int. Conf. Proc* (1991), 929.
75. Hoffman, R. Berner, I. Gouzman, C. Cytermann, H. Geller, L. Levine, M. Kenny, *Diamond and Related Materials*, **4**, (1995), 292.
76. S. Praver, *Diamond and Related Materials* **4** (1995) 862-872.
77. Lux and R. Haubner "Nucleation and Growth of Low-pressure Diamond", *Diamond and Diamond-like films and coatings*, Edited by Robert E. Clausing, Linda L. Horton, John C Angus, and Peter Koidl, *NATO ASI Series B* **266**, 579.

78. S. Yugo, T. Kimura, H.Kanai: JNDF Tokyo, p2-20.
79. B.E. Williams, J.T. Glass, R.F. Davis: SPIE, Vol. 877, Micro-Optoelectronica Materials (1988) pp. 56-63
80. B.E. Williams, D.A. Asbury, B.R. Stones, J.T. Glass : Nato ASI.
81. S. Abraham, C. J. Mchargue, R. E. Clausing, L. Heatherly, and J. D. Hunn, Diamond Relat. Mater., 4 (1995)261
82. P. O. Joffreau, R. Haubner, B. Lux : J. Ref. Met.-Hard Mat., Vol. 7, Nr.4, 1988, 186-194.
83. Anger, A. Gicquel, Z. Z. Wang, M. F. Ravet Diamond and Related Materials 4 (1995) 759-764
84. J. J. Dubray, W. A. Yarbrough, and C. G. Pantano "Physico-Chemical Aspects Of Surface Treatments For Diamond Nucleation, *Diamond and Diamond-like films and coatings*, Edited by Robert E. Clausing, Linda L. Horton, John C Angus, and Peter Koidl, NATO ASI Series B 266, 619 (1991).
85. W.A. Yarbrough and R. Messier, *Science*, 247, 688(1990).
86. K. Hirabayashi, Y. Taniguchi, O. Takamatsu, T. Ikeda, K. Ikoma, N. Iwasaki-Kurihara, *Appl.Phys.Lett.*, 53 1815 (1988).
87. J. A. Baglio, B. C. Farnsworth, S. Hankin, C Sung, J Hefter, and M Tabasky "Studies On The Formation Of Diamond Nucleation Sites On <100> Silicon Substrates" in *Diamond and Diamond-like films and coatings*, Edited by Robert E. Clausing, Linda L. Horton, John C Angus, and Peter Koidl, NATO ASI Series B 266, 635 (1991).
88. R. Badzian, T. Badzian, L. Pilione: 3<sup>rd</sup> Int. Conf. On Sufr. Mod. Techn., pp.51-61, Aug.28-sept.1,1989, Neuchatel, Switzerland.

89. K. Hirabayashi, K. Ikoma, Y. Taniguchi, N. I. Kurihara: JNDF Tokyo P 2-03.
90. L. Vandenbulk, P. Bou, R. Herbin: Journal de Physique, Colloque C5, Supp. To n°5, Vol.50 May 1989, 177-188.
91. W. A. Yarborough: MRS 1987, Nov.30-Dec.5, N 3.8, Boston, MS.
92. S. Yougo and T. Kimura in "First Int. Conf. On the New Diamond Sci. and Techn., Program & Abstracts, "24-26 september, 1988 (JNDF, Tokyo), p.130.
93. Chalmers: "Principles of Solidification", New York 1934.
94. A. Porter, K E Easterling, "Phase Transformations in Metals and Alloys", second edition, Chapman & Hall, 1992.
95. P.A. Denning, and D.A. Stevenson, in Proceedings of the Second International Conference on The New Diamond Science and Technology, edited by R.Messier and J.T.Glass (Japan New Diamond Forum, Washington DC,1990);
96. P.A. Denning and D.A. Stevenson in Proceedings of the First International Conference on The Applications of Diamond films and Related materials, edited by Y. Tzeng, M. Yoshikawa, M. Marakawa and A.Feldman (Elsevier, New York, 1991), p383
97. S. Yugo, A Izumi, T Kanai, T Muto and T Kimura, in Second International Conference on the New Diamond Science and Technology, edited by R. Messier, J T Glass, J E Butler and R Roy (mater. Res. Soc.,Pittsburgh, PA,1991)p385.
98. R. Badzian, T Badzian : Surface and Coatings Technology, **36**, (1988), 283-293
99. Y. Chakk, R. Kalish and A. Hoffman, Diamond Relat. Mater., **5** (1996)1074.
100. D.M. Li, R. Hernberg, and T. Mäntylä, Diamond and Related Materials, **7**, (1998), 188-192

101. P. Karve, S. R. Sainkar, S. T. Kshirsagar, *Materials letters*. **34**,(1998) 387-391
102. S. Iijima, Y. Aikawa, and K. Baba, *Appl. Phys. Lett.* **57** (1990) 2646
103. S. Iijima, Y. Aikawa, and K. Baba, *J. Mater. Res.* **6** (1991) 1491
104. K. Suzuki, A. Sawabe, H. Yasuda, and T. Inuzaka, *Appl. Phys. Lett.* **50** (1987) 728
105. Sawabe and T. Inuzula, *Thin Solid Films* **137** (1986) 89
106. P. Change, D. L. Flamm, D. E. Lbbotson, and J. A. Mucha, *J. Apply. Phys.* **63** (1988)1744
107. K. Higuchi and S. Noda *Diamond Relat. Mater.* **1** (1993) 220
108. R. Kirkpatrick, B. W. Wart and N. P. Economou, *J. Vac Sci Technol.*, **B7** (1989) 1947
109. S. J. Lin, S. L. Lee, J. Hwang and T. S. Lin, *J. Electrochem. Soc.*, **139** (1992) 3255
110. M. A. Brewer, I. G. Brown, P. J. Evans and A. Hoffman, *Appl. Phys. Lett*, **63** (1992)1631
111. J. Mchargue "Ion Implantation and Ion-beam Mixing". *Surface Modification Engineering Volume I. Fundamental Aspects*, Editor RAM Kossowsky, CRC press
112. D. Clark, P. J. Kemmy, E. W. J. Mitchell, *Discussion Faraday Soc.* **31** (1961) 96
113. "*The Stopping and Range of Ions in Matter*", vol 2-6, Pergamon Press, 1977-1985]
114. J. Verhoeven, "Fundamentals of Physical Metallurgy", (1975), 47.

115. E. S. Zanoria, T. R. Watkins, K. Breder, L. Riester, M Bashkansky, J. Reintjes, J. G. Sun, W. A. Ellingson, and P. J. Blau, *Journal of Materials Engineering and Performance*, **7(4)** (1998) 533
117. Piercy, G.R., Brown, F., Davies, J.A., and McCargo, M. (1963), *Phys. Rev. Lett.* **10**, 399. First experimental evidence for channeling - from range studies in Al.
118. Robinson, M.T. and Oen, U.S. (1963a), *Appl. Phys. Lett.* **2**, 30.
119. Robinson, M.T. and Oen, U.S. (1963b), *Phys. Rev.* **132**, 2385. First predictions of channeling by computer simulations.
120. A.A. Morrish, Pehr E. Pehrsson, Effects of surface pretreatments on nucleation and growth of diamond films on a variety of substrates, april 29, 1991;
121. Sumio Iijima, Yumi Aikawa, and Kazuhiro Baba, Early formation of chemical vapor depositions diamond films, *Appl Phys Lett* **57** (25), 17 december 1990].
122. Carl Mchargue, personal discussion.
123. A. sawabe and T. Inuzaka, *Thin Solid Films*, **137** (1986) 89.
124. C.P. Chang, D.L. Flamm, D.E. Ibbotson and J.A. Mucha, *J. Appl Phys*, **63** (1988) 1744.
125. L.A. Christel, J.F. Gibbons, and T.W. Sigmon, Displacement criterion for amorphization of silicon during ion implantation, *J. Appl. Phys.* **52**(12), December 1981.
126. C.D. Clark, P. Kemmey, and E.W.J. Mitchell, *Disc. Faraday Soc.* **31**, 96 (1961)
127. J. Washburn, C. S. Murty, D Sadana, P. Byrne, R. Gronsky, N. Cheung and R. KilaasThe Crystalline to Amorphous Transformation in Silicon, *Nuclear Instruments and Methods* **209/210** (1983) 345-350



128. G. Wolf, in J. K. Hirvonen (ed.), Ion Implantation, Treatise Mater. Sci Technol.,**18** (1980) 403.
129. W. J. M. J. Josquin, Radiat. Eff., **47** (1980) 221.
130. J. F. Gotzlich, K. Habegger, H. Ryssel, H. Kranz and E. Traumuller, Radiat. Eff., **47** (1980) 203.
131. B. R. Stoner, G. H. M. Ma, S.D. Wolter, and J.T. Glass, Phys. Rev. B **45** (1992) 11067
132. W. Kulisch, B. Sobisch, M. Kuhr, R. Beckmann, Characterization of the bias nucleation process, Diamond and Related Materials **4** (1995) 401-405
133. D. K. Milne, P.G. Roberts, P. John, M.G. Jubber, M. Liehr, J.I.B. Wilson, Epitaxy of diamond on silicon, Diamond and Related Materials **4** (1995) 394-400
134. P.C. Yang, T.J.Kistenmacher, D.A. Tucker, W. Liu, F.R. Sivazlian, S.P. Bozeman, B.R. Stoner, J.T. Prater, J.T. Glass and R.F. Davis, Nucleation and Growth of Oriented Diamond Films on Ni Substrates, Applications of Diamond films and Related Materials: Third International Conference, 1995 Editors: A. Feldman, Y. Tzeng, W. A. Yarbrough, M. Yoshikawa, and M. Murakawa
135. Zhangda Lin, Jie Yang, Kean Feng and Yan Chen, HETERO-EPITAXY OF DIAMOND FILM ON SILICON, Applications of Diamond films and Related Materials: Third International Conference, 1995 Editors: A. Feldman, Y. Tzeng, W. A. Yarbrough, M. Yoshikawa, and M. Murakawa.
136. W.Zhu, X.H.Wang, B.R. Stoner, G.H.M. Ma, H.S.Kong, M.W.H. Braun, and J.T. Glass, Phys. Rev. B**47** (1993) 6529.
137. J. Gyulai, "Radiation damage and annealing in Ion Implantation" P69-117 in Handbook of Ion Implantation Technology, Edited by J.F. Ziegler (worth-Holland, Amsterdam, 1992).

138. T. Evans pp. 408-419 in The Properties of Diamond, ed., J. E. Field (Academic Press, London, 1979).
139. G. Braunstein, A. Talmi, R. Kalish, T. Bernstein, and R. Beserman, Rad. Effects, 48 (1980) 139.
140. M. Teicher and R. Beserman, J. Appl. Phys., 53 (1982) 1467
141. G. Braunstein and R. Kalish, J. Appl. Phys; 54 (1983)2106];
142. R.E. Clausing personal discussion.
143. R.S. Muller, Sensors and Actuators, vol A21-A23, (1990),1.
144. J. D. Hunn, S. P. Withrow, C. W. White, R. E. Clausing, and L. Heatherly, Appl. Phys. Lett. 65 (24), 12 December 1994.
145. J. D. Hunn, C. P. Christensen, Solid State Technology, (1994), 57.

## VITA

Samer Sima'an Ackleh was born in Nazareth, Israel in 1971. He grew up in Nazareth until attending Cumberland College in Williamsburg Kentucky in 1988. He obtained his Bachelor of Science in Mathematics and Physics in May 1992. He then attended the University of Tennessee to pursue his graduate studies. He obtained his Master of Science in Physics in May 1995, and a Ph.D. in Metallurgical Engineering in December 1999. He is currently working as a Response Center Engineer at Hewlett Packard in Atlanta Georgia.